E-ISSN: 2148-6247

Turkish Journal of PHARMACEUTICAL SCIENCES

An Official Journal of the Turkish Pharmacists' Association, Academy of Pharmacy

Volume: 22 Issue: 2 April 2025

www.turkjps.org

PubMed Central PubMed Scopus TRDİZİN

galenos

Turkish Journal of
PHARMACEUTICAL SCIENCES

Turkish Journal of
PHARMACEUTICAL SCIENCES

Prof. Robert Rapoport, Ph.D.
ORCID: orcid.org/0000-0001-8554-1014
Cincinati University Faculty of Pharmacy, Department of Pharmacology and Cell Biophysics, Cincinati, USA
robertrapoport@gmail.com

Prof. Tayfun Uzbay, Ph.D.
ORCID: orcid.org/0000-0002-9784-5637
Üsküdar University Faculty of Medicine, Department of Medical Pharmacology, İstanbul, Türkiye
tayfun.uzbay@uskudar.edu.tr

Prof. Wolfgang Sadee, Ph.D.
ORCID: orcid.org/0000-0003-1894-6374
Ohio State University, Center for Pharmacogenomics, Ohio, USA
wolfgang.sadee@osumc.edu

Advisory Board

Turkish Journal of
PHARMACEUTICAL SCIENCES

Please refer to the journal's webpage (https://www.turkjps.org/) for "Editorial Policy" and "Instructions to Authors".

The editorial and publication process of the **Turkish Journal of Pharmaceutical Sciences** are shaped in accordance with the guidelines of ICMJE, WAME, CSE, COPE, EASE, and NISO. The Turkish Journal of Pharmaceutical Sciences is indexed in **PubMed, PubMed Central, Thomson Reuters / Emerging Sources Citation Index, Scopus, ULAKBİM, Türkiye Citation Index, Embase, EBSCO Host, Türk Medline, Cabi, CNK**I.

The journal is published online.

Owner: Turkish Pharmacists' Association, Academy of Pharmacy

Responsible Manager: Mesut Sancar

galenos yayınevi

Publisher Contact
Address: Molla Gürani Mah. Kaçamak Sk. No: 21/1
34093 İstanbul, Türkiye
Phone: +90 (530) 177 30 97
E-mail: info@galenos.com.tr/yayin@galenos.com.tr
Web: www.galenos.com.tr | **Publisher Certificate Number:** 14521

Publication Date: May 2025
E-ISSN: 2148-6247
International scientific journal published bimonthly.

Turkish Journal of
PHARMACEUTICAL SCIENCES

CONTENTS

Original Articles

Turk J Pharm Sci 2025;22(2):71-76
DOI: 10.4274/tjps.galenos.2025.48380

ORIGINAL ARTICLE

Development and Characterization of Mucoadhesive Films Containing Metronidazole for Vaginal Drug Delivery

Sinem SAAR, Fatmanur TUĞCU DEMİRÖZ*

Gazi University Faculty of Pharmacy, Department of Pharmaceutical Technology, Ankara, Türkiye

ABSTRACT

Objectives: Bacterial vaginosis (BV) is a common disease in women of reproductive age. Metronidazole (MET) is an antibiotic used to treat BV *via* the oral or vaginal route. Vaginal films are dosage forms that combine the properties of solid and gel formulations and increase patient compliance. This study aims to develop and characterize vaginal film formulations containing MET for the treatment of BV.

Materials and Methods: Film formulations were prepared using the solvent casting method with poly(vinyl alcohol), hydroxypropyl methylcellulose K100M, and mixtures of these polymers. Polyethylene glycol 400 was added to the formulations as a plasticizer. The moisture content, average thickness, and weight of the film formulations were examined. Also, the mechanical properties (tensile strength and elongation at break) and *ex vivo* mucoadhesion properties of the films were determined with vaginal tissue. The release of MET from the films was investigated using Franz diffusion cells.

Results: The moisture content of the formulations was found to be less than 10%. It was observed that tensile strength and elongation at break values decreased when MET was loaded onto the films. Mucoadhesion values decreased with MET loading and the work of mucoadhesion values was found to be 0.070±0.053, 0.067±0.039, and 0.150±0.061 for F4, F5, and F6, respectively. The release of MET was found to be 92.7%, 65.5%, and 87.6% for F4, F5, and F6, respectively.

Conclusion: Mucoadhesive films can be used as an alternative dosage form for vaginal delivery of MET in the treatment of BV.

Keywords: Metronidazole, bacterial vaginosis, vaginal drug delivery, vaginal film

INTRODUCTION

Bacterial vaginosis (BV) is a common disease in women characterized by an increase in facultative and anaerobic bacteria by suppressing the normal vaginal flora.[1,2] Various drugs, such as Ampicillin, Penicillin, and Metronidazole (MET), are used to treat BV1. MET is an antibiotic used to treat infections in the digestive, reproductive, and integumentary systems that inhibit nucleic acid synthesis.[3] MET is a preferred agent for treating various diseases with its low cost, acceptable side effect profile, and pharmacokinetic and pharmacodynamic properties.[4,5] MET is associated with low levels of antimicrobial resistance.[6] MET-containing oral or vaginal formulations are commonly used to treat BV. MET is well tolerated and diffuses to all tissues.[7]

Vaginal drug administration is frequently used because of its large surface area, high permeability, ease of self-administration, and both local and systemic effects.[8,9] Different dosage forms, such as gel, suppository, tablet, emulsion, nanoparticle, liposome, and film, are used for vaginal drug administration.[10-14]

Films are solid dosage forms that release active substances by dissolving when placed on a mucosal surface. Film

***Correspondence:** fatmanur@gazi.edu.tr, **ORCID-ID:** orcid.org/0000-0002-9468-3329
Received: 07.02.2024, **Accepted:** 07.02.2025 **Publication Date:** 14.05.2025

Cite this article as: SAAR S, TUĞCU DEMİRÖZ F. Development and characterization of mucoadhesive films containing metronidazole for vaginal drug delivery. Turk J Pharm Sci. 2025;22(2):71-76

formulations have several advantages such as fast and accurate dosing, leakage prevention, ease of use without an applicator, and increased stability.[15] The acceptability of vaginal films over other vaginal formulations, such as gels, foams, and suppositories, has been demonstrated.[15] The solvent casting method, which is based on removing the solvent by pouring the polymer solution on glass, teflon, and plastic, is widely used in the production of vaginal films.[16] Film formulations can be prepared using different polymers such as poly(vinyl alcohol) (PVA), pectin, carrageenan, sodium carboxymethyl cellulose, and hydroxyethyl cellulose, individually or in combinations with different polymers.[17] Hydroxypropyl methylcellulose (HPMC), a non-ionic water-soluble polymer with its swelling and dissolution properties in aqueous media, is frequently used to develop different dosage forms, such as films, gels, nanofibers, and tablets.[13,17-19] PVA is a biodegradable, water-soluble, crystalline, and synthetic polymer used in various industrial and medical applications.[20,21] PVA is a polymer also used in commercial film formulations.[22]

Kawarkhe and Poddar[23] developed film formulations containing MET to be applied vaginally to treat local infections. They investigated the effect of the HPMC and Carbopol ratio and the different plasticizers on film formulation during production. The physical, mechanical, and mucoadhesive properties of the films were evaluated. The solvent casting method successfully produced the optimum film formulation containing MET. Film formulations containing MET have also been developed for buccal administration to treat periodontal diseases.[24]

In our previous work, we developed nanofiber and gel formulations that are containing MET for vaginal use.[25] As an alternative to these formulations, the authors aimed to develop a new, inexpensive, and organic solvent-free dosage form that can be used for vaginal application. For this purpose, mucoadhesive and controlled-release film formulations containing MET have been developed using HPMC, PVA, and mixtures of these polymers. The physical, mechanical, *ex vivo* mucoadhesive, and *in vitro* diffusion properties of the developed films were investigated. In this study, the most suitable vaginal film formulations for MET vaginal administration were evaluated.

MATERIALS AND METHODS

Materials

MET was a generous gift from Abdi İbrahim Pharmaceutical Company, Türkiye. HPMC-K100M was purchased from Colorcon, England. PVA was kindly donated by Wacker Chemical Corporation. Polyethylene glycol 400 (PEG400) was acquired from Merck, Germany. All chemicals and reagents were of analytical grade.

Preparation of vaginal films

HPMC, PVA, or a mixture of the two was used as the film-forming polymer, and PEG400 was used as a plasticizer. To prepare the HPMC film, the polymer was dissolved in distilled water. During the preparation of the PVA film, hot water (80-90 °C) was used. When the polymers were mixed with water, a plasticizer was added to the solution, resulting in a homogeneous mixture. PVA was completely dissolved in hot water to prepare the film containing both polymers. Then, HPMC was added to the PVA solution and mixed until a homogeneous mixture was formed. The ingredients of the formulations and their amounts are shown in Table 1. The films prepared using the solvent casting method were poured into petri dishes. The air in the solutions was removed by sonication. Film formulations were dried in the oven at 40 °C.[26]

Thermal analysis of vaginal films

Thermal properties of MET, polymers, and formulations were characterized using differential scanning calorimetry (DSC) (Shimadzu, DSC-60, Japan). Samples (2-3 mg) were weighed, sealed in aluminum pans, and scanned at a heating rate from 25 to 300 °C.

Weight and thickness of vaginal films

To evaluate the weight homogeneity, three films were cut into 1x1 cm pieces and weighed on a digital scale, and their average weight was calculated. To determine the thickness of the films, random points on the film were measured with a micrometer (Mitutoyo Digital Micrometer, Japan), and the average of these values was determined as film thickness.

Moisture content of vaginal films

The moisture content of vaginal film formulations was evaluated by heating film samples to 130 °C using a moisture analyzer (Sartorius Moisture Analyzer, Germany).

Mechanical properties of vaginal films

(TA.XT. Plus Texture Analyzer, Stable Micro Systems, UK) was used to determine the mechanical characterization of vaginal films. The films were cut to 3x1 cm in size and clamped between the mini tensile grips. Elongation at break and tensile strength of the films were calculated at the point of rupture, while the upper part of the apparatus moved upwards with a fixed lower part. For all formulations, stress-strain graphs were used for measurement parameters such as tensile strength and elongation at break values, and measurements were repeated three times for each film.

Table 1. Content of vaginal film formulations

	Formulation code					
	F1	F2	F3	F4	F5	F6
Content *(w/w)*						
MET	-	-	-	0.05	0.05	0.05
PVA	0.5	-	0.25	0.5	-	0.25
HPMC	-	0.5	0.25	-	0.5	0.25
PEG400	0.5	0.5	0.5	0.5	0.5	0.5
Distilled water	qs 50 g					

MET: Metronidazole, PVA: Poly(vinyl alcohol), HPMC: Hydroxypropyl methylcellulose, PEG400: Polyethylene glycol 400, qs: Quantum satis

Ex vivo mucoadhesion studies of vaginal films

The sheep vagina was used as a model tissue for mucoadhesion studies. Mucoadhesion properties of the films were determined with a texture analyzer equipped with a 50 N load cell. The film formulation was attached to the upper probe of the device with double-sided tape. Vaginal tissue was placed in the inferior attachment. The contact time of the probe used was 60 seconds, the force applied by the probe to the vaginal tissue was 0.2 N, and the experiments were carried out at a speed of 1 mm/s. The force required to separate the films from vaginal tissue was determined as mucoadhesive strength. The work of mucoadhesion was measured using the area under the curve (AUC) of the force-distance graph. The work of mucoadhesion was calculated with the formula (mJ/cm^2)=AUC/(πr^2).[27]

In vitro drug release of vaginal films

Franz diffusion cells were used for the *in vitro* release of MET from vaginal films. *In vitro* diffusion studies were performed with a dialysis membrane (12 kDa, Sigma®, USA). For this study, the film formulation was placed in the donor compartment. The release from the films was sampled at certain time intervals (0.5, 1, 1.5, 2, 3, 4, 6, and 8 h). The samples were withdrawn from the receptor phase (pH 4.5 phosphate buffer) and replaced with fresh buffer. The amount of MET released was determined at 320 nm in an ultraviolet (UV) spectrometer (Cary 60 UV-vis, Agilent Technologies, US). All the release studies were conducted under sink conditions.

RESULTS

Thermal properties of vaginal films

DSC thermograms of MET, polymers, and formulations are given in Figure 1. The characteristic peak of MET was observed around 160 °C, which corresponds to the melting point in the thermogram. According to the literature, pure PVA has a melt peak temperature of 202.7 °C. Similarly, it was found to be 195 °C in our study.

Weight and thickness of vaginal films

The average weight of the films increased with MET loading. In the MET-loaded film formulations, the highest average weight was observed in the F4 formulation (10.0±0.9 mg/cm^2) and the lowest in the F5 formulation (5.1±0.5 mg/cm^2). The difference in vaginal film thickness and MET loading was significant between F1 and F4, while the addition of MET to the other formulations was not found to be significant (p<0.05). The change in the weight of the films with MET loading was found to be statistically non-significant (p>0.05).

Moisture content of vaginal films

It was observed that the moisture content of the MET-loaded films was generally higher. The moisture content of film formulations is less than 10%, as seen in Table 2. F4 formulation containing MET showed a higher percentage of moisture content than other formulations.

Mechanical properties of vaginal films

Vaginal films must have sufficient strength to withstand mechanical effects during manufacture, use, and application.[28] In our film formulations, the presence of the MET changed the mechanical properties. When the mechanical properties of blank and MET-loaded films are examined, it has been found that the addition of MET reduces the tensile strength, as seen in Table 2. The change observed with MET loading was found to be statistically insignificant (p>0.05). The F6 formulation showed higher tensile strength compared to the F5 and F4 formulations containing MET (p>0.05). When the elongation at break values was examined, a significant difference was observed between F1 and F4 with the loading of MET into the films (p<0.05).

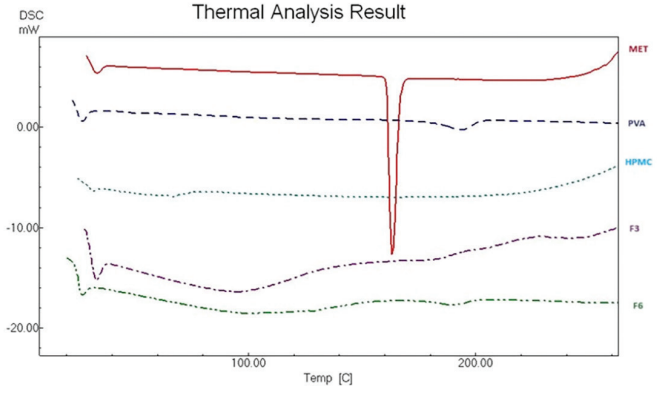

Figure 1. DSC thermograms of MET, PVA, HPMC, F3 and F6 formulations

DSC: Differential scanning calorimetry, MET: Metronidazole, PVA: Poly(vinyl alcohol), HPMC: Hydroxypropyl methylcellulose

Table 2. Different properties of vaginal film formulations

Formulations	Properties				
	Thickness (μm)	Average weight (mg/cm^2)	Moisture content (%)	Tensile strenght (MPa)	Elongation at break (%)
F1	81.7±3.80	6.6±0.40	4	4.68±0.838	239.90±78.749
F2	62.7±1.50	4.9±0.20	4.2	10.96±4.624	121.47±47.626
F3	80.7±4.00	5.4±0.40	7.95	9.779±2.379	88.487±19.673
F4	162.7±38.10	10.0±0.90	8	3.64±0.896	90.687±19.725
F5	46±4.6	5.1±0.50	7.2	7.143±1.881	86.143±17.439
F6	85.3±17.7	7.9±3.1	4.7	7.349±2.680	46.290±20.773

Mucoadhesion studies of vaginal films

The values of the work of mucoadhesion for the film formulations are shown in Figure 2. Mucoadhesion values decreased with MET loading in the formulations. The highest mucoadhesion value of the formulations loaded with MET was observed in formulation F6, prepared with a combination of polymers.

In vitro drug release of vaginal films

The release profiles of MET from the different film formulations were compared. The release profiles of MET were found to be 92.7%, 65.5%, and 87.6% for F4, F5, and F6, respectively (Figure 3). However, approximately 80% of MET release from our formulations occurred within an hour. In our study, the slowest release was observed in the F5 formulation prepared with HPMC.

DISCUSSION

Film formulations were successfully developed using the solvent-casting method. Film formulations were developed with HPMC, PVA, and a mixture of these polymers. The films prepared were transparent, soft, and flexible. This shows that the two polymers can blend completely with the plasticizer to form a new polymer matrix. The formulations developed using HPMC have a more transparent and colorless appearance than those consisting of PVA or polymer mixtures.

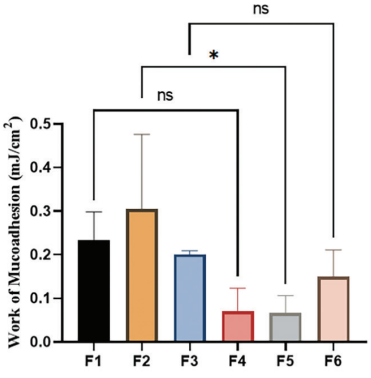

Figure 2. Work of mucoadhesion values of film formulations from sheep vaginal tissue

ns: Not significant, *: $p<0.05$, n=3

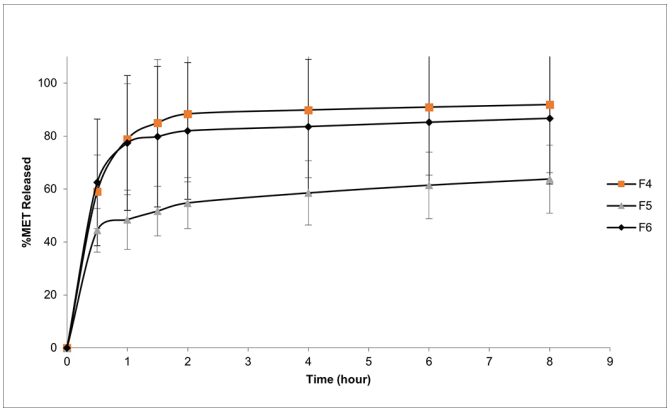

Figure 3. *In vitro* diffusion profiles of F4, F5 and F6 formulations

When DSC analysis was performed, the disappearance of the MET endothermic peak indicated that the drug transformed from a crystalline to a partially amorphous state.[29] The amorphous structure of the drug resulted in increased solubility.[30]

Different thicknesses and weights may be due to the polymer type and amount in the film formulations.

The moisture content of film formulations must be at a certain level so that the formulations are not dry and brittle. Dobaria et al.[30] found the moisture content to be 7.66±0.51% *(w/w)* in the vaginal film formulation they developed to prevent *Candida* infections. The researchers stated that the small amount of moisture content in the films would help them remain stable and prevent them from becoming completely dry and brittle. Cautela et al.[31] found the moisture content of the films containing PVA and pectin to be from 5% to 8.7%. In addition, the moisture content of the commercially available Vaginal Contraceptive Film® (VCF®) (Apothecus, Oyster Bay, NY, USA) was found to be 13.1%. The moisture content of film formulations is less than commercially available VCF®, as seen in Table 2.

Film formulations should have moderate tensile strength and high elongation at break.[32] A decrease in elongation at break values was observed in film formulations prepared with a mixture of HPMC and PVA, relative to the films containing a single polymer. In addition, an increase in tensile strength values was observed in comparison to formulations containing PVA. PEG400 can change the mechanical properties of the film by weakening the intermolecular interactions between polymer chains, with a hydrogen-bonding effect.[32] A suitable vaginal film formulation is recommended to have high tensile strength and an elongation at break value.[33] Akil et al.[15] found that while the tensile strength value of the 0.5 mg dapivirine-containing film was 777.59±19.99 N/cm^2 in the vaginal film formulations, the 1.25 mg dapivirine-containing film's tensile strength was 538.24±57.17 N/cm^2. Increasing the amount of dapivirine changed the films' mechanical properties. Similarly, drug loading changed the mechanical properties of our film formulations. Tensile strength and elongation at break values in our blank film formulations are higher than in the MET-loaded formulations. Higher tensile strength and elongation at break values were obtained in F1 and F4 formulations prepared with PVA.

Retention of vaginal films in the vagina is desirable for therapeutic efficacy and helps reduce frequent dosing.[28] HPMC is a non-ionic polymer, and its mucoadhesiveness is due to physical or hydrogen bonding with mucus components, which can relieve dryness and irritation even if mucus secretions are reduced.[28] With their mucoadhesive properties, the films may help prevent vaginal leakage and will increase the effectiveness of MET by providing better contact of the formulations with the vagina. Notario-Pérez et al.,[16] in their study, prepared film formulations containing zein and HPMC. The film formulation prepared with HPMC remained in the biological sample longer until corrosion was complete. The F6 formulation, prepared with HPMC and PVA, has the highest mucoadhesion value and was expected to remain in the vagina for longer than the other formulations.

The release profiles of MET shown in Figure 3 can be related to the swelling properties of the polymers. Drug release from films occurs by the swelling of the films, which allows gels that can control release.[17] In Kawarkhe and Poddar's[23] study, MET releases were observed over 60 minutes in films prepared with Carbopol and HPMC.

The highest release was obtained in the F4 formulation prepared with PVA (92.7%), while the slowest MET release was obtained from the F5 formulation prepared with HPMC (65.5%). The slow release of MET from our film formulations prepared with HPMC may be due to its high molecular weight or high viscosity. Sudeendra et al.[28] prepared a film formulation using clotrimazole-loaded HPMC, chitosan, and sodium CMC with different types of plasticizers in their study. It was observed that the release of the formulations decreased with the increase in HPMC and sodium CMC ratios. It has been stated that HPMC slows the release by reducing the penetration of water, forming a viscous gel.[28]

CONCLUSION

Film formulations were successfully produced using the solvent-casting method. Mechanical properties and release profiles of the films were investigated. MET-loaded vaginal films are developed for many different purposes and provide various advantages over gel formulations, such as prolonged retention, reduced messiness, and reduced leakage. Film formulations can be a cost-effective dosage form that can be administered vaginally for BV treatment. F6 film formulation, prepared with the combination of PVA and HPMC polymers, showed good mucoadhesive properties and a good drug release profile for vaginal application. More detailed morphological, mechanical, *ex vivo*, and *in vivo* studies are required to determine the optimum film formulation.

Ethics

Ethics Committee Approval: Not required.

Informed Consent: Not required.

Acknowledgment

The authors would like to thank Abdi İbrahim Pharmaceutical Company for kindly providing Metronidazole for research purposes.

Footnotes

Authorship Contributions

Concept: F.T.D., Design: F.T.D., Data Collection or Processing: F.T.D., S.S., Analysis or Interpretation: S.S., FTD., Literature Search: F.T.D., S.S., Writing: F.T.D., S.S.

Conflict of Interest: The authors declare no conflicts of interest.

Financial Disclosure: The authors declared that this study received no financial support.

REFERENCES

1. Afzali E, Siahposh A, Haghighi-Zadeh MH, Farajzadeh A, Abbaspoor Z. The effect of Quercus (Oak Gal) vaginal cream versus metronidazole vaginal gel on bacterial vaginosis: a double-blind randomized controlled trial. Complement Ther Med. 2020;52:102497.
2. Mondal AS, Sharma R, Trivedi N. Bacterial vaginosis: a state of microbial dysbiosis. Med Microecol. 2023;16:100082.
3. Coletti Zabala TL, Zerbatto ME, Perotti EBR, Smacchia AM, Ombrella A, Pidello AR. Efecto del metronidazol suplementado con hidroquinona en la adherencia de *Lactobacillus acidophilus* en células vaginales ovinas. Rev Argent Microbiol. 2016;48:313-319.
4. Freeman CD, Klutman NE, Lamp KC. Metronidazole. A therapeutic review and update. Drugs. 1997;54:679-708.
5. Stover KR, Riche DM, Gandy CL, Henderson H. What would we do without metronidazole? Am J Med Sci. 2012;343:316-319.
6. Verwijs MC, Agaba SK, Darby AC, van de Wijgert JHHM. Impact of oral metronidazole treatment on the vaginal microbiota and correlates of treatment failure. Am J Obstet Gynecol. 2020;222:157.
7. Finegold SM. Pharmacology and mode of action of prymnesin. Marine Pharmacognosy. 1980:241-263.
8. Acartürk F. Mucoadhesive vaginal drug delivery systems. Recent Pat Drug Deliv Formul. 2009;3:193-205.
9. Tuğcu-Demiröz F, Acartürk F, Erdoğan D. Development of long-acting bioadhesive vaginal gels of oxybutynin: formulation, *in vitro* and *in vivo* evaluations. Int J Pharm. 2013;457:25-39.
10. das Neves J, Nunes R, Machado A, Sarmento B. Polymer-based nanocarriers for vaginal drug delivery. Adv Drug Deliv Rev. 2015;92:53-70.
11. Caramella CM, Rossi S, Ferrari F, Bonferoni MC, Sandri G. Mucoadhesive and thermogelling systems for vaginal drug delivery. Adv Drug Deliv Rev. 2015;92:39-52.
12. Tuğcu-Demiröz F. Vaginal delivery of benzydamine hydrochloride through liposomes dispersed in mucoadhesive gels. Chem Pharm Bull (Tokyo). 2017;65:660-667.
13. Tuğcu-Demiröz F, Acartürk F, Özkul A. Preparation and characterization of bioadhesive controlled-release gels of cidofovir for vaginal delivery. J Biomater Sci Polym Ed. 2015;26:1237-1255.
14. Tuğcu-Demiröz F. Development of *in situ* poloxamer-chitosan hydrogels for vaginal drug delivery of benzydamine hydrochloride: textural, mucoadhesive and *in vitro* release properties. Marmara Pharm J. 2017;21:762-770.
15. Akil A, Parniak MA, Dezzuitti CS, Moncla BJ, Cost MR, Li M, Rohan LC. Development and characterization of a vaginal film containing dapivirine, a Non-nucleoside Reverse Transcriptase Inhibitor (NNRTI), for prevention of HIV-1 sexual transmission. Drug Deliv Transl Res. 2011;1:209-222.
16. Notario-Pérez F, Cazorla-Luna R, Martín-Illana A, Galante J, Ruiz-Caro R, das Neves J, Veiga MD. Design, fabrication and characterisation of drug-loaded vaginal films: state-of-the-art. J Control Release. 2020;327:477-499.
17. Notario-Pérez F, Martín-Illana A, Cazorla-Luna R, Ruiz-Caro R, Bedoya LM, Peña J, Veiga MD. Development of mucoadhesive vaginal films based on HPMC and zein as novel formulations to prevent sexual transmission of HIV. Int J Pharm. 2019;570:118643.

18. Rüzgar G, Birer M, Tort S, Acartürk F. Studies on improvement of water-solubility of curcumin with electrospun nanofibers. FABAD J Pharm Sci. 2013;38:143-149.

19. Bhise MR, Mohod SP, Narkhede MB, Sapkal SB. HPMC based extended release matrix tablet of gabapentin by direct compression method. Turk J Pharm Sci. 2014;11:45-53.

20. Traore YL, Fumakia M, Gu J, Ho EA. Dynamic mechanical behaviour of nanoparticle loaded biodegradable PVA films for vaginal drug delivery. J Biomater Appl. 2018;32:1119-1126.

21. Baker MI, Walsh SP, Schwartz Z, Boyan BD. A review of polyvinyl alcohol and its uses in cartilage and orthopedic applications. J Biomed Mater Res B Appl Biomater. 2012;100:1451-1457.

22. Gong T, Zhang W, Parniak MA, Graebing PW, Moncla B, Gupta P, Empey KM, Rohan LC. Preformulation and vaginal film formulation development of microbicide drug candidate CSIC for HIV prevention. J Pharm Innov. 2017;12:142-154.

23. Kawarkhe S, Poddar SS. Designing of the mucoadhesive intravaginal spermicidal films. Indian J Pharm Sci. 2010;72:652-655.

24. El-Kamel AH, Ashri LY, Alsarra IA. Micromatricial metronidazole benzoate film as a local mucoadhesive delivery system for treatment of periodontal diseases. AAPS PharmSciTech. 2007;8:E75.

25. Tuğcu-Demiröz F, Saar S, Tort S, Acartürk F. Electrospun metronidazole-loaded nanofibers for vaginal drug delivery. Drug Dev Ind Pharm. 2020;46:1015-1025.

26. Machado RM, Palmeira-de-Oliveira A, Martinez-De-Oliveira J, Palmeira-de-Oliveira R. Vaginal films for drug delivery. J Pharm Sci. 2013;102:2069-2081.

27. Cevher E, Sensoy D, Taha MA, Araman A. Effect of thiolated polymers to textural and mucoadhesive properties of vaginal gel formulations prepared with polycarbophil and chitosan. AAPS PharmSciTech. 2008;9:953-965.

28. Sudeendra BR, Umme H, Gupta RK, Shivakumar HG. Development and characterization of bioadhesive vaginal films of clotrimazole for vaginal candidiasis. Acta Pharmaceutica Sciencia. 2010;52:416-425.

29. Calvo NL, Svetaz LA, Alvarez VA, Quiroga AD, Lamas MC, Leonardi D. Chitosan-hydroxypropyl methylcellulose tioconazole films: A promising alternative dosage form for the treatment of vaginal candidiasis. Int J Pharm. 2019;556:181-191.

30. Dobaria NB, Badhan AC, Mashru RC. A novel itraconazole bioadhesive film for vaginal delivery: design, optimization, and physicodynamic characterization. AAPS PharmSciTech. 2009;10:951-959.

31. Cautela MP, Moshe H, Sosnik A, Sarmento B, das Neves J. Composite films for vaginal delivery of tenofovir disoproxil fumarate and emtricitabine. Eur J Pharm Biopharm. 2019;138:3-10.

32. Zhang W, Parniak MA, Sarafianos SG, Cost MR, Rohan LC. Development of a vaginal delivery film containing EFdA, a novel anti-HIV nucleoside reverse transcriptase inhibitor. Int J Pharm. 2014;461:203-213.

33. Chatterjee A, Bhowmik BB, Awasthi D. Prolong release bioadhesive vaginal film of anti-HIV drug (zidovudine): formulation and *in vitro* evaluation. Int J Pharm Sci Res. 2010;1:28-37.

Turk J Pharm Sci 2025;22(2):77-82
DOI: 10.4274/tjps.galenos.2025.40070

ORIGINAL ARTICLE

Synthesis and Characterization of Sodium Carboxymethylcellulose from *Sansevieria trifasciata* as an Alternative Raw Material for Capsule Shell

Azimatur RAHMİ[1]*, Bella Vista OLVIA[2], Iza Ayu SAUFANI[3]

[1]Republic of Indonesia Defense University Faculty of Military Mathematics and Natural Sciences, Department of Chemistry, West Java, Indonesia
[2]Mohammad Natsir University Faculty of Pharmacy, Department of Pharmacy, West Sumatra, Indonesia
[3]Universitas Negeri Medan Faculty of Engineering, Department of Nutrition, North Sumatra, Indonesia

ABSTRACT

Objectives: Capsules are pharmaceutical preparations that are enclosed in hard or soft capsule shells made of gelatin. Because gelatin is typically generated from non-halal materials, there is a need for alternative raw materials for making capsule shells, one of which is carboxymethyl cellulose (Na-CMC), which is synthesized from cellulose.

Materials and Methods: This study aims to find alternative raw materials for the manufacture of capsule shells from cellulose-containing *Sansevieria trifasciata* leaves. Then, the isolated cellulose was treated with sodium Na-CMC using the alkalization and carboxymethylation methods.

Results: The cellulose that was produced fulfills the requirements for continuing the synthesis of Na-CMC. The yield of Na-CMC produced was 83.83%, with a pH of 6; dispersed in water and insoluble in ethanol and ether; a degree of substitution of 0.83; and a water content of 12%. The Fourier Transform Infrared Spectroscopy study results show the presence of functional groups such as O-H at 3332 cm^{-1}, C-H at 2930 cm^{-1}, C=C at 2050 cm^{-1}, O-Na at 1588.82 cm^{-1}, and C-O at 1020.16 cm^{-1}. The resulting capsule shell has the following properties: transparency, a slightly cream color, a somewhat firm texture, no odor, and a moisture content of 20%.

Conclusion: As a result, it is possible to establish that Na-CMC from the *S. trifasciata* leaves can be used as a raw material for capsule shells.

Keywords: Capsule shell, Na-CMC, *Sansevieria trifasciata*

INTRODUCTION

Capsules are solid preparations consisting of one or more drugs or other inert materials that are enclosed in a soluble hard or soft shell. Hard capsules are generally made of gelatin but can also be made of starch or other suitable materials.[1] Commercially available hard-shell capsules are generally made from gelatin, which is produced from the bone and skin of cows, pigs, or buffalo. Gelatin hard-shell capsules were introduced in 1931 by Arthur Cotton. One of the advantages of hard-shell capsules is that they can deliver both solid and liquid medicines. This indicates that the presence of hard-shell capsules is important as a drug delivery system (DDS).[2,3]

According to several sources, it is known that the most widely produced source of gelatin is derived from pork skin, namely 44.5% (136,000 tons), the second from cow skin, 27.6% (84,000 tons), the third from cow bones, 26.6% (81,000 tons), and the rest comes from another 1.3% (4,000 tons). The use of pork skin as the main source of gelatin manufacture started in 1930 in Europe. This is due to the limited availability of raw materials and high prices. In this case, pigs are abundant, while the

***Correspondence:** azimatur.rahmi046@gmail.com, **ORCID-ID:** orcid.org/0000-0002-7700-0864
Received: 01.07.2023 **Accepted:** 07.02.2025 **Publication Date:** 14.05.2025

Cite this article as: RAHMİ A, OLVIA BV, SAUFANI IA. Synthesis and characterization of sodium carboxymethylcellulose from *Sansevieria trifasciata* as an alternative raw material for capsule shells. Turk J Pharm Sci. 2025;22(2):77-82

consumers, Indonesian people, are mostly Muslim, and pigs are among the animals that are forbidden by Islam. Because of that, many studies have been carried out to find alternative materials, such as materials that are obtained from polysaccharides or natural polymers.[4]

Polysaccharides play a crucial role in plant life processes because they can form glycoconjugates with proteins and lipids, resulting in biological macromolecules. The primary wall's principal polysaccharides are cellulose, hemicellulose, and pectin. Cellulose is one of the most abundant natural biopolymers, found in the cells of many plants and algae.[5] Cellulose has three reactive hydroxyl groups that create inter- and intramolecular hydrogen bonds per anhydroglucose repeat unit. This second bond has a significant impact on cellulose's chemical reactivity and solubility.[6]

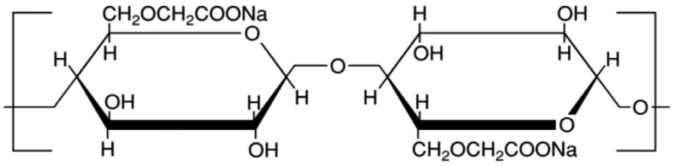

Figure 1. Sodium carboxymethyl cellulose (Na-CMC)[7]

Sodium carboxymethyl cellulose (Na-CMC) is a water-soluble organic polymer, which is produced by partial substitution of 2, 3, and 6 hydroxymethyl groups of cellulose by hydrophobic carboxymethyl groups. The chemical structure of Na-CMC, as illustrated in Figure 1, provides further insight into its composition and properties, highlighting the specific modifications that enable its solubility and functionality in various applications.

Na-CMC was chosen as an alternative to gelatin in the manufacture of capsule shells because it has a lower water content value than gelatin, which gives it a longer shelf life and makes it more resistant to damage due to physical, chemical, and microorganism factors.[8] It was demonstrated that the addition of CMC binder at 2.00% and 3.00% improved pellet water stability.[9]

Plants with a high cellulose content can be used to produce Na-CMC. Some plants, such as cassava peel, are used for cellulose isolation to serve as raw materials for Na-CMC, which contains 80-85% cellulose.[10] Meanwhile, the literature indicates that Pontederia crassipes plants contain 66.87% cellulose,[11] Elaeis guineensis fibers contain 59.6% cellulose,[12] and Imperata cylindrical stems contain 44.28% cellulose.[13]

Sansevieria trifasciata is a single-seeded or monocotyledonous plant that is one of the most popular ornamental plants, and it can be used as an alternative source of cellulose.[14] It contains chemicals such as flavonoids, saponins, and tannins.[15] Among other advantages, *S. trifasciata* survives extreme conditions of temperature and light, and it is resistant to various types of pollutants. The results of research by the United States Space Agency have proven that the mother-in-law's tongue plant can reduce sick-building syndrome naturally. Room conditions are affected by pollutants due to increased concentrations of carbon dioxide gas, cigarette smoke containing nicotine, and the use of air conditioners.[16]

Based on the above description of the cellulose content of *S. trifasciata*, the researchers wanted to use the mother-in-law's tongue as an alternative raw material for capsule shells derived from cellulose.

MATERIALS AND METHODS

Tools and materials

Tools

The equipment used in this research includes Fourier Transform InfraRed (FTIR) (Perkin Elmer Frontier C90704 Version 10.6.1), Magnetic Stirrer (DLAB MS7-H550-5), Instrument Moisture Content Analyzer, oven (Memmert), hot plate (IKA HS7-C-MAG), Grinder (Miyako), 40 mesh sieve, scale (Fujika), mortar and stamper, pH paper, plastic container, filter, tea-bag, and glassware (Iwaki).

Materials

The materials used in this study were *S. trifasciata* (5 kg wet), sodium hydroxide (NaOH) (Merck), nitric acid (HNO_3) (Merck), hydrogen peroxide (H_2O_2) (Brataco), hydrochloric acid (HCl) (Merck), acetic acid 70% (Merck), isopropyl (Merck), glycerin (Brataco), sodium chloroacetate (Brand), methanol 70% (Merck), methanol absolute (Merck), ethanol (Merck), ether (Merck), aquadest (Smart Lab).

Works procedure

Sampling

The study of *S. trifasciata* leaves was carried out in Jorong Kubang Bunguk, Situjuah Batur, Situjuah Limo Nagari District, Lima Puluh Kota Regency, West Sumatra, Indonesia.

Identification of S. trifasciata

Identification of the *S. trifasciata* was carried out at the Herbarium of Biology Department of Andalas University.

Sample preparation

S. trifasciata was weighed to obtain the wet weight. Then it was washed and dried. The drying process is carried out with the help of indirect sunlight. After drying, it was reduced in size with a grinder and sieved using a 100 mesh sieve. The *S. trifasciata* powder was weighed to determine the dry weight.

Cellulose isolation

50 g of *S. trifasciata* powder was hydrolyzed using 400 mL of 4% HNO_3 at 80 °C for 2 hours on a magnetic stirrer. The sample was then filtered and bleached with 200 mL of 15% H_2O_2 at 80 °C for 1 hour. Then delignification was carried out using 200 mL of 2N NaOH at 80 °C for 1 hour,[17] and the mixture was then filtered and bleached using 200 mL of 15% H_2O_2 at 80 °C for 1 hour. Then, the samples were placed in the oven at 70 °C for 24 hours.[18]

Synthesis of Na-CMC

A total of 6 grams of *S. trifasciata* cellulose was alkaliized by adding 100 mL of isopropyl alcohol and 20 mL of 20% NaOH in a beaker and heated at 30 ˚C for 90 minutes. Six grams of sodium chloroacetate were added to the mixture, and then stirred for 3.5 hours at 70 ˚C. The mixture was filtered and neutralized with 50 mL of acetic acid, followed by rinsing with methanol, filtered again, and then oven-dried at 50 ˚C.[19]

Characterization of Na-CMC

Organoleptic

Examination organoleptic examination was carried out under the Indonesian Pharmacopoeia 3rd edition, which included an examination of shape, smell, taste, and color. The examination involved direct observation using multiple senses.

Examination of pH

One gram of Na-CMC was dissolved in 100 mL of distilled water, and then the mixture was heated at a temperature of 60 ˚C and stirred until dissolved. The heated mixture is cooled at room temperature, and then the pH is determined with a pH meter.[20]

The examination of the solubility of

Na-CMC obtained was observed for its solubility in water, ethanol, and ether.

Inspection of moisture content

The determination of water content is carried out using the gravimetric method. In the gravimetric procedure, weigh 1 gram of sample in a dish whose weight is known, and heat it in an oven at 105 ˚C for 5 hours. After that, the cup containing the sample is put in a desiccator for 15 minutes and then weighed. Repeat the weighing every 1 hour and 30 minutes until the weight remains constant.

Swelling ratio test

Measurement of the swelling of Na-CMC in water was conducted to calculate the absorption capacity expressed in the swelling ratio. Measurements were carried out using distilled water at a temperature of 22 ˚C with a tea bag as part of the process. Before immersion, the weight of the tea bag (Wo) and dry Na-CMC (W1) were measured. Then, it was immersed in distilled water, and every 10 minutes, the weight was measured (W1). Before weighing, the tea bags were hung for 15 minutes to remove the remaining water that was not absorbed by the Na-CMC.[21]

Determination of the degree of substitution (DS)

Nought point five grams of Na-CMC was added to 10 mL of 2 N HNO_3 solution, and allowed to stand for 2 hours; then filtered, and the residue was baked in an oven at 60 ˚C to dry. Samples that have been in the oven are combined with 100 mL of distilled water and 25 mL of 0.3 N NaOH solution, then titrated with 0.3 N HCl.[22]

FTIR

FTIR analysis characteristics were used to determine the functional groups of Na-CMC. The first step of this analysis is to make a pellet by mixing Na-CMC with KBr. The fibers were ground with KBr until they became homogeneous, forming a fine powder. After being homogeneous, a certain amount of the powder is taken and then inserted into the pellet-making tool. The pellet that has been formed is put into an infrared spectrometer. After all the spectra were formed, they were analyzed and matched with data from the literature.[22]

Preparation of a of capsule

Capsule shells were made by dissolving 0.78 grams of Na-CMC in aqua dest, then adding 5 grams of carrageenan, which had also been dissolved in aqua dest. Then, the capsule shell was printed using a manual mold. The molded capsule shell is allowed to dry, then removed from the mold and trimmed.

Evaluation of capsule shell

Organoleptic

Organoleptic examination was carried out using the five senses, which included examination of shape, smell, taste, and color.

Water content test

One gram of capsule shell is weighed and put in a tared container. Dry at 105 ˚C for 5 hours. Continue drying and weighing at intervals of 1 hour until the weight remains constant.[21]

RESULTS

The isolation of cellulose from *S. trifasciata* was aimed at obtaining an active compound for the synthesis of Na-CMC. The characterization was conducted based on standardization parameters, as shown in Table 1. Table 2 presents the yield

Table 1. Characterization of Na-CMC *Sansevieria trifasciata*

Parameters	Terms FI	Na-CMC
Form	Powder	Powder
Color	White or white ivory ivory	White
Odor	Odorless or almost odorless	Slightly smelly acid
Moisture content	<10%	12%

Na-CMC: Carboxymethyl cellulose

Table 2. Yield and moisture content of *Sansevieria trifasciata*

Powder of *S. trifasciata*	Cellulose	Yield	Water content
50 grams	20 grams	40%	7 %

Table 3. Yield and pH

Parameters	
Yield	pH
88.83%	6

Table 4. Swelling test results

Time	10 minutes	20 minutes	30 minutes	40 minutes	50 minutes	60 minutes
Weight	6.38 mg	7.32 mg	7.29 mg	7.69 mg	8.13 mg	8.33 mg

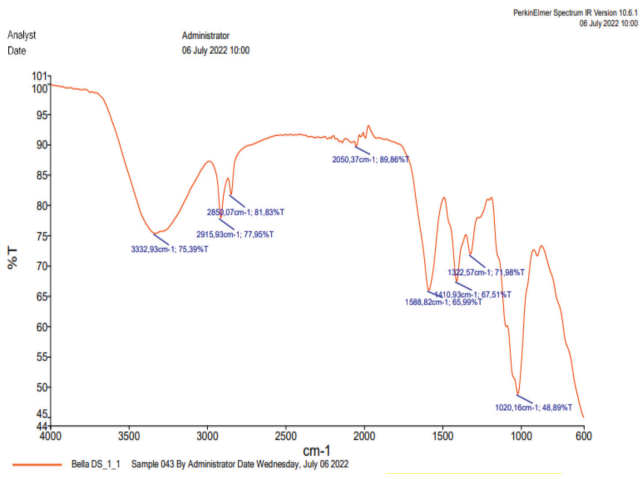

Figure 2. A spectrum of Na-CMC FTIR analysis *Sansevieria trifasciata*
Na-CMC: Carboxymethyl cellulose, FTIR: Fourier Transform InfraRed

and moisture content of cellulose, while the pH after the alkalization process is shown in Table 3. The parameter used to evaluate and calculate the adsorption capacity of Na-CMC was the swelling ratio (Table 4). The analysis of functional groups in Na-CMC was performed using IR spectroscopy that showed at Figure 2.

DISCUSSION

Cellulose isolation is the separation of cellulose and non-cellulose components such as lignin and hemicellulose.[22] The bleaching process aims to whiten the cellulose that is still brown and, at the same time, remove the remaining lignin.[18]

Alkalization is a process using NaOH 20% NaOH, aiming to activate the OH groups on the cellulose molecule. This process facilitates the development of cellulose and substitution reactions involving the sodium chloroacetate reagent. The expansion of cellulose causes the breaking of hydrogen bonds in the cellulose structure. In the alkalization stage, a substitution reaction occurs between the hydroxyl group and NaOH, which produces cellulose alkali in the form of a light brown, viscous solution. At this stage, an organic solvent is used as an inert reaction medium, where the alkalization and carboxymethylation processes can react simultaneously and can also increase the DS.[23]

The quantity of reagents employed in the carboxymethylation process has a significant impact on the quality of the Na-CMC produced.[22]

The reactions that occur in the alkalization and carboxymethylation processes are as follows:

RcellulosaOH + NaOH + ClCH2COONa → RcellulosaOCH$_2$COONa + NaCl+H$_2$O

In addition to the reaction for the formation of Na-CMC, there is also a reaction between NaOH and sodium chloroacetate to form side products, sodium glycolate, and sodium chloride, based on the reaction as follows:

NaOH + ClCH$_2$COONa → HO-CH$_2$COONa + NaCl

This reaction occurs between NaOH and ether, and the conditions of this reaction must be optimized to minimize the by-products formed.[18] Because of its strong hydrophilicity, the resultant Na-CMC water content still contains many water molecules, which may be determined by gravimetric measurements and validated by mass structure analyses.[24]

Na-CMC and glycerin can affect physical stability, as measured using a viscometer, and already comply with the Indonesian National Standard number 12-3524-1995. However, if the concentration of glycerin is reduced further, it will not significantly affect the thickness of the paste. However, if the concentration of Na-CMC is too high, it will result in poor spreadability of the toothpaste gel, which can affect other parameters such as pH and organoleptic properties.[25] The average amount of hydroxyl groups in the cellulose structure substituted by carboxymethyl or sodium carboxymethyl groups at carbons 2, 3, and 6 is referred to as the DS,[26] and is one of the parameters in determining the quality of Na-CMC. The higher the DS produced, the better the quality of Na-CMC because its solubility in water is greater. Meanwhile, the more by-products produced, the lower the quality of Na-CMC.[22] The DS obtained depends on the time and raw materials used in the synthesis process, but the value of the DS generally varies between 0.6 and 0.95[27] and ranges from 0.4 to 1.5.[24] After removing the water, the swelling test was performed until the equilibrium development value was attained, which can be estimated using the formula:[28]

$$\text{Swelling ratio} = \frac{wt - wo - w1}{w1}$$

The swelling Na-CMC can be affected by the hydrophilicity of the carboxylate groups in the hydrogel structure. Because of the limited space available for free water to enter the hydrogel network, the swelling capacity of Na-CMC is diminished. The swelling process can be initiated by the passage of water molecules through the matrix, the relaxing of polymer chains by hydration, and the expansion of the polymer network following relaxation. When Na-CMC is submerged in deionized water, the hydrophilic polymer chains generate osmotic pressure inside the hydrogel, causing the hydrogel matrix to form.[28] Functional group analysis using FTIR was carried out to prove the presence of specific functional groups in Na-CMC. Figure 2 shows a peak at a wavelength of 3332.93 cm-1, which indicates the presence of OH, so hydrogen bonding groups are formed between hydrogen atoms in one hydroxyl group in one glucose monomer and oxygen atoms from another hydroxyl group in a glucose monomer in cellulose polymer chains. The O-Na group was seen at a wavelength of 1410.93 cm-1, some clusters at a wavelength of 2915.93 cm-1, and the presence of a peak at a wavelength of 2850.07 cm-1 indicated a CH strain. At a wavelength of 1020.16 cm-1, the CO strain and the structure of the cellulose component are shown; at a wavelength of 1588.82 cm-1, the C=C group symmetrical stretch of the aromatic ring of lignin is shown.[24] Hendradi et al.'s[29] FTIR analysis revealed the production of covalent imine linkages between chitosan and

glutaraldehyde. Furthermore, adding glutaraldehyde or genipin as crosslinkers reduced the mechanical strength of the implant. The humidity of the capsule normally fluctuates between 13 and 16%. If it is stored in a relatively high-humidity environment, the humidity rises, and the stiff capsule shell becomes warped.[30] The development of hard capsules to replace gelatin in DDSs is moving forward. Hard capsules are manufactured in six basic steps: dipping, spinning, drying, stripping, trimming, and joining.[2]

CONCLUSION

After conducting basic research to identify substitute ingredients for capsule production, it was determined that Na-CMC from *S. trifasciata* could be used as a raw material. Its characteristics include a powder-like shape, a bone-white color, a strong smell, a pH of 6, a water content of 12%, and a substitution degree of 0.83. This Na-CMC from *S. trifasciata* needs to be thoroughly developed and tested by further researchers before it can be manufactured and sold as a formulation material for capsule shells, such as average molecular weight must be determined for the cellulose obtained, and compare the capsule from gelatin cost, production method, equipment used, materials, etc.

Ethics

Ethics Committee Approval: This study did not involve human subjects, animal experimentation, or the collection of personal and identifiable data.

Informed Consent: Patient consent was not applicable.

Footnotes

Authorship Contributions

Concept: A.R., Design: A.R., B.V.O., I.A.S., Data Collection or Processing: B.V.O., Analysis or Interpretation: A.R., B.V.O., Literature Search: A.R., Writing: A.R., B.V.O., I.A.S.

Conflict of Interest: The authors declare no conflicts of interest.

Financial Disclosure: The authors declared that this study received no financial support.

REFERENCES

1. Chappidi, S. R. Capsules and it 's technology : an overview. Int J Pharm Drug Anal. 2014;2:727-733.
2. Fauzi MARD, Pudjiastuti P, Wibowo AC, Hendradi E. Preparation, properties and potential of carrageenan-based hard capsules for replacing gelatine: a review. Polymers. 2021;13:2666.
3. Pudjiastuti P, Wafiroh S, Hendradi E, Darmokoesoemo H, Harsini M, Fauzi M, Nahar L, Sarker S. Disintegration, in vitro dissolution, and drug release kinetics profiles of k-Carrageenan-based nutraceutical hard-shell capsules containing salicylamide. Open Chemistry. 2020;18:226-231.
4. GMIA. Gelatin Handbook. USA: Gelatin manufacturers institute of America; 2012.
5. Che Nan, Nur Fitrah, Norhazlin Zainuddin, Mansor Ahmad. Preparation and swelling study of CMC hydrogel as potential superabsorbent. Pertanika J Sci & Technol. 2019;27:489-498.
6. Ibrahim Atef A, Adel Abeer M, Abd El-Wahab Zeinab H, Al-Shemy Mona T. Utilization of carboxymethyl cellulose based on bean hulls as chelating agent. Synthesis, characterization and biological activity. Carbohydrate Polymers. 2011;83:94-115.
7. Guo, Jian-Hwa, Skinner GW, Harcum WW, Barnum PE. Pharmaceutical applications of naturally occurring water-soluble polymers. Pharmaceutical Science & Technology Today. 1998;1:254-261.
8. Pujokaroni Agustu S, Ichiura H. Sintesis dan karakterisasi sodium karboksimetil selulosa dari serabut kelapa sawit. J Trop AgriFood. 2022;3:101.
9. Yusoff Nor A, Ihwan MZ, Jalilah MS, Rahmah S, Hassan M. Evaluation of carboxymethyl cellulose (CMC) binder and squid oil attractant in the formulation of litopenaeus vannamei diet. J Ilm Perikanan Kelautan. 2021;13:279-287.
10. Santoso Shella P, Sanjaya N, Ayucitra A. Pemanfaatan kulit singkong sebagai bahan baku pembuatan Natrium Karbosimetil Selulosa. J Teknik Kimia Indones. 2018;11:124.
11. Indriyati W, Kusmawati R, Sriwidodo S, Hasanah AN, Musfiroh I. Karakterisasi carboxymethyl cellulose sodium (Na-CMC) dari Selulosa Eceng Gondok [Eichhornia crassipes (Mart.) Solms.] yang Tumbuh di Daerah Jatinangor dan Lembang. Indones J Pharm Sci Technol. 2016;3:99.
12. Indriani Hasan A, Meydinariasty A, Sriwijaya PN. Sintesis dan karakterisasi Na-CMC dari α-selulosa serabut kelapa sawit. J Pendik dan Teknol Indones. 2021;1:375-381.
13. Nur'ain, Nur'ain, Nurhaeni N, Ridhay A. Optimasi kondisi reaksi untuk sintesis karboksimetil selulosa (Cmc) dari batang jagung (Zea Mays L.). Kovalen. 2017;3:112.
14. Wolela Asaye D. Extraction and characterization of natural cellulose fibers from sanseveria trifasciata plant. Trends Text Eng Fashion Technol. 2019;5.
15. Septiani G, Susanti S, Sucitra F. Effect of different extraction method on total flavonoid contents of Sansevieria trifasciata P. leaves extract. J Farm Galenika (e-Journal). 2021;7:143-150.
16. Kahar K, Karmini M, Kamaludin A. Ekstrak lidah mertua (Sansevieria sp.) efektif dalam mereduksi volatile organic compound (VOC)-benzena dalam ruang. J Kesehat Lingkung. 2022;19:1-6.
17. AscencioJ, Chandel AK, Philippini R, Silva SS. Comparative study of cellulosic sugars production from sugarcane bagasse after dilute nitric acid, dilute sodium hydroxide and sequential nitric acid-sodium hydroxide pretreatment. Biomass Conv Bioref. 2019;10:813-822.
18. Golbaghi L, Khamforoush M, Hatami T. Carboxymethyl cellulose production from sugarcane bagasse with steam explosion pulping: Experimental, modeling, and optimization. Carbohydr Polym. 2017;174:780-788.
19. Rahim EA, Turumi GS, Bahri S, Jusman, Syamsuddin. Pemanfaatan selulosa dari rumput gajah (Pennisetum purpureum) pada sintesis karboksimetil selulosa (CMC). Kovalen J Riset Kimia. 2021;7:146-153.
20. Adi Setyono H, Nani Heryani. Sintesis, pengujian, dan karakterisasi hidrogel berbasis sodium carboxymethyl cellulose dan chitosan. Widyariset. 2020;5:1.
21. Rahmania Fitriani J, Patihul Husni. Potensi karboksimetil selulosa (Cmc) bersumber dari tumbuhan eceng gondok [Eichhornia crassipes (Mart.) Solms] sebagai eksipien farmasi. Scientia J Farmasi 2017;7:141.
22. Mulyatno Hendrik A, Pratama OI, Inayati I. synthesis of carboxymethyl cellulose (CMC) from banana tree stem: influence of ratio of cellulose with

sodium chloroacetate to properties of carboxymethyl cellulose. Equilib J Chem Eng. 2017;1:33.

23. Jia F, Liu H-J, Zhang G-G. Preparation of carboxymethyl cellulose from corncob. Procedia Environ Sci. 2016;31:98-102.
24. Ibrahim Atef A, Adel Abeer M, El-Wahab ZH, Al-Shemy MT. Utilization of carboxymethyl cellulose based on bean hulls as chelating agent. Synthesis, characterization and biological activity. Carbohydr Polym. 2011;83:94-115.
25. Mahmoud A, Fahmy A, Naser A, Saied MA. Novel sulfonated poly(vinyl alcohol)/carboxy methyl cellulose/acrylamide-based hybrid polyelectrolyte membranes. Sci Rep. 2022;12:22017.
26. Alizadeh Asl Saeid, Mousavi M, Labbafi M. Synthesis and characterization of carboxymethyl cellulose from sugarcane bagasse. J Food Process Technol. 2017;8
27. Maulina Z, An A, Rihayat T. Pengaruh variasi konsentrasi naoh dan berat natrium monokloroasetat pada pembuatan (carboxymethyl cellulose) Cmc dari serat daun nenas (pineapple-leaf fibres). J Sains Teknol Reaksi. 2019;17.
28. Sulta N, Zainuddin N, Ahmad MB, Masarudin J. Preparation, characterization and swelling studies of carboxymethyl sago starch hydrogel. 2019.
29. Hendradi E, Hariyadi DM, Adrianto MF. The effect of two different crosslinkers on in vitro characteristics of ciprofloxacin-loaded chitosan implants. Res Pharm Sci. 2018;13:38-46.
30. Rasool Hassan, Bassam A. Overview on pharmaceutical formulation and drug design. Pharm Anal Acta. 2012;3:10.

Turk J Pharm Sci 2025;22(2):83-90
DOI: 10.4274/tjps.galenos.2025.44902

ORIGINAL ARTICLE

Integrating a Pharmacovigilance and Response Unit Team for a Better Adverse Drug Reaction Reporting and Management: Insights from a Prospective Cross-Sectional Study

Vinodkumar MUGADA[1]*, Satya Sai Srinivas ALLADA[1], Chaitanya RVS KOPPALA[2], Srinivasa Rao YARGUNTLA[3]

[1]Vignan Institute of Pharmaceutical Technology, Department of Pharmacy Practice, Duvvada, India
[2]Vignan Institute of Pharmaceutical Technology, Department of Pharmacology, Duvvada, India
[3]Vignan Institute of Pharmaceutical Technology, Department of Pharmaceutics, Duvvada, India

ABSTRACT

Objectives: The multidisciplinary team approach improves adverse drug reaction (ADR) reporting and management. Our study aims to integrate a pharmacovigilance (PV) and Response Team within the general medicine department to improve ADR reporting and management.

Materials and Methods: We conducted a prospective cross-sectional study for seven months in four general medicine wards. We proposed a PV and response unit team (PRUT), comprising a nursing student, and a Doctor of Pharmacy (intern). After the team received interventional educational training, we integrated them with the physician and head nurse of each general medicine inpatient ward. We then evaluated the effectiveness of the team in ADR reporting and management using a feedback survey.

Results: In this study, comorbidities (30.69%) and polypharmacy (≥5 drugs) (26.25%) were major predisposing factors. Among drug-related problems in 125 patients, inappropriate drug use (28.80%) and unclear dose timing (21.60%) were predominant. Gastrointestinal disorders were common (44.73%), with dose adjustment being the top management strategy (36.84%). Over 71% supported the PRUT for improving patient safety and reducing medication errors, noting high effectiveness in consultation (85.92%) and in reducing the ADR reporting burden (87.32%). There is a statistically significant association between the level of agreement on the effectiveness of PRUT among healthcare professionals ($p<0.01$). Most healthcare professionals agreed on PRUT's effectiveness without any reports of low agreement levels.

Conclusion: The PRUT effectively reported and managed ADRs. A multidisciplinary approach improves ADR reporting and management.

Keywords: Adverse drug reaction, pharmacovigilance, inappropriate drug use, dose adjustment, polypharmacy, pharmacovigilance, and response unit team

INTRODUCTION

Adverse drug reaction (ADR) management is crucial in reducing patient morbidity, minimizing healthcare costs, and improving the quality of medical care. Initiatives for ADR monitoring and reporting are instrumental in protecting patient safety by providing essential insights into drug efficacy and safety, initiating risk management strategies, and quantifying ADR occurrences.[1, 2] The primary responsibility of detecting, documenting, and reporting ADRs falls upon healthcare professionals (HCPs) -namely medical doctors, nurses, and pharmacists.

***Correspondence:** viptpharmd@gmail.com, **ORCID-ID:** orcid.org/0000-0002-9364-9874
Received: 14.02.2024, **Accepted:** 07.02.2025 **Publication Date:** 14.05.2025

Cite this article as: MUGADA V, ALLADA SSS, RVS KOPPALA C, YARGUNTLA SR. Integrating a pharmacovigilance and response unit team for a better adverse drug reaction reporting and management: Insights from a prospective cross-sectional study. Turk J Pharm Sci. 2025;22(2):83-90

Their vigilance in daily practices is crucial for ADR prevention, as research suggests that adherence to current medical protocols and the evaluation of potential ADR risk factors could significantly reduce ADR incidences.[3]

Risk communication, a cornerstone of ADR management, involves educating patients, their families, and healthcare colleagues about the dangers of specific medications, aiming to reduce exposure to potential adverse drug effects. Despite its significance, studies highlight a gap in effectively communicating medication-related risks to patients at the time of discharge. This represents a crucial area that needs improvement in ADR communication strategies.[4] This observation highlights the important need for improved risk communication methods to strengthen patient safety and care standards.

In response to such challenges, a Dutch study explored the feasibility and impact of integrating Junior-Adverse Drug Event Managers (J-ADEMs), comprising medical students, within hospital settings to supervise and report ADRs. The findings indicated that the J-ADEM framework effectively enhances ADR detection and management, supports physicians in reporting tasks, and provides students with helpful pharmacovigilance (PV) expertise.[5]

Furthermore, extensive research in India has thoroughly reported ADR patterns, severities, causality, and organ-specific impacts, highlighting the importance of such studies.[6,7] However, the integration of specialized ADR management teams within the Indian healthcare context remains unexplored. Our study aims to fill this gap by evaluating the practicality and efficacy of a multidisciplinary ADR management team within a general medicine inpatient department. This innovative approach seeks to strengthen patient safety and elevate the standard of care through refined ADR management and reporting protocols.

MATERIALS AND METHODS

Study setting and duration

The study was conducted in four in-patient departments of General Medicine for a duration of seven months (01/04/2023 to 30/11/2023).

Study participants

Third-year Nursing students and sixth-year Doctor of Pharmacy internship students.

Sampling technique

We employed the judgmental sampling technique because it helps to select participants with expertise or characteristics that are important to the research study.[8]

PV and Response Unit Team (PRUT)

The PRUT team contains a nursing student and a Pharm.D intern. The Pharm.D intern must spend six months in the general medicine department, while nursing students will visit the hospital regularly as part of the curriculum. The competent team coordinates with the attending physician and the head nurse of the respective general medicine inpatient wards. The primary responsibility of the nursing student is to collect the best possible patient medication history and to update the intern and physician on clinical and objective measures. The primary responsibility of the Pharm.D intern is to evaluate the predisposing factors of ADRs and to conduct prescription auditing.

If the Pharm.D intern finds any medication errors and drug therapy problems, then these issues will be communicated to the nursing student and physician. If the team observes any ADR, they will inform the physician and report it on the ADR form recommended by the PV Programme of India (PvPI). In case of any discrepancy in filling out the ADR form, they will contact the PV associate in the nearby ADR Monitoring Center to clarify it. The team, with the help of the physician, will prepare a management plan and implement it effectively.

Educational training for the team

We adapted and developed an educational training module for the team from previous studies.[9,10] The training was carried out for four weeks, and each module included a 45-minute lecture. We covered the basics of PV, ADR reporting, case-report-based ADR reporting, identifying predisposing factors, taking the best possible medication history, and a real-life practical demonstration. We then estimated the knowledge and competency of the students using a questionnaire, which contained a few multiple-choice questions, fill-in-the-blank answers, and one case study.

PRUT impact survey

We framed a predetermined questionnaire with 10 statements to evaluate the impact of PRUT on patient safety, PV, and healthcare practice. The statements covered the effectiveness of the PRUT in improving ADR reporting, the role of collaboration among HCPs, the reduction in medication errors, the importance of prescription audits, the understanding of PV, proactive patient safety measures, the quality of ADR surveillance, the effectiveness of consultations for validating ADRs, the impact on ADR reporting burden, and the overall necessity of the PRUT in healthcare. We used a three-point Likert scale for each response, with a score of 3 for "Agree," a score of 2 for "Neutral," and a score of 1 for "Disagree." The maximum score was 30, whereas the minimum score was 10. Scores ranging from 25 to 30 indicate a high level of agreement with the effectiveness and importance of the PRUT, whereas a score between 16 and 24 represents a moderate level of agreement, and a score of 10 to 15 indicates a low level of agreement.

Validity and reliability of the survey questionnaire

We assessed the content validity of the questionnaire by involving one PV associate and a physician specialized in pharmacology. Each expert evaluated whether the statements accurately reflected the constructs of interest. They rated the relevance of each statement on a 4-point scale, where 1 represented "not relevant" and 4 indicated "highly relevant." After both experts completed their evaluations, we calculated the Content Validity Index (CVI), following the guidelines of Polit and Beck.[11] We considered statements with a CVI of 0.80 or higher to be acceptable, indicating that they were relevant and

valid for assessing the impact of the PRUT on patient safety, PV, and healthcare practice.

Given that Streiner[12] recommends a minimum sample size of 30 for a reliable estimate of Cronbach's alpha, we conducted a pilot test with 30 HCPs. We then used Cronbach's alpha to assess the internal consistency of the questionnaire and obtained a value of 0.85, indicating strong internal consistency among the items. This result confirmed that the questionnaire reliably measured the intended constructs.

Pharmaceutical Care Network Europe (PCNE) classification of drug-related problems (DRPs)

We used the PCNE classification of DRPs in our study.[13] The classification contains three primary domains for problems, nine primary domains for causes, and five primary domains for interventions. It also contains the acceptance of the intervention proposals and the status of DRP.

Study procedure

Initially, we explained the aim and objectives of our study to nursing students and Pharm.D interns and identified the interested candidates. Fourteen nursing students and 18 Pharm.D intern students were willing to participate. We then screened their preliminary knowledge of PV with a questionnaire containing a few multiple-choice questions. Post-screening, we started a four-week educational training module for these students. After the educational training module, 12 out of 14 nursing students and 13 out of 18 Pharm.D interns were eligible to form a team (PRUT). We then divided them into pairs, consisting of one nursing intern and one Pharm.D intern, for each general medicine inpatient ward. Additional nursing students and Pharm.D interns were also used when required (Figure 1). To carry out their primary roles and responsibilities, we introduced the new team to the head nurse and attending physician in the respective wards.

Statistical analysis

Socio-demographic details, including age, gender, comorbidities, smoking and alcohol history, and clinical details, including past medical history, previous drug allergies, drug-related problems, previous and current ADRs, and predisposing factors for ADRs, were collected. Feedback on the impact of PRUT from physicians and nurses was also gathered. The qualitative data were represented as frequencies and percentages, whereas the quantitative data were represented as means and standard deviations where appropriate. The chi-square test was used to assess the association between the HCPs level of agreement on the effectiveness of PRUT. A p value <0.05 was considered statistically significant. Jeffrey's Amazing Statistical Programme (version 0.18.3) was used for statistical analysis.

Ethical approval

The study was approved by the Vignan Institute of Pharmaceutical Technology Ethical Committee (approval number: VIPT/IEC/359/2023, date: 28.03.2023). We obtained written informed consent from the participants who were willing to participate. We assured the participants of the confidentiality of the data.

RESULTS

Table 1 outlines the socio-demographic details of the patients (n=358). The majority of patients fall between 56 and 70 years of age group (37.7%), followed by those in the age group 41-55 years (24.68%). Males are more predominant (58.38%) than females. The most common comorbidities in our study were hypertension (26.7%) and diabetes mellitus (23.99%). Among 101 patients who reported ADRs, nausea and vomiting were the most frequent (32.67%), followed by severe itching (20.79%). Pantoprazole (32.48%) was the most frequently prescribed past medication, followed by metformin and glimepiride (18.98%).

Table 2 highlights the identified predisposing factors (n=720) among the patients. The most common predisposing factor was comorbidity (30.69%), followed by polypharmacy (26.25%) and age (18.47%). As illustrated in Table 3, the most common drug-related problem identified among the patients in our study was an inappropriate drug (28.80%), followed by unclear timing or omission of dose instructions (21.60%), and unavailability of the prescribed drug (18.40%).

Table 4 summarises the ADRs (n=76) identified among the patients. Gastrointestinal disorders are the most commonly reported ADRs, occurring in 44.73% of the patients. Dermatological reactions, including skin rash and itching, are the second most frequent, affecting 34.21% of patients. Respiratory system-related ADRs, such as dry cough and breathlessness, are observed in 14.47% of cases, while musculoskeletal reactions, including myalgia and pedal edema, are reported in 6.58% of patients. The most frequently employed management strategy was dose adjustment (36.84%), followed by symptomatic treatment (15.79%) and withdrawal of the offending drug (15.79%) (Table 5).

Table 6 outlines the impact of PRUT survey results conducted among 41 healthcare professionals. A significant majority (87.8%) observed an improvement in ADR surveillance since its implementation. Additionally, 85.3% agreed that the consultation process within the PRUT is effective in assessing the severity and validity of suspected ADRs, and the same percentage

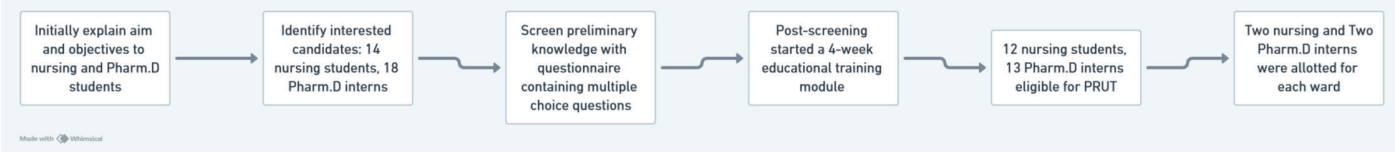

Figure 1. Study procedure for selecting the eligible participants for including in PRUT

PRUT: Pharmacovigilance and response unit team

Table 1. Socio-demographic and clinical details of the patients (n=358)

S. no.	Characteristic	Frequency (%)
1	**Age (in years)**	
	<10	05 (1.39)
	11-25	34 (9.49)
	26-40	51 (14.24)
	41-55	89 (24.86)
	56-70	135 (37.70)
	>70	44 (12.29)
2	**Gender**	
	Male	209 (58.38)
	Female	149 (41.62)
3	**Comorbidities (n=221)**	
	Gastrointestinal disorders	18 (8.14)
	Musculoskeletal disorders	19 (8.60)
	Thyroid disorders	21 (9.50)
	More than two comorbidities	51 (23.07)
	Diabetes mellitus	53 (23.99)
	Hypertension	59 (26.70)
4	**Previous drug allergies (n=7)**	
	Diclofenac	4 (57.14)
	Cefixime	3 (42.86)
5	**Previous drug related ADRs (n=101)**	
	Stevens Johnson syndrome	2 (1.98)
	Weight gain	8 (7.92)
	Weakness/fatigue	9 (8.91)
	Injection site reaction	10 (9.90)
	Skin rash	18 (17.82)
	Severe itching	21 (20.79)
	Nausea and vomiting	33 (32.67)
6	**Past medications (n=274)**	
	Nifedipine	12 (4.38)
	Levothyroxine	16 (5.84)
	Amlodipine	19 (6.93)
	Ibuprofen	19 (6.93)
	Aceclofenac and paracetamol	28 (10.22)
	Metoprolol	39 (14.23)
	Metformin and glimepiride	52 (18.98)
	Pantoprazole	89 (32.48)

S. no.: Serial number, ADRs: Adverse drug reactions

considered the PRUT an essential component of healthcare for ensuring drug safety and efficacy. Most respondents (82.9%) also emphasized the importance of pharmacists' role in prescription audits and acknowledged the PRUT's contribution to proactive patient safety by categorizing patients based on their ADR predisposition. Overall, the feedback highlights strong support (85.3%) for PRUT's positive impact on patient care and safety. However, a chi-square test for independence showed that there was no significant association between the profession and level of agreement on PRUT team effectiveness (p=0.40). The chi-square test and survey both show that physicians and nurses largely agree on the effectiveness of PRUT. There are no significant differences in their perceptions, with both groups consistently expressing high agreement on PRUT's positive impact in areas like patient safety and ADR reporting.

DISCUSSION

We observed alignment with findings on common predisposing factors in two studies.[14,15] In contrast, one study highlighted polypharmacy as the predominant predisposing factor.[16] As people age, the occurrence of comorbid conditions increases, leading to the need for multiple medications, a situation known as polypharmacy. Advanced age is associated with changes in the body that affect how drugs are processed, increasing the risk of ADRs. These changes include reduced heart function, lower kidney filtration, and smaller liver size, which impact how drugs are absorbed, metabolized, distributed, and eliminated from the body.[17]

When individuals have multiple health conditions at the same time, the overall effectiveness of treatments often does not

Table 2. Predisposing factors identified among the patients (n=720)

S. no.	Predisposing factor	Frequency (%)
1	Impaired/abnormal liver function	37 (5.14)
2	Impaired/abnormal renal function	39 (5.42)
3	Previous drug related ADR	101 (14.03)
4	Age	133 (18.47)
5	Polypharmacy (≥5 drugs)	189 (26.25)
6	Comorbidities	221 (30.69)

S. no.: Serial number, ADR: Adverse drug reaction

Table 3. ADRs identified among the patients (n=125)

S. no.	Drug related problem	Frequency (%)
1	No indication for drug	09 (7.20)
2	Inappropriate combination of drugs	13 (10.40)
3	Dosage regimen not frequent enough	17 (13.60)
4	Prescribed drug not available	23 (18.40)
5	Dose timing instructions unclear or missing	27 (21.60)
6	Inappropriate drug	36 (28.80)

S. no.: Serial number, ADRs: Adverse drug reactions

Table 4. Adverse drug reactions identified among the patients (n=76)

S. no.	Organ system	Adverse drug reaction	Frequency (%)
1	Musculoskeletal	Myalgia (2), pedal edema (3)	05 (6.58%)
2	Respiratory	Dry cough (8), breathlessness (3)	11 (14.47)
3	Dermatology	Skin rash (8), itching all over the body (3), itching over hands (2), erythema (5), pruritis (4), fixed drug eruption (2), and urticaria (2)	26 (34.21)
4	Gastrointestinal Disorders	Nausea and vomiting (12), abdominal discomfort (3), abdominal pain (4), diarrhea (5), and constipation (5), and gastritis (8)	34 (44.73)

S. no.: Serial number

Table 5. Management strategies for ADRs

S. no.	Management strategy	Frequency (%)
1	Preventive measures	07 (9.21%)
2	Monitoring and supportive care	08 (10.52)
3	Switching medications	09 (11.84)
4	Withdrawal of the offending drug	12 (15.79)
5	Symptomatic treatment	12 (15.79)
6	Dose adjustment	28 (36.84)

S. no.: Serial number, ADRs: Adverse drug reactions

Table 6. Feedback survey of physician and nurse perceptions on the effectiveness of PRUT (n=41)

S. no.	Question	Agree n (%)	Disagree n (%)	Neutral n (%)
1	Do you believe that the PRUT enhances patient safety by improving ADR reporting?	33 (80.5)	5 (12.2)	3 (7.3)
2	Do you agree that the collaboration between physicians, pharmacists, nurses, and PV associates in the PRUT leads to more comprehensive patient care?	32 (78)	5 (12.2)	4 (9.8)
3	Have you found that the PRUT's efforts have led to a noticeable reduction in medication errors in your practice?	33 (80.5)	5 (12.2)	3 (7.3)
4	Is the pharmacist's role in conducting prescription audits crucial for identifying potential drug interactions and incorrect dosages?	34 (82.9)	4 (9.8)	3 (7.3)
5	Have the PRUT's activities improved your understanding of PV and its importance in clinical practice?	31 (75.6)	4 (9.8)	6 (14.6)
6	Do you agree that the PRUT promotes a proactive approach in patient safety by categorizing patients based on their predisposition to ADRs?	34 (82.9)	3 (7.3)	4 (9.8)
7	Have you observed an improvement in the quality of ADR surveillance since the implementation of the PRUT in your facility?	36 (87.8)	3 (7.3)	2 (4.9)
8	Is the consultation process with the physician and nurses within the PRUT effective in validating the severity and validity of suspected ADRs?	35 (85.3)	4 (9.8)	2 (4.9)
9	Do you agree that the PRUT significantly decreases the burden of ADR reporting and management for nurses and physicians, allowing them to focus more on patient care?	33 (80.5)	5 (12.2)	3 (7.3)
10	Overall, do you believe that the PRUT is an essential component of the healthcare system for ensuring drug safety and efficacy?	35 (85.3)	4 (9.8)	2 (4.9)

S. no.: Serial number, PRUT: Pharmacovigilance and response unit team, ADR: Adverse drug reaction, PV: Pharmacovigilance

meet expectations. As people age, treatments also tend to be less effective. Polypharmacy, the use of multiple medications, poses a major challenge in clinical practice because it can cause drug interactions that reduce the effectiveness of treatments. Even though each medication is prescribed to treat a specific condition, using many drugs together can complicate the patient's health outcomes due to such interactions.[18] This situation emphasizes the importance of careful monitoring and evaluation of all prescribed medications by HCPs. Such oversight is necessary to balance the benefits of each drug against the risks of polypharmacy.

The team identified 125 drug therapy problems in total. The most common issue was the prescription of inappropriate drugs, which made up 28.80% of the problems. This was followed by unclear or missing dose timing instructions (21.60%) and the unavailability of prescribed drugs (18.40%). These findings are consistent with previous research, where three studies, numbered 19-21, also reported inappropriate drug prescriptions as the most frequent drug therapy problem.

The prescription of inappropriate drugs in public hospitals may stem from several factors. These include limited access to updated drug information, high patient-to-physician ratios that lead to rushed clinical decisions, and the absence of standardized treatment protocols. Additionally, a lack of adequate training on current pharmacotherapy guidelines among HCPs contributes to this issue. Donnenberg et al.[22] emphasize the need for improving prescribing skills and integrating clinical pharmacology education into medical training.

The team identified a significant gap in the physicians' knowledge regarding established guidelines for prescribing potentially inappropriate medications to the elderly, such as the Screening Tool of Older Person's Prescriptions criteria and the American Geriatrics Society Beers criteria. One clear example of this was the prescription of glimepiride to elderly patients. Glimepiride is generally not recommended for older adults due to the increased risk of prolonged hypoglycemia, a serious condition.[23] Despite this, the PRUT team found instances where glimepiride had been prescribed to elderly patients.

In this study, gastrointestinal-related ADRs were the most common, accounting for 44.73%, followed by dermatological reactions at 34.21%. This result is consistent with the findings of Singh et al.[24], who reported a similar pattern. However, two other studies identified dermatological reactions as the most frequent ADRs.[25,26]

The prevalence of ADRs is closely related to the presence of specific diseases within a patient group and the medications used to treat them. For example, in the general medicine department involved in this study, many patients were treated with drugs known for causing gastrointestinal side effects, such as non-steroidal anti-inflammatory drugs commonly used for pain management. This may explain the higher reporting of gastrointestinal-related ADRs in these cases.[27] On the other hand, the increased use of medications like antibiotics and antiepileptics, which are often associated with dermatological reactions, points to a different pattern of ADR prevalence, as noted by two studies.[28,29] Elderly patients with multiple comorbidities are especially vulnerable to gastrointestinal complications, which can be linked to the challenges of polypharmacy and the use of drugs affecting the gastrointestinal system.

In this study, dose adjustment was the most frequently used strategy for managing ADRs, accounting for 36.84% of cases. This finding differs from two studies 7; 28, which found that adding another medication or discontinuing the offending drug was a more common approach for managing ADRs. This variation highlights the different management strategies that can be used in specific clinical contexts. Dose adjustment is crucial in managing ADRs. Jiang et al.[30] emphasized that modifying the dosing regimen or discontinuing the suspected drug is a common approach in clinical practice. Precision dosing, which considers patient-specific factors and biomarkers, can help prevent ADRs.[31] However, healthcare providers must have access to detailed dosage information, especially regarding lower effective doses, to make informed dose adjustments and reduce ADR occurrence.[32]

The positive response observed in this study may be due to a reduced burden on physicians, who often face time constraints because of their demanding patient care duties. Gupta et al.[33] found that 73% of physicians cited time constraints as a major reason for underreporting ADRs. Other contributing factors to underreporting included limited awareness of reporting protocols, reluctance to report known reactions, and fear of legal consequences.[33] Mwakawanga et al.[34] also reported that fewer HCPs) participated in ADR reporting, viewing the process as difficult, time-consuming, and unnecessary for every ADR. In contrast, the PRUT team in this study successfully addressed these issues by reporting 76 ADRs, highlighting the value of a multidisciplinary approach to PV.

The effectiveness of a team approach involving medical students was demonstrated by Reumerman et al.,[5] who created the JJ-ADEM team. This group of medical students (from 1st to 6th year) was responsible for reporting and managing ADRs in inpatients. The J-ADEM approach proved beneficial, as physicians were supported in ADR reporting, patients received better care, and students gained valuable PV experience.

Patidar et al.[35] involved physicians, pharmacists, and nurses in spontaneous reporting method where they actively searched for suspected ADRs. A passive method also encouraged prescribers to report any suspected ADRs. All physicians were briefed on the study and the harmful effects of ADRs, which led to increased reporting. Reminders were regularly sent to ensure consistent reporting throughout the study.[35] This setting differs from the current study's environment, which is a 35-bed internal medicine ward in a private hospital. The previous study was conducted in an 800-bed public hospital with four general medicine wards, each with an average capacity of 15 beds, where physicians managed both inpatient and outpatient care. PV sensitization efforts, such as lectures, workshops, and induction programs, had a positive impact on ADR reporting.[36] These programs improved the completeness of ADR forms

between 2018 and 2020. However, no such programs have been conducted in the current hospital for the past five years.[36]

Study limitations

The study has several limitations. The region where the study was conducted, which is home to over 150 pharmacy colleges and 250 nursing colleges, offers easy access to a large pool of students. This advantage may not be present in other regions. Both the Doctor of Pharmacy and the new Bachelor of Pharmacy curricula have now incorporated PV concepts. To further improve ADR reporting, it would be beneficial to include a mandatory two-month PV training at a nearby public hospital as part of the Bachelor of Pharmacy curriculum. Other limitations include the small sample size and the limited generalizability of the findings. Furthermore, the lack of baseline data on medication errors, drug therapy problems, and ADR reports required the study to rely on feedback surveys to evaluate the effectiveness of the PRUT.

CONCLUSION

The PRUT effectively reported and managed the ADRs. Most physicians and nurses also had a high level of agreement on the effectiveness of this team. Incorporating mandatory PV activities for nursing and pharmacy students in nearby public hospitals can improve the reporting and management of ADRs.

Ethics

Ethics Committee Approval: The study was approved by the Vignan Institute of Pharmaceutical Technology Ethical Committee (approval number: VIPT/IEC/359/2023, date: 28.03.2023).

Informed Consent: Informed consent was obtained.

Acknowledgment

We are grateful to the principal and management of Vignan Institute of Pharmaceutical Technology and the enthusiastic students who participated and cooperated till the end of the study. We are also grateful to the physicians and head nurses for their cooperation and active participation.

Footnotes

Authorship Contributions

Concept: V.K.M., Design: V.K.M., S.R.Y., Data Collection or Processing: V.K.M., S.S.S.A., C.R.V.S.K., Analysis or Interpretation: V.K.M., S.S.S.A., C.R.V.S.K., S.R.Y., Literature Search: V.K.M., S.S.S.A., C.R.V.S.K., S.R.Y., Writing: V.K.M., S.S.S.A., C.R.V.S.K., S.R.Y.

Conflict of Interest: The authors declare no conflicts of interest.

Financial Disclosure: The authors declared that this study received no financial support.

REFERENCES

1. Wolfe D, Yazdi F, Kanji S, Burry L, Beck A, Butler C, Esmaeilisaraji L, Hamel C, Hersi M, Skidmore B, Moher D, Hutton B. Incidence, causes, and consequences of preventable adverse drug reactions occurring in inpatients: a systematic review of systematic reviews. PLoS One. 2018;13:e0205426.
2. Sahu RK, Yadav R, Prasad P, Roy A, Chandrakar S. Adverse drug reactions monitoring: prospects and impending challenges for pharmacovigilance. Springerplus. 2014;3:695.
3. O'Donnell C, Demler TL, Dzierba C. Perceptions and barriers of adverse drug reaction reporting within inpatient state psychiatric facilities. Ment Health Clin. 2022;12:247-253.
4. Graudins LV, Ly J, Trubiano J, Aung AK. More than skin deep. Ten year follow-up of delayed cutaneous adverse drug reactions (CADR). Br J Clin Pharmacol. 2016;82:1040-1047.
5. Reumerman M, Tichelaar J, Richir MC, van Agtmael MA. Medical students as adverse drug event managers, learning about side effects while improving their reporting in clinical practice. Naunyn Schmiedebergs Arch Pharmacol. 2021;394:1467-1476.
6. Valder BK, Neelamma P, Nalini GK, Sahana G. A study to assess, monitor, and reporting of adverse drug reactions in a tertiary care teaching hospital: HIMS, HASSAN. Asian J Pharm Clin Res. 2023;16:201-203.
7. Venkatasubbaiah M, Dwarakanadha Reddy P, Satyanarayana SV. Analysis and reporting of adverse drug reactions at a tertiary care teaching hospital. Alexandria J Med. 2018;54:597-603.
8. Campbell S, Greenwood M, Prior S, Shearer T, Walkem K, Young S, Bywaters D, Walker K. Purposive sampling: complex or simple? Research case examples. J Res Nurs. 2020;25:652-661.
9. Herrera Comoglio R. Undergraduate and postgraduate pharmacovigilance education: a proposal for appropriate curriculum content. Br J Clin Pharmacol. 2020;86:779-790.
10. Pagotto C, Varallo F, Mastroianni P. Impact of educational interventions on adverse drug events reporting. Int J Technol Assess Health Care. 2013;29:410-417.
11. Polit DF, Beck CT. The content validity index: are you sure you know what's being reported? Critique and recommendations. Res Nurs Health. 2006;29:489-497.
12. Streiner DL. Starting at the beginning: an introduction to coefficient alpha and internal consistency. J Pers Assess. 2003;80:99-103.
13. Pharmaceutical Care Network Europe. Working groups item detail [Internet]. Pcne.org; [cited 2024 Aug 30]. Available from: https://www.pcne.org/working-groups/2/drug-related-problem-classification/10.
14. Sriram S, Ghasemi A, Ramasamy R, Devi M, Balasubramanian R, Ravi TK, Sabzghabaee AM. Prevalence of adverse drug reactions at a private tertiary care hospital in South India. J Res Med Sci. 2011;16:16-25.
15. Haile DB, Ayen WY, Tiwari P. Prevalence and assessment of factors contributing to adverse drug reactions in wards of a tertiary care hospital, India. Ethiop J Health Sci. 2013;23:39-48.
16. Kuruvilla A. PDG30 A study on adverse drug reaction related hospital admissions of a tertiary care hospital in South India. Value Health. 2021;24(Suppl 1):S92.
17. Sychev DA, Ostroumova OD, Pereverzev AP, Kochetkov AI, Ostroumova TM, Klepikova MV, Ebzeeva EY. Advanced age as a risk factor of drug-induced diseases. Safety and Risk of Pharmacotherapy. 2021;9:15-24.
18. Fitzgerald SP, Bean NG. An analysis of the interactions between individual comorbidities and their treatments-implications for guidelines and polypharmacy. J Am Med Dir Assoc. 2010;11:475-484.

19. Movva R, Jampani A, Nathani J, Pinnamaneni SH, Challa SR. A prospective study of incidence of medication-related problems in general medicine ward of a tertiary care hospital. J Adv Pharm Technol Res. 2015;6:190-194.

20. Kumar MV, Pasha MM, Varshith G, Pravalika B, Shameela M. Drug related problems ıdentified by clinical pharmacist in a tertiary care hospital in South India: an observational study. Indian J Pharm Pract. 2022;15:198-204.

21. Anshila MK, Nambiar PD, Augustine VD, Saseendran M, Shabraya AR, Siva S. Evaluation of drug related problems in patients with chronic disease at tertiary care teaching hospital. Int J Health Sci Res. 2020;10:144-155.

22. Donnenberg VS, Burris JF, Wiernik PH, Cohen LJ, Korth-Bradley JM. How to fix the dangerous lack of clinical pharmacology education in the medical profession: the generation of core entrustable professional activities in clinical pharmacology for entering residency. J Clin Pharmacol. 2016;56:1177-1179.

23. O'Mahony D, Cherubini A, Guiteras AR, Denkinger M, Beuscart JB, Onder G, Gudmundsson A, Cruz-Jentoft AJ, Knol W, Bahat G, van der Velde N, Petrovic M, Curtin D. STOPP/START criteria for potentially inappropriate prescribing in older people: version 3. Eur Geriatr Med. 2023;14:625-632.

24. Singh H, Dulhani N, Kumar B, Singh P, Tewari P, Nayak K. A pharmacovigilance study in medicine department of tertiary care hospital in Chhattisgarh (Jagdalpur), India. J Young Pharm. 2010;2:95-100.

25. Lihite RJ, Lahkar M, Das S, Hazarika D, Kotni M, Maqbool M, Phukan S. A study on adverse drug reactions in a tertiary care hospital of Northeast India. Alexandria J Med. 2017;53:151–156.

26. James J, Rani J. A prospective study of adverse drug reactions in a tertiary care hospital in South India. Asian J Pharm Clin Res. 2020;13:89-92.

27. Singh G, Triadafilopoulos G. Epidemiology of NSAID induced gastrointestinal complications. J Rheumatol Suppl. 1999;56:18-24.

28. Lobo MG, Pinheiro SM, Castro JG, Momenté VG, Pranchevicius MC. Adverse drug reaction monitoring: support for pharmacovigilance at a tertiary care hospital in Northern Brazil. BMC Pharmacol Toxicol. 2013;14:5.

29. Coleman JJ, Pontefract SK. Adverse drug reactions. Clin Med (Lond). 2016;16:481- 485.

30. Jiang H, Lin Y, Ren W, Fang Z, Liu Y, Tan X, Lv X, Zhang N. Adverse drug reactions and correlations with drug-drug interactions: a retrospective study of reports from 2011 to 2020. Front. Pharmacol. 2022;13:1-14.

31. Polasek TM, Kirkpatrick CMJ, Rostami-Hodjegan A. Precision dosing to avoid adverse drug reactions. Ther Adv Drug Saf. 2019;10:2042098619894147.

32. Cohen JS. Dose discrepancies between the Physicians' Desk Reference and the medical literature, and their possible role in the high incidence of dose-related adverse drug events. Arch Intern Med. 2001;161:957-964.

33. Gupta R, Malhotra A, Malhotra P. A study on determinants of underreporting of adverse drug reactions among resident doctors. Int J Res Med Sci. 2018;6:623-627.

34. Mwakawanga DL, Kilonzi M, Philipo EG, Martine A, Mbilinyi T, Kileo NF, Mkinga B, Shonyella CJ, Mohamedi JA, Clement A, Mwasomola D, Mushy SE, Sirili N. Pharmacovigilance and adverse drug reactions reporting: healthcare providers' experiences from southern highland Tanzania. Adv Pharmacol Pharm Sci. 2023;2023:5537592.

35. Patidar D, Rajput MS, Nirmal NP, Savitri W. Implementation and evaluation of adverse drug reaction monitoring system in a tertiary care teaching hospital in Mumbai, India. Interdiscip Toxicol. 2013;6:41-46.

36. Thakare V, Patil A, Jain M, Rai V, Langade D. Adverse drug reactions reporting: five years analysis from a teaching hospital. J Family Med Prim Care. 2022;11:7316-7321.

Turk J Pharm Sci 2025;22(2):91-103
DOI: 10.4274/tjps.galenos.2025.66350

ORIGINAL ARTICLE

Formulation and Optimization of Pyrazinamide-Loaded Solid Lipid Nanoparticles by Employing a Design of Experiments Approach

Nimitt CHOKSHI, Preksha VINCHHI, Shreyansh CHAUHAN, Mayur PATEL*

Nirma University Institute of Pharmacy, Department of Pharmaceutics, Gujarat, India

ABSTRACT

Objectives: Tuberculosis (TB) remains a major worldwide health challenge causing morbidity and mortality, necessitating novel approaches for its effective therapy. Pyrazinamide (PYZ), a nicotinamide analogue, is a key frontline drug significantly involved in the treatment of TB. However, its dose-dependent hepatotoxicity is a major concern that needs to be addressed. The aim of the current research was to develop PYZ-loaded solid lipid nanoparticles (PYZ-SLNs) as a potential therapeutic intervention for treating TB.

Materials and Methods: The PYZ-SLNs were formulated by a high-pressure homogenization technique and optimized using a 23-factorial design. The drug concentration, emulsifier concentration, and homogenization cycles were considered critical formulation and processing parameters to study their effects on essential attributes of quality of PYZ-SLNs, i.e., entrapment efficiency (EE%), drug loading (DL%), and particle size.

Results: The optimized PYZ-SLNs showed a particle size of 401±08 nm, EE% of 86.24±1.15, DL% of 14.38±0.85. The *in vitro* lipolysis studies revealed that PYZ-SLNs exhibited an anti-lipolytic effect due to stabilization by poloxamer 188. Moreover, the *in vitro* gastrointestinal (GI) stability results demonstrated that the PYZ-SLNs were stable in GI tract media (at pH 1.2, pH 4.5, pH 6.8, and pH 7.4). The *in vitro* drug release studies showed the best fit with the Hixon-Crowell model. The accelerated stability studies revealed no significant changes in PYZ-SLNs for 6 months.

Conclusion: PYZ-SLNs could be a promising carrier for the treatment of TB via the oral intestinal lymphatic pathway, circumventing its hepatic first-pass metabolism and thereby preventing hepatic adverse effects.

Keywords: Full factorial design, lipolysis model, long-chain lipids, lymphatic delivery, drug release kinetics

INTRODUCTION

Tuberculosis (TB) is a major worldwide health issue causing morbidity and mortality. It is an ailment that strikes in conditions of malnutrition, poverty, and limited healthcare access. Approximately 10.6 million people developed TB, and 1.3 million people died from TB in 2022, as per the World Health Organization Global TB Report. Primarily, developing countries such as India, Bangladesh, Pakistan, Philippines, Nigeria, and Indonesia bear the brunt of the worldwide TB burden.[1] The currently available TB treatment lasts from 6 months to 12 months, depending on its type.[2-6] The drug treatment for TB is complex due to its adverse effects, multiple drug regimens, and longer duration. Thus, effective drug formulations are necessary that can provide sustained release over a ,more extended period and thereby increase medication adherence in patients.[7]

A nicotinamide analogue, pyrazinamide (PYZ), is an essential frontline drug utilized for TB treatment. PYZ has a noteworthy role in shortening the TB treatment schedule from a duration of 9 to 12 months to a schedule of 6 months.[8] The capability of PYZ to shorten the schedule is due to its activity against a population of persistent tubercle bacilli dwelling in acidic pH

***Correspondence:** drmayurmpatel@gmail.com, **ORCID-ID:** orcid.org/0000-0002-9057-5769
Received: 06.03.2024, **Accepted:** 07.02.2025 **Publication Date:** 14.05.2025

Cite this article as: CHOKSHI N, VINCHHI P, CHAUHAN S, PATEL M. Formulation and optimization of pyrazinamide-loaded solid lipid nanoparticles by employing a design of experiments approach. Turk J Pharm Sci. 2025;22(2):91-103

environments that are not destroyed by other TB drugs. The acidic pH facilitates the intracellular accumulation of pyrazinoic acid, the active derivative of PYZ formed by the conversion of PYZ by pyrazinamidase. Due to high dosing frequency and high drug payload, the regimen for PYZ bactericidal activity is limited to two months. A PYZ dose of 15-30 mg/kg, or 1.5 to 2 g (depending on the patient's weight) is generally given. However, dose-dependent hepatotoxicity is a severe adverse effect of PYZ. Furthermore, major adverse effects of PYZ also include gouty arthritis, hyperuricemia, and, in rare cases, nephritis.[2,3,6,9,10]

Several research studies have been conducted on formulating and developing nano-carriers to deliver PYZ, namely, liposomes,[9] colloidosomes,[11] polymeric nanoparticles,[6,12] *etc*. Liposomes are potential carriers offering unique advantages; however, issues such as rapid leakage of water-soluble drugs, low encapsulation efficiency, instability in plasma, and poor storage stability persist.[12] Moreover, polymeric nanocarriers often require organic solvents in their fabrication, leading to toxicity and environmental risk.[13] Additionally, researchers explore inhalation therapy to deliver PYZ. However, challenges in using specialized delivery devices and implementing them on a large scale are some of the drawbacks that need to be addressed.[14]

The oral route is the most convenient for drug delivery. The key contributing factors affecting the oral bioavailability of drugs are gastric mean residence time, pH of the gastrointestinal (GI) tract, and drug solubility and permeability. Moreover, the pre-systemic metabolism also affects the bioavailability of drugs. The lymphatic pathway is a preferable alternative for avoiding first-pass metabolism. Several colloidal nano-carriers such as nano-micelles, self-emulsifying delivery systems, polymeric nanoparticles, liposomes, microemulsions, and solid lipid nanoparticles (SLNs) have been explored for achieving oral delivery via intestinal lymphatic transport.[15-17]

SLNs have emerged as promising nanoparticles as they amalgamate the benefits of all colloidal carriers mentioned and thereby improve the effectiveness of encapsulated drugs. They enhance the drug's lymphatic uptake. They are taken up *via* lymphatic circulation and enter blood vessels *via* jugular and subclavian veins, thus preventing the first-pass metabolism of the drug, and thereby reducing hepatic adverse effects.

Incorporating PYZ in SLNs would also promote drug efficacy, lessen the drug dose, and provide a sustained release.[18-20] Furthermore, it has been reported that the drug must have log $P \geq 4.7$ to be suitable for lymphatic uptake. PYZ exhibits a log *P* of -1.884; hence, it cannot enter the lymphatics and thereby undergoes hepatic first-pass metabolism.[21] Thus, based on the facts above, there is a dire need to develop therapeutic strategies that reduce PYZ hepatic toxicity.

To surmount the limitations associated with PYZ therapy, we propose an encapsulation of PYZ in SLNs to reduce hepatic adverse effects. The fabricated PYZ-SLNs contain long-chain lipids that facilitate absorption through the lymphatic system compared to medium or short-chain lipids. Moreover, the SLNs were developed utilizing poloxamer 188 (surfactant), which develops a steric crown on the SLNs surface, thus decreasing their contact with pancreatic and gastric lipase. Thus, poloxamer 188 plays a significant role in maintaining the integrity of PYZ-SLNs during its migration *via* the GI tract into the lymphatic system (Figure 1).[22]

MATERIALS AND METHODS

Materials

PYZ (99% pure) was obtained as a gift sample from S. Kant Healthcare Ltd., Mumbai, India. Stearylamine and stearic acid were acquired from Himedia Laboratories in Mumbai, India. Compritol 888 ATO (Glyceryl di- and tri-behenate) was acquired as a kind gift from Gattefosse India Pvt. Ltd., Mumbai, India. Glyceryl monostearate was donated by Hallstar, USA. Softisan 154 and Dynasan (114, 116, and 118) were donated by CremerOleo, Germany. Crodamol cetyl palmitate was acquired as a gratis sample from Croda, Mumbai, India. Tween 80, tween 20, sorbitan monooleate (span 80), and sorbitan monolaurate (span 20) were acquired from Central Drug House (CDH) Pvt. Ltd., New Delhi, India. Cremophor EL, cremophor RH 40, poloxamer 407 (P407), poloxamer 188 (P188), and solutol HS 15 samples were acquired as samples from BASF India Ltd., Mumbai, India. Soy Lecithin (Source: Soy), lipoid S 75 phospholipon 90 H, and phospholipon 90 G were acquired as samples from Lipoid GmbH, Germany. Sephadex G-50 (grade: coarse) was procured from MP Biomedicals, USA. Mannitol was acquired from CDH, New Delhi, India. The solvents used were of high performance liquid chromatography (HPLC) grade, and all additional chemicals were of analytical grade.

Surfactants and solid lipids screening

The lipids were heated to 10 °C higher than their melting temperature in a glass vial. PYZ (in increments of 2 mg) was incorporated into the melted lipid, which was stirred at

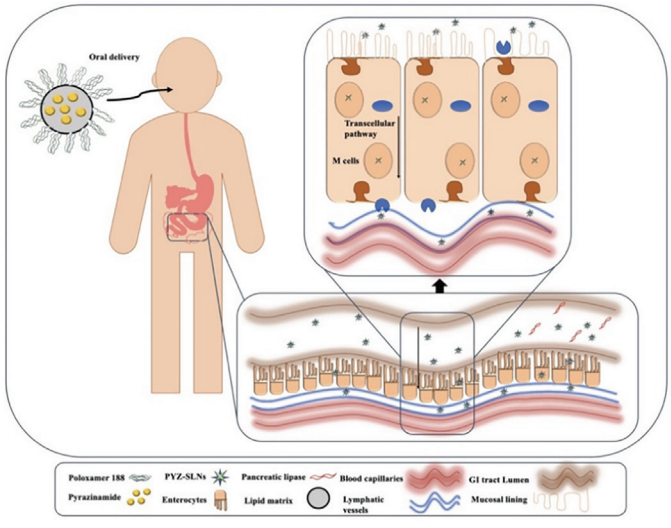

Figure 1. Schematic representation of the mechanism of oral absorption of PYZ-SLNs *via* the intestinal lymphatic system

PYZ-SLNs: Pyrazinamide-loaded solid lipid nanoparticles

100 rpm for 24 h by employing a water bath incubator shaker (EIE Instruments Pvt. Ltd., Ahmedabad). To confirm whether insoluble drug crystals were present or absent, the lipid melts were examined against a black-and-white background. The solubility of the drug was also assessed in several surfactant solutions (1% *w/v*) that were kept at a temperature of 25±2 °C. All the above-mentioned studies were carried out in triplicate sets.[23-26]

Preparation of PYZ-SLNs

The high-pressure homogenization method was used for the fabrication of PYZ-SLNs.[27-29] In brief, soy lecithin (0.3% *w/v*), stearyl amine (0.1% *w/v*), and stearic acid (1% *w/v*) were heated (10 °C above the melting point of the lipids) in a beaker using a water bath to obtain a uniform lipid phase. In the lipid melt phase, PYZ (30% *w/w*) was added and dissolved with constant stirring. Poloxamer 188 (3% *w/v*) was melted at a temperature similar to the lipid phase to obtain an aqueous surfactant solution. A high-speed stirrer (12000 rpm) (RQ 122/D Remi mechanical stirrer, Remi Mumbai, India) was used to mix aqueous surfactant solution and melted lipid phase, to form a pre-emulsion. A high-pressure homogenizer (GEA Lab Homogenizer PandaPLUS 200, Niro Soavi, Italy) was employed for the nanonization of pre-emulsion. It was subjected to 12 homogenization cycles at 1200 bar pressure in the homogenizer. The formulated SLNs were then lyophilized after the addition of cryoprotectant (Mannitol: 5% *w/v*) employing a bench-top freeze-dryer (FD-10-MR, Labfreez Instruments, Beijing, China) and were stored in a cool place.[26,30-35]

Statistical analysis

Statistical optimization of PYZ-SLNs

The PYZ-SLNs were optimized for various processing and formulation variables by applying the design of experiments using Design Expert software (Stat-Ease, Inc., Minneapolis, MN, USA). The preliminary batches (data not shown) were fabricated and characterized to investigate the formulation and processing variables influencing the PYZ-SLNs. A 2^3 full factorial design (two levels and three factors) was applied to optimize PYZ-SLNs. A 2^3 full factorial design estimates the impact of three factors (screened *via* preliminary trials) at two levels (high and low) on the dependent variables.

PYZ-SLNs characterization studies

Determination of particle size, polydispersity index (PDI), and zeta potential (ZP)

The particle size analysis was conducted by employing Zetasizer Nano ZS90 (Malvern Panalytical Ltd., Malvern, UK), which functions based on the principle of dynamic light scattering. The sample was diluted, for particle size analysis, to the required concentration using water for injection. Particle size distribution results were acquired, indicating the PDI of formulated PYZ-loaded SLNs. Each sample had a run time of 120 seconds. The ZP calculates the particle's electrophoretic mobility in an electric field using about 12 to 15 runs for every measurement. All the above-mentioned studies (D90, PDI, and ZP) were carried out in triplicate sets.[24,25,33-35]

Evaluation of DL% and EE%

The DL% and EE% of the PYZ-SLNs were estimated based on the size exclusion chromatography principle by utilizing the Sephadex G-50 minicolumn and centrifugation technique (as discussed elsewhere).[34,36]

The drug-loaded SLNs, after centrifugation, collected from Sephadex G-50 mini column were diluted (20 times) using a 2:1 ratio of dichloromethane, methanol to determine the entrapped drug ($W_{entrapped}$). A validated HPLC method was utilized to analyze the EE% of the aforementioned sample. All the above-mentioned procedures were carried out in triplicate. The following formula was used to calculate the EE%:

$$EE\% = \frac{W_{entrapped}}{W_{total}} \times 100 \quad \text{(Equation 1)}$$

Where $W_{entrapped}$ is the amount of entrapped PYZ in the SLNs (Separated *via* Sephadex G-50 column), W_{total} is the whole PYZ quantity that was added into the formulation.

The following formula was used to calculate the DL%:[37]

$$DL\% = \frac{W_{entrapped}}{\text{Quantity of solids added}} \times 100 \quad \text{(Equation 2)}$$

Differential scanning calorimetry (DSC) analysis

A Shimadzu DSC 60 A (Kyoto, Japan) linked to a TDA trend line program was utilized for calorimetric analysis. Samples were weighed (5 mg) in an aluminum pan, while an empty aluminum pan served as the reference. Thermograms were scanned at 10 °C per minute from 40 °C to 300 °C. Thereafter, the samples were cooled down to 40 °C using liquid nitrogen.[26,32-34,38]

Transmission electron microscopy (TEM) analysis

The PYZ-SLN's morphology was examined by using a CM-200 TEM (Philips, the Netherlands). On Formvar-coated TEM grids (Ted Pella, Redding, CA), SLNs (diluted 50X) were mounted and then negatively stained with phosphotungstic acid. The PYZ-SLNs sample was dried for 5 min at 25 °C and then observed using a TEM with a resolution of 0.23 nm at 200 kV.[19,24-26,33,34,39,40]

Powder X-ray diffraction (PXRD) studies

To investigate the crystallinity of PYZ and the SLNs' structure after preparation, an X-ray diffractometer (Bruker D8 Discover, Germany) was used. The diffraction patterns of pure PYZ, stearic acid (solid lipid), blank SLNs, and optimized PYZ-SLNs (batch 11) were analyzed. The samples (500 mg) were kept in the sample compartment and exposed to Ni-filtered Cu Kα-radiation at a wavelength of 1.5406 Å at 30 kV, 10 mA. Each diffractogram was recorded from 10° to 40° two theta angles, and plots (intensity *vs.* 2θ) were generated utilizing software OriginPro 2017 (OriginLab Corporation, USA).[24,25,33,34,40]

In vitro characterization studies of PYZ-SLNs

In vitro release study

Using the dialysis membrane method, the *in vitro* release from PYZ-SLNs was conducted in various solutions: 0.1 N HCl (pH

1.2) to mimic gastric pH phosphate-citrate buffer (pH 4.5) to mimic endosomal alveolar macrophage and phosphate buffer (pH 6.8 and 7.4) to mimic intestinal pH.[41-45] The volume of various release media for conducting the *in vitro* release study was 100 mL. The freeze-dried SLNs (comprising the 10 mg equivalent of entrapped PYZ) were added to the dialysis tube (molecular weight cut-off 12-14 KDa, HiMedia Laboratories Pvt. Limited, Mumbai) for the investigation. The beaker containing dialysis tubing suspended in the media was maintained at 37.0±0.5 ˚C with magnetic stirring (5-MLH Remi, Remi labworld, India) at a speed of 100 rpm. The 5 mL aliquots were drawn at predetermined time points (0, 1, 2, 4, 6, 8, 12, 24, 36, 48, 60, 72, 96, and 120 hours) and replenished with an equal amount of fresh release media to sustain the sink conditions. A validated HPLC technique was used to analyze the samples and determine the quantity of drug released.[25,26,33,34]

Drug release kinetics

The drug release data were further subjected to drug dissolution (DD) solver to determine the drug release kinetics.[46] Various mathematical models, namely first order, zero order, Higuchi, Weibull, the Hixon-Crowell, and the Korsemeyer-Peppas were evaluated to determine the drug release mechanism from SLNs. The release data were fitted to all the above-mentioned models in the DD solver program and the scatter plots were generated with the fitted curve. The model with the highest R-square value and highest *f*-value was the best fit for dissolution profiling. The formula for the models to which the release data were fitted is mentioned below:

$$\text{First order: } F = 100 \cdot (1 - e^{-k1 \cdot t}) \quad \text{(Equation 3)}$$

$$\text{Zero order: } F = k_0 \cdot t \quad \text{(Equation 4)}$$

$$\text{Higuchi: } F = k_{\text{H}} \cdot t^{0.5} \quad \text{(Equation 5)}$$

$$\text{Weibull: } F = F_{\max} \cdot \left[1 - e^{-\frac{(t-Ti)^{\beta}}{\alpha}}\right] \quad \text{(Equation 6)}$$

$$\text{Hixon-Crowell: } F = 100 \cdot [1 - (1 - k_{\text{HC}} \cdot t)^3] \quad \text{(Equation 7)}$$

$$\text{Korsemeyer-Peppas: } F = k_{\text{KP}} \cdot t^n \quad \text{(Equation 8)}$$

Where, in all models, F is the fraction (%) of drug released in time t, k_1 is first order release constant, k_0 is zero order release constant, is the Higuchi release constant, is the maximum drug released at infinite time, α (scale parameter) defines the time scale of the process, β (shape parameter) characterizes a curve as exponential, sigmoid, or parabolic; k_{HC} is release constant in the Hixson-Crowell model, is the korsemeyer-peppas release constant incorporating the geometric and structural characteristics of the formulation, and *n* is the diffusional exponent defining the release mechanism.[47]

In vitro lipolysis test

The *in vitro* lipolysis test of PYZ-SLNs was conducted as per the previously described procedure using simulated empty-state intestinal conditions.[48] A lipolytic medium was prepared and reacted with the formulated PYZ-SLNs. It contained calcium chloride (5 mM), sodium taurodeoxycholate (5 mM), sodium chloride (150 mM), soy lecithin (1.25 mM), pancreatic lipase (0.525 g/300 IU/mL), and sodium dodecyl sulphate (0.5% *w/v*). The lipolytic medium was buffered with tris-maleate (pH 6.8). Herein, simulated digestive media (14 mL) was mixed with PYZ-SLNs (6 mL). The above blend was stored at 37±0.5 ˚C in a thermostatic water bath. The entire lipolysis process was maintained at pH 6.8 by using an Auto Titrator (Titra+, LabIndia Analytical Instruments Pvt. Ltd., Thane, India). The autotitrator used 200 mM sodium hydroxide to counterbalance the fatty acid generated by the lipid digestion. When the pH change at 15 minute intervals was less than 0.05 units, the digestive process was considered to be complete.

$$\textit{Extent of lipolysis } (\%) = \frac{V \times C \times M.W}{3 \times \rho \times v} \times 100 \quad \text{(Equation 9)}$$

Where V is the titrant volume utilized amidst the digestion at 6.8 pH, C is the titrant concentration, M.W denotes the lipids molecular weight (g/mol) utilized for the formulation of SLNs, 3 describes that one triglyceride molecule can release a maximum of 3 fatty acids, ρ indicates the lipid density (g/mL), ν is the lipids volume in SLNs within the lipolysis medium.[24-26,33,34]

In vitro investigation of GI stability of PYZ-SLNs

GI stability of PYZ-SLNs was assessed by determining their EE%, PDI, and particle size across different pH ranges, viz. pH 1.2 (0.1 N HCl), pH 4.5 (sodium acetate buffer), pH 6.8 (PBS), and pH 7.4 (PBS), simulating the GI physiology of humans. To assess the stability of the formulated PYZ-SLNs, they were kept at pH 1.2 and 4.5 for 2 h, and incubated at pH 6.8 and 7.4 for 6 h.[19,49,50]

Stability analysis of PYZ-SLNs

The stability studies of the optimized lyophilized PYZ-SLNs were conducted according to the previously reported literature.[19,51] The lyophilized PYZ-SLNs were stored in amber-colored glass vials, sealed, and placed in an upright position in a stability chamber (Nova Instruments Pvt. Ltd. in Ahmedabad). Thereafter, the SLNs were stored at 8 ˚C, 30±2 ˚C/65±5% RH (intermediate conditions), and 40±2 ˚C/75±5% RH (accelerated conditions) for 6 months to assess their stability. At predetermined intervals, namely, initial, 1 month, 3 months, and 6 months, samples were investigated for ease of redispersibility, any alterations in physical appearance, EE%, PDI, and particle size.[24-26,32,33]

RESULTS

Lipid excipients and surfactants screening

Solid lipids screening

The solid lipid was selected based on the criterion that the drug has maximum solubility in that lipid. PYZ has a log *p* of -1.884 as it is lipophilic in nature. The results showed that stearic acid had the highest solubility of PYZ (Figure 2A). The partitioning of PYZ in various solids was evaluated.[23] Stearic acid was selected for developing PYZ-SLNs because PYZ partitioning was highest in stearic acid.

Screening of surfactants

The surfactant was selected based on the least solubility of PYZ in it. As shown in Figure 2B, the investigation was carried out using different surfactant solutions (1% *w/v*). Drug moieties are incorporated in the lipid matrix and are strongly associated with the solid lipid core due to surfactants with low drug solubility. It was necessary to select surfactants with the lowest solubility of PYZ. Drug moieties are materialized in the lipid matrix and are strongly associated with the solid lipid core by surfactants having a low drug solubility.[33,34] It was necessary to select surfactants having the least solubility for PYZ. The PYZ solubility was found to be highest in polysorbate 80 (20 mg/mL), followed by cremophor RH40 (18 mg/mL), polysorbate 40 (16 mg/mL), polysorbate 20 (16 mg/mL), and cremophor EL (16 mg/mL). PYZ was found to be moderately soluble in poloxamer 407 (14 mg/mL) and solutol HS15 (14 mg/mL). The solubility of PYZ in P188 was the lowest (12 mg/mL). Thus, P188 was selected for formulating PYZ-SLNs.

It has been reported that P188 provides an anti-lipolytic effect in the GI tract. A steric crown is created on SLNs surface, which reduces the interaction of SLNs with pancreatic and gastric lipase.[50-52] Batches CSP2 (1% *w/v* P188) and CSP3 (3% *w/v* P188) were subjected to an *in vitro* lipolysis study. Batch CSP2 degraded by 21.23±1.86%, while batch CSP3 degraded by 10.12±0.69% (Figure 2C). Thus, 3% *w/v* P188 was selected for the optimization of PYZ-SLNs as it resulted in minimum lipolysis.

PYZ-SLNs optimization by response surface methods

Optimization of PYZ-SLNs utilizing 2^3 factorial design

Based on the preliminary trial results (data not shown), it was observed that among various formulation and process variables, the parameters viz. homogenization cycles, emulsifier concentration, and drug concentration demonstrated significant impact on particle size, DL%, and EE% of PYZ-SLNs. The emulsifier concentration influenced particle size and EE%, while the drug concentration primarily impacted DL% and EE%. The homogenization cycles impacted the EE% and particle size of PYZ-SLNs. To comprehensively optimize the PYZ-SLNs, these primary observations were taken into account, and a 2^3 factorial design (two levels and three factors) was applied, as shown in Table 1 and Table 2. The following mathematical model was used to derive equations showing the link between independent and dependent variables:

$$Y = B_0 + B_1X_1 + B_2X_2 + B_3X_3 + B_{12}X_1X_2 + B_{13}X_1X_3 + B_{23}X_2X_3 + B_{123}X_1X_2X_3 \quad \text{(Equation 10)}$$

Where X_1, X_2, and X_3 are the factors (chosen from primary studies), Y_i is the dependent variable, B_1 to B_{33} is the regression coefficients range and B_0 is the intercept.

3D response surface plots were generated, and data were investigated by employing Design-Expert 10 software (version 10.0.6) (Stat-Ease, Inc., Minneapolis, MN, USA). To identify a design space with higher desirability, restraints were applied to responses.

The responses [particle size (D90), EE%, and DL%] achieved at various levels of the independent variables (X_1, X_2, and X_3) were put through multiple linear regression to obtain second-order polynomial Equations (11), (12), and (13). The equations are mentioned below:

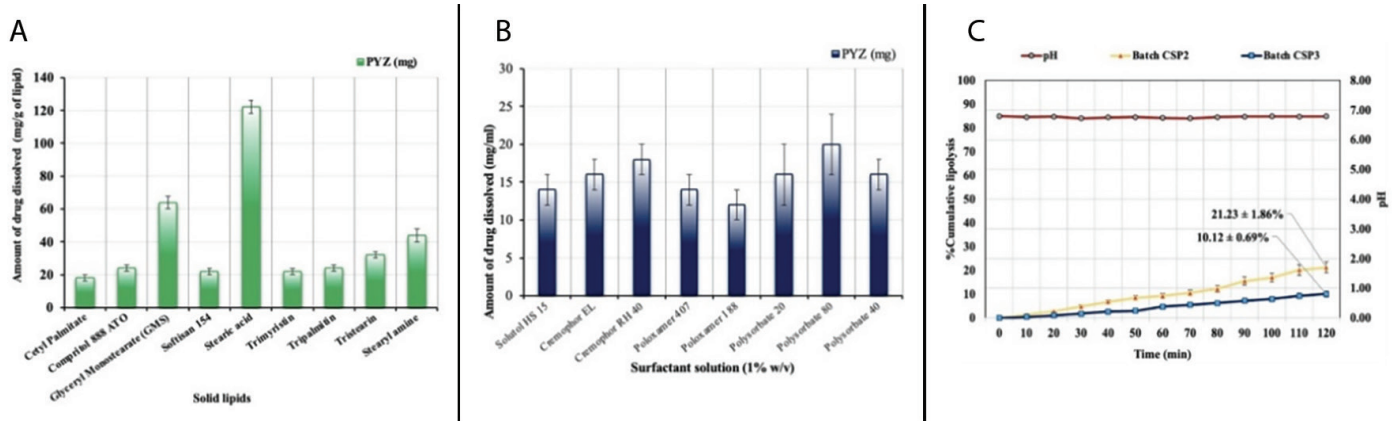

Figure 2. Solubility studies of PYZ in (A) solid lipids, (B) surfactant solutions (1% *w/v*), and (C) % cumulative lipolysis of formulation batches *versus* time profile (mean ± SD, n=3)

PYZ: Pyrazinamide, SD: Standard deviation

$$Y_1 = +446.30 + 0.28 * X_1 - 10.42 * X_2 - 26.09 * X_3 + 3.79 * X_1 * X_2 + 4.51 * X_1 * X_3 - 7.57 * X_2 * X_3 - 6.24 * X_1 * X_2 * X_3 \quad \text{(Equation 11)}$$

$$Y_2 = +83.55 + 1.03 * X_1 + 1.38 * X_2 - 0.51 * X_3 + 0.38 * X_1 * X_2 + 0.15 * X_1 * X_3 - 0.31 * X_2 * X_3 + 0.076 * X_1 * X_2 * X_3 \quad \text{(Equation 12)}$$

$$Y_3 = +12.08 + 2.28 * X_1 + 0.32 * X_2 - 0.19 * X_3 + 0.072 * X_1 * X_2 + 0.011 * X_1 * X_3 - 0.21 * X_2 * X_3 - 0.043 * X_1 * X_2 * X_3 \quad \text{(Equation 13)}$$

The equations signify the influence of X_1, X_2, and X_3 (independent variables) on Y_1, Y_2, and Y_3 (dependent responses). The correlation coefficient R^2 values were established to be 0.9484, 0.7094, and 0.9317 for dependent responses Y_1, Y_2, and Y_3, respectively, signifying a good match.

Table 1. 2^3 factorial design-independent and dependent variables

	Factors	Coded levels	
	Independent variables	Low level (-1)	High level (+1)
X_1	Drug concentration (*w/w* %)	10	30
X_2	Emulsifier concentration (*w/v* %)	0.2	0.3
X_3	Homogenization cycles	8	12
	Dependent variables	Constraints	
Y_1	D90 (nm)	D90<500 nm	
Y_2	Entrapment efficiency %	Maximum	
Y_3	Drug loading %	Maximum	

The impact of factors and independent variables on particle size is shown in Figure 3A-C. Equation (11) indicates that the X_2 and X_3 variables have a notable inverse effect on the PYZ-SLNs particle size. This suggests that the particle size (D90) of PYZ-SLNs is reduced with increasing homogenization cycles (X_3). The possible cause of the decrease in particle size might be the cavitation forces in the high-pressure homogenizer leading to the reduction of PYZ-SLNs to nano-scale size.[53,54] Moreover, the particle size of PYZ-SLNs reduces with an increase in emulsifier (X_2) concentration. This might be owing to increased stabilization of pre-emulsion by an emulsifier, leading to a diminution in particle size as well as its aggregation.[53]

The impact of the factors on EE% is represented in Figure 3D-F. It is evident from Equation (12) that factors X_1 and X_2 have a positive impact, whereas factor X_3 has a negative impact on EE% of PYZ-SLNs. The direct correlation between the drug concentration and EE% is described by the Equation. The EE% increases with an increase in drug concentration, which might be due to the increased drug availability for accommodation in a lipid matrix. The EE% rises as the emulsifier (X_2) concentration increases. The high drug solubilization and incorporation into the lipid core could be responsible for an increase in EE%.[53,55] The EE% was negatively impacted by homogenization cycles (X_3). The EE% decreased as the number of homogenization cycles increased. This might be owing to the increased surface area of particles caused by the cavitational forces generated with increased cycles of homogenization, resulting in drug leaching during SLN formation.[53,54] The impact of factors on response DL% is represented in Figure 3G-I. It is clear from Equation (13) that the variables X_1 and X_2 have a positive impact on DL%. The increase in drug concentration was attributed to more drug able to be incorporated into the lipid matrix. Furthermore, the drug is more solubilized in the lipid matrix with the addition of an emulsifier. Thus, an increase in emulsifier concentration increases the DL%. It was found that as the homogenization cycles increased, the DL% was reduced. This could be the

Table 2. Components of experimental batches (mean ± SD, n=3)

Batch no.	(X_1)	(X_2)	(X_3)	Particle size (nm) (Y_1)		EE (Y_2) %		Drug loading (Y_3) %	
				Observed	Predicted	Observed	Predicted	Observed	Predicted
P1	-1	-1	-1	521±15	517.99	81.2±3.1	80.62	5.71±0.61	5.27
P2	1	-1	-1	470±9	460.98	84.7±2.7	82.96	15.21±1.15	13.89
P3	-1	1	-1	453±10	452.12	82.4±1.4	82.18	5.81±0.37	5.64
P4	1	1	-1	478±14	475.35	87.6±2.4	86.93	15.70±1.24	15.18
P5	-1	-1	1	417±12	416.48	80.1±0.4	79.79	5.24±0.26	4.99
P6	1	-1	1	447±11	445.43	83.6±2.7	82.68	14.80±1.52	14.04
P7	-1	1	1	395±8	395.19	79.4±3.4	79.21	5.21±0.62	5.05
P8	1	1	1	404±6	404.56	86.3±1.7	85.74	14.82±0.96	14.33
P9*	0	-0.5	-0.5	439±14	433.25	81.9±2.5	83.29	10.70±0.58	11.98
P10*	0	0	0.5	440±12	462.66	79.2±4.2	83.04	9.12±0.59	11.96

*: Checkpoint batches, SD: Standard deviation, no.: Number, EE: Entrapment efficiency

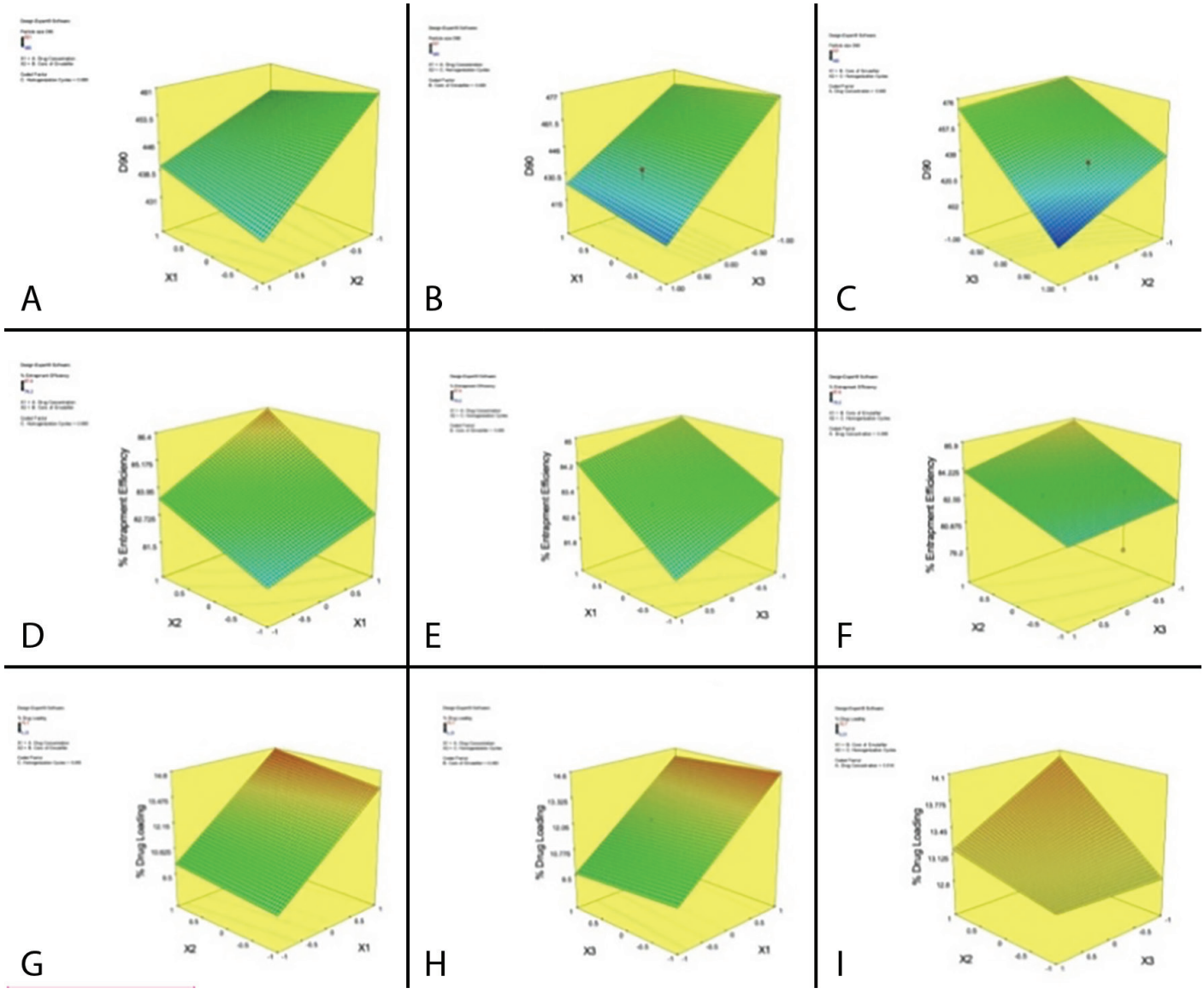

Figure 3. Effect of independent variables on particle size, EE%, and DL% (dependent variables)
EE: Entrapment efficiency, DL: Drug loading

result of greater homogenization cycles, which further cause drug leaching during the preparation of SLNs.

Optimization and validation

The 3D RSP results were based on polynomial models, which depicted the impact of significant independent factors on responses. Two additional checkpoint batches, P9 and P10, with the predicted values, were prepared to verify the validity of the optimization process. The checkpoint batches were prepared, and the variance between the observed and predicted values was examined using the Student's *t*-test (Table 2). The outcomes showed a high degree of closeness between observed and predicted values, and the difference between them was not significant ($p>0.05$). As a result, the obtained mathematical Equation was found to be accurate in predicting the responses Y_1, Y_2, and Y_3 (Table 3).

Table 3. Comparison of observed and predicted values of PYZ-SLNs (optimized batch P11) (mean ± SD, n=3)

Formulation	Characterisation		
	Y_1 (nm)	Y_2 (%)	Y_3 (%)
Batch P11 (Predicted value)	404	85.74	14.33
Batch P11 (Observed value)	401±08	86.24±1.15	14.38±0.85
Bias# %	0.75	-0.58	-0.35

#Bias % = (Predicted value - Observed value)/Observed value x 100, SD: Standard deviation, PYZ-SLNs: Pyrazinamide-loaded solid lipid nanoparticles

The software Design-Expert 10 (version 10.0.6) was used to create optimum conditions for PYZ-SLNs, with a desirability value of 0.878. The optimized batch P11 was selected by setting the criteria of particle size <500 nm, and DL% and

EE% as being the highest. For the optimization batch, the software projected the following process parameters: drug concentration (PYZ) =30% *w/w*, emulsifier concentration (Soy lecithin) =0.3% *w/v*, and homogenization cycles =12. Furthermore, the Design-Expert 10 software predicted that the optimized batch P11 would have a particle size of 404 nm (Figure 4), with 85.74% (EE%) and 14.33% (DL%). Table 3 shows that the predicted values produced by the software and the practical values (P11-optimized PYZ-SLNs) were in good agreement.

In vitro drug release analysis of PYZ-SLNs

The lyophilized PYZ-SLNs (batch P11) *in vitro* drug release study was conducted at different pH values: 1.2 (0.1 N HCl), 6.8, and 7.4 (PBS), 4.5 (citrate-phosphate buffer) (Figure 5A and B). At a pH of 1.2, the PYZ-SLNs (Batch P11) exhibited ~10% drug release in 2 h. However, at pH 4.5, 6.8, and 7.4, the PYZ-SLNs (Batch P11) were observed to have a biphasic drug release pattern, releasing about 90% of the drug in 5 days (120 h) at different pH ranges. This pattern consisted of an initial burst release (~30% in 12 h) and thereafter, a sustained release (~90% in 120 h). The drug release pattern was found to be the same in the entire pH range. Therefore, it was concluded that the *in vitro* release of PYZ-SLNs was pH-independent.

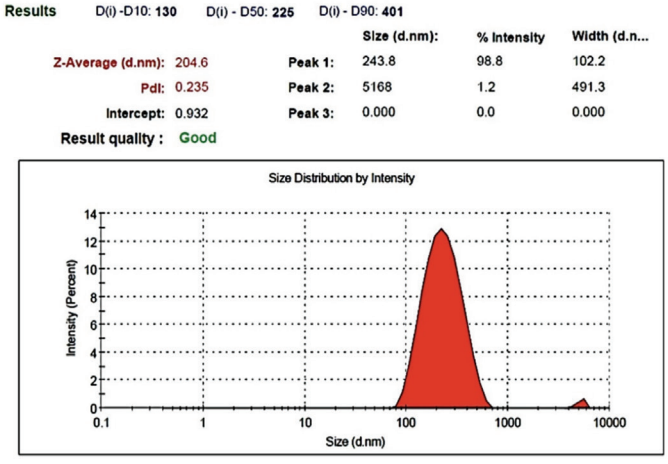

Figure 4. Particle size and particle size distribution of optimized PYZ-SLNs (Batch P11)

PYZ-SLNs: Pyrazinamide-loaded solid lipid nanoparticles

Drug release kinetics

Furthermore, the optimized PYZ-SLNs, (Batch P11), *in vitro* drug release profile was fitted to first-order, zero-order, Baker-Lonsdale, Hixson-Crowell, Korsmeyer-Peppas, Higuchi, and Weibull models (Table 4). To further describe the drug release mechanism, the best model with the lowest *f*-value and the highest R-square value was selected. The Hixson-Crowell model (Figure 5C) best fits the drug release profile of the PYZ-SLNs (Batch P11), with the lowest *f*-value and the highest R-squared when compared to other models (Table 4). The Hixson-Crowell model explains drug release through a dissolution mechanism, which depends on the surface area of the drug particles in contact with the aqueous phase. Hence, the larger the surface area, the faster the particle dissolution.[56,57]

DSC analysis

DSC analysis demonstrates the alterations in thermal behavior occurring because of the interactions amongst lipid components and drug during fabrication of PYZ-SLNs.[58-60] The pure PYZ transition temperature (Figure 6A) was determined to be 191.78 °C (endothermic peak) by DSC analysis.[61,62] The stearic acid (lipid excipient) transition temperature (Figure 6B) was determined to be 60.44 °C. Due to the addition of excipients such as soy lecithin and stearylamine (emulsifier), the blank SLNs peak (Figure 6C) was altered to 69.38 °C. Furthermore, in optimized PYZ-SLNs batch P11 (Figure 6D), the peak for the pure drug was not obtained. This might be attributed to the encapsulation of PYZ in a distributed form inside the SLN lipid core.

Morphological examination by TEM analysis

The TEM analysis of the PYZ-SLNs (batch P11) showed that the particles had a smooth surface and even size and shape (Figure 7A). There was no discernible particle aggregation, and the mean diameter was <500 nm. These analyses validate the outcomes of the DLS method.

PXRD analysis

The OriginPro 2017 software (OriginLab Corporation, USA) was used to analyze the diffraction patterns of the PYZ-SLNs (Batch

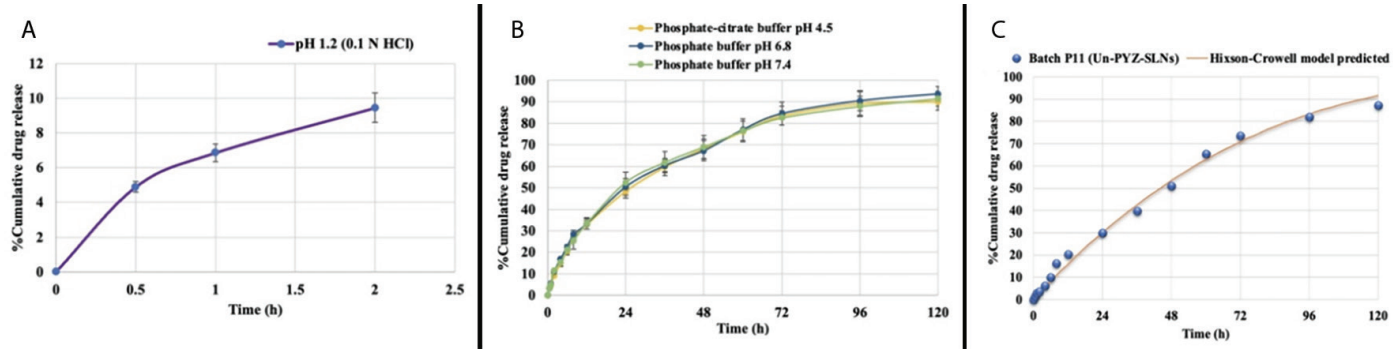

Figure 5. Dissolution profile of batch P11 in (A) pH 1.2 (0.1 N HCl), (B) phosphate-citrate buffer (pH 4.5) and phosphate buffer (pH 6.8 and 7.4); (C) Hixson-Crowell model for batch P11 (mean ± SD, n=3)

SD: Standard deviation

Table 4. *F*-values and R^2 of optimized PYZ-SLNs (batch P11) for different kinetic models

Parameters	Zero order model	First order model	Higuchi model	Hixcon-Crowell model	Korsmeyer-Peppas model	Baker lonsdale model	Weibull model
R^2	0.8923	0.9892	0.9695	0.9923	0.9861	0.9627	0.9683
F-value	544.83	23.80	114.22	11.65	24.18	102.48	120.74

PYZ-SLNs: Pyrazinamide-loaded solid lipid nanoparticles

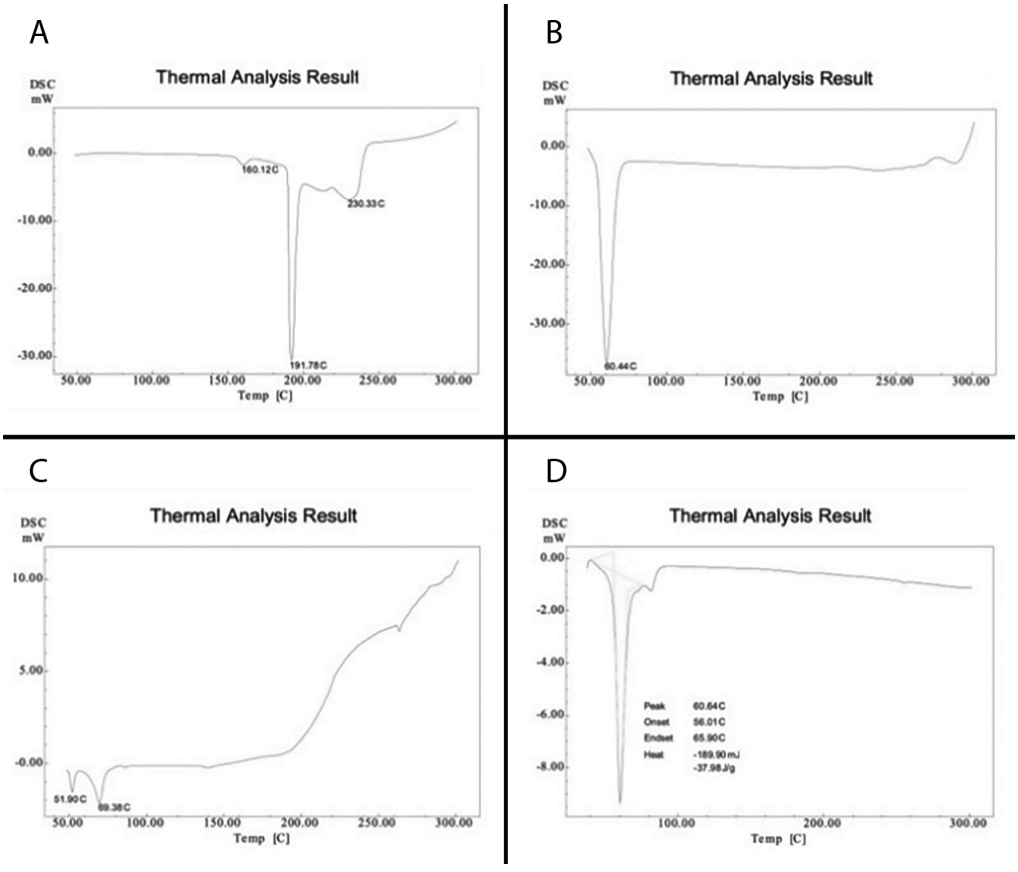

Figure 6. DSC of (A) pure PYZ powder, (B) stearic acid (lipid), (C) blank SLNs, (D) optimized PYZ-SLNs (batch P11)
DSC: Differential scanning calorimetry, PYZ-SLNs: Pyrazinamide-loaded solid lipid nanoparticles

P11) and PYZ, as shown in Figure 7B. The p-XRD patterns of PYZ showed its crystalline character, as clear sharp peaks were observed in the 2θ scale. In the PYZ-SLNs (Batch P11), the data showed a decline in the relative integrated peak intensity, and there was no discrete PYZ peak, signifying that PYZ was encapsulated in the lipid core of the SLNs in an amorphous form. Therefore, it can be concluded that the PYZ, which was incorporated into the lipid core of SLNs, was completely solubilized and changed into an amorphous state.

GI stability studies (in vitro)

PYZ-SLNs were uniformly distributed without any drug precipitation, according to the outcomes of stability studies (Table 5). Furthermore, after being incubated with different United States Pharmacopeia buffers, with a pH range of 1.2 to 7.4, statistically non-significant (p>0.05) variations in PDI values, EE%, and particle size were observed.

Stability studies for PYZ-SLNs

The stability of SLNs was determined at freezer (8 ˚C), intermediate conditions (30±2 ˚C/RH 65±5%), and accelerated conditions (40±2 ˚C/RH 75±5%) for 6 months. At predetermined intervals (initial, 1 month, 3 months, and 6 months), samples were analyzed for any alterations in physical appearance, ease of redispersibility, EE%, PDI, and particle size (D90). Table 6 represents the stability results for the lyophilized formulations (PYZ-SLNs). The lyophilized powder had a fluffy appearance, and upon reconstitution with water, it was found to be easily re-dispersed. Furthermore, there were no noteworthy changes in the parameters, suggesting that the prepared nanoparticles were stable and had a long shelf-life.

DISCUSSION

The PYZ-SLNs were fabricated using a high-pressure homogenization technique. In the preliminary trials, it was

Table 5. *In vitro* GI stability studies for PYZ-SLNs (batch P11) (mean ± SD, n=3)

Medium	Particle size (nm)		PDI		EE%	
	Pre-incubation	Post incubation	Pre-incubation	Post incubation	Pre-incubation	Post incubation
pH 1.2 (0.1 N HCl)	401±08	406±07	0.235±0.03	0.237±0.04	86.24±1.15	85.37±1.79
Sodium acetate buffer pH 4.5	401±08	404±06	0.235±0.03	0.238±0.03	86.24±1.15	85.70±0.64
Phosphate buffer pH 6.8	401±08	403±03	0.235±0.03	0.240±0.05	86.24±1.15	85.12±1.40
Phosphate buffer pH 7.4	401±08	404±09	0.235±0.03	0.236±0.04	86.24±1.15	85.29±1.62

GI: Gastrointestinal, SD: Standard deviation, PYZ-SLNs: Pyrazinamide-loaded solid lipid nanoparticles, EE: Entrapment efficiency, PDI: Polydispersity index

Table 6. Stability evaluation of PYZ-SLNs (batch P11) (mean ± SD, n=3)

Stability testing condition	PYZ-SLNs		
	Particle size (nm)	PDI	EE (%)
Initial*	401±08	0.235±0.03	86.24±1.15
5±3 °C**			
1 month	402±08	0.236±0.04	86.02±0.47
3 months	404±09	0.239±0.03	85.35±0.84
6 months	410±12	0.242±0.05	84.85±1.06
30±2 °C/65±5% RH**			
1 month	403±09	0.237±0.04	85.88±0.76
3 months	404±08	0.240±0.05	85.16±0.94
6 months	413±11	0.242±0.07	83.67±1.12
40±2 °C/75±5% RH**			
1 month	405±08	0.239±0.05	85.68±1.18
3 months	412±10	0.242±0.06	84.15±1.61
6 months	417±11	0.244±0.08	82.79±2.08

*: Fresh samples, **: Lyophilized samples, SD: Standard deviation, PYZ-SLNs: Pyrazinamide-loaded solid lipid nanoparticles, EE: Entrapment efficiency, PDI: Polydispersity index

observed that three parameters, namely, homogenization cycles, drug concentration, and emulsifier concentration, had a noteworthy impact on DL%, EE%, and particle size of PYZ-SLNs. A 2^3 factorial design was applied to optimize PYZ-SLNs. By employing Design-Expert software, the 3D response surface plots were generated and investigated. The independent variables emulsifier concentration (X_2) and homogenization cycles (X_3) had a significant reverse impact on particle size of PYZ-SLNs. With the increase in homogenization cycles, the decrease in particle size might be owing to the cavitation forces in the high-pressure homogenizer, leading to the reduction of PYZ-SLNs to nano-scale.[53,54] Moreover, an increase in emulsifier concentration reduced the particle size of PYZ-SLNs. This might be owing to increased stabilization of pre-emulsion by an emulsifier, leading to a diminution in particle size as well as its aggregation.[53] Furthermore, the drug concentration and emulsifier concentration had a positive impact on the EE% of PYZ-SLNs. The high drug solubilization and incorporation into the lipid core could be responsible for an increase in EE%.[53,55] The EE% decreased with an increase in homogenization cycles (X_3). This might be owing to the increased surface area of particles owing to the cavitational forces generated with increased cycles of homogenization resulting in drug leaching during SLN formation.[53,54] Thereafter, the impact of independent variables on DL% showed that an increase in drug concentration and emulsifier concentration led to an increase in DL%. The increase in drug concentration was attributed to more drug accessible to get incorporated into the lipid matrix. Furthermore, the drug gets solubilized more in the lipid matrix with the addition of an emulsifier as it acts as a solubilizer. Thus, an increase in emulsifier concentration increases the DL%. However, an increase in homogenization cycles led to a decrease in DL%. This could be the result of greater homogenization cycles which further cause drug leaching during the preparation of SLNs.[53,54]

To validate the optimization process, checkpoint batches (P9 and P10) with predicted values were prepared. The predicted and observed values represented a high degree of closeness

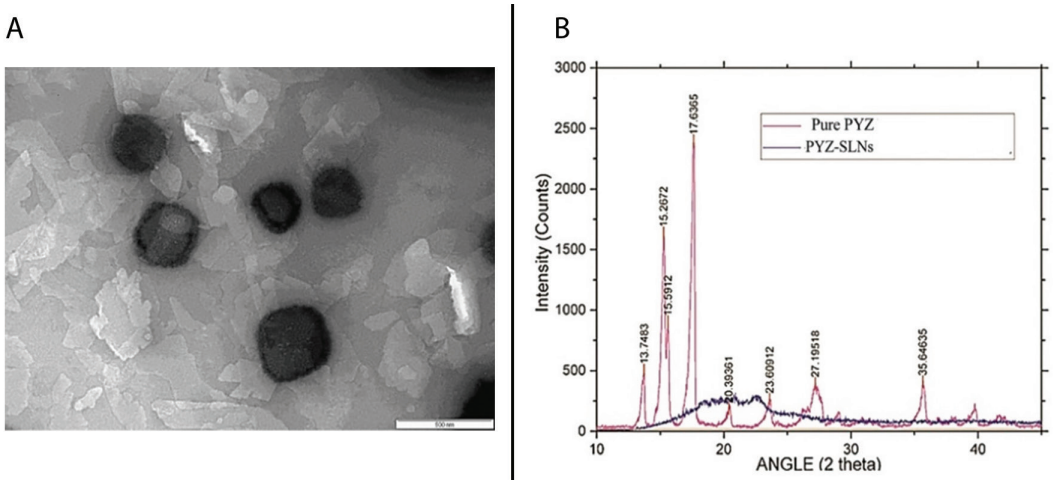

Figure 7. (A) TEM images of batch P11; (B) PXRD patterns of Pure PYZ and batch P11 (PYZ-SLNs)
TEM: Transmission electron microscopy, PXRD: Powder X-ray diffraction, PYZ-SLNs: Pyrazinamide-loaded solid lipid nanoparticles

as the difference among them was not significant (p>0.05). Thus, the obtained mathematical Equation was accurate in predicting the responses Y_1, Y_2, and Y_3. The optimized batch (P11) was fabricated by setting the optimum conditions (particle size: <500 nm and DL% and EE% of highest). The predicted and observed values of the P11 batch were in close agreement.

The *in vitro* drug release from the optimized batch P11 (lyophilized), evaluated in different pH media, represented an initial burst release followed by a sustained release. Further, the Hixson-Crowell model was found to provide the best fit for the PYZ-SLNs drug release profile as it had the highest R-square and lowest *f*-value. The Hixson-Crowell model explains the drug release by a dissolution mechanism, which depends on the outer surface of the aqueous phase. Hence, the larger the surface area, the faster the particle dissolution.[56,57] DSC analysis demonstrates the alterations in thermal behavior occurring because of the interactions among lipid components and drug during fabrication of PYZ-SLNs.[58-60] Herein, the DSC results of optimized PYZ-SLNs (P11 batch) did not show the peak of the pure drug. This might be attributed to the encapsulation of PYZ in a distributed form inside the SLNs lipid core.[61,62] Moreover, the TEM analysis results did not depict any particle aggregation. The TEM results validated the outcomes of the DLS method. The PXRD indicated a decrease in peak intensity and did not detect any PYZ peaks. Thus it was concluded that the PYZ was incorporated into the lipidic core of SLNs solubilized, and changed into an amorphous state. Furthermore, the PYZ-SLNs were determined to be stable under accelerated stability conditions for 6 months, as there were no changes in EE%, D90, PDI, or their physical appearance.

CONCLUSION

The current research work emphasizes the prospects of SLNs as an efficient carrier for oral delivery of the anti-tubercular drug PYZ. For optimizing the formulated PYZ-SLNs systematically, three factors and a two-level fractional factorial design were applied. The *in vitro* drug release study represented a biphasic release of PYZ-SLNs, consisting of an initial burst release followed by sustained release, fitting best with the Hixson-Crowell model, indicative of a release *via* a diffusion mechanism. The *in vitro* lipolysis analysis showed that PYZ-SLNs demonstrated an anti-lipolytic action in the fasted-state simulated intestinal (lipase-containing) fluid. PYZ-SLNs demonstrated good resistance *in vitro* and easily withstood varied GI tract-resembling media. The accelerated stability assessment confirmed that the PYZ-SLNs were stable even after 6 months, indicating their long shelf-life. Hence, from the aforementioned outcomes, it may be inferred that the optimized and formulated PYZ-SLNs can avert the PYZ degradation in varied GI media, and can be employed as a promising nano-based treatment for TB.

Ethics

Ethics Committee Approval: Not required.

Informed Consent: Not required.

Acknowledgment

Authors are thankful to the Institute of Pharmacy, Nirma University, Ahmedabad, Gujarat, India for providing the necessary facilities to generate the manuscript that is a part of Doctor of Philosophy (Ph.D.) research work of Mr. Nimitt Chokshi, submitted to Nirma University, Ahmedabad, India.

Footnotes

Authorship Contributions

Concept: N.C., M.P., Design: N.C., M.P., Data Collection or Processing: N.C., P.V., S.C., M.P., Analysis or Interpretation: N.C., P.V., M.P., Literature Search: N.C., S.C., Writing: N.C., P.V., S.C., M.P.

Conflict of Interest: The authors declare no conflicts of interest.

Financial Disclosure: The authors are highly grateful to Department of Science and Technology, Fund for Improvement of S&T Infrastructure (grant number: SR/FST/LSI-607/2014), Government of India for providing the necessary funding to establish equipment facility in laboratory.

REFERENCES

1. Programme GT. Global tuberculosis report 2023 [Internet]. 2023. Available from: https://iris.who.int/
2. El-Ridy MS, Abdelbary A, Nasr EA, Khalil RM, Mostafa DM, El-Batal AI, Abd El-Alim SH. Niosomal encapsulation of the antitubercular drug, pyrazinamide. Drug Dev Ind Pharm. 2011;37:1110-1118.
3. Rojanarat W, Nakpheng T, Thawithong E, Yanyium N, Srichana T. Inhaled pyrazinamide proliposome for targeting alveolar macrophages. Drug Deliv. 2012;19:334-345.
4. Sosnik A, Carcaboso AM, Glisoni RJ, Moretton MA, Chiappetta DA. New old challenges in tuberculosis: potentially effective nanotechnologies in drug delivery. Adv Drug Deliv Rev. 2010;62:547-559.
5. Thomas J, Bagyalakshmi J. Design, development and characterization of pyrazinamide niosomal dosage form. Am J Pharmtech Res. 2013;3:532-544.
6. Varma JN, Kumar TS, Prasanthi B, Ratna JV. Formulation and characterization of pyrazinamide polymeric nanoparticles for pulmonary tuberculosis: efficiency for alveolar macrophage targeting. Indian J Pharm Sci. 2015;77:258-266.
7. Chiang SS, Starke JR. Mycobacterium tuberculosis. In: Principles and Practice of Pediatric Infectious Diseases. Elsevier; 2023. p. 806-823.e4.
8. Zhang N, Savic RM, Boeree MJ, Peloquin CA, Weiner M, Heinrich N, Bliven-Sizemore E, Phillips PPJ, Hoelscher M, Whitworth W, Morlock G, Posey J, Stout JE, Mac Kenzie W, Aarnoutse R, Dooley KE; Tuberculosis Trials Consortium (TBTC) and Pan African Consortium for the evaluation of antituberculosis antibiotics (PanACEA) networks. Optimising pyrazinamide for the treatment of tuberculosis. Eur Respir J. 2021;58:2002013.
9. El-Ridy MS, Mostafa DM, Shehab A, Nasr EA, Abd El-Alim S. Biological evaluation of pyrazinamide liposomes for treatment of *Mycobacterium tuberculosis*. Int J Pharm. 2007;330:82-88.
10. Stehr M, Elamin AA, Singh M. Pyrazinamide: the importance of uncovering the mechanisms of action in mycobacteria. Expert Rev Anti Infect Ther. 2015;13:593-603.
11. Singh A, Das SS, Ruokolainen J, Kesari KK, Singh SK. Biopolymer-capped pyrazinamide-loaded colloidosomes: *In vitro* characterization and bioavailability studies. ACS Omega. 2023;8:25515-25524.
12. Pham DD, Fattal E, Tsapis N. Pyrazinamide-loaded poly(lactide-co-glycolide) nanoparticles: optimization by experimental design. J Drug Deliv Sci Technol. 2015;30:384-390.
13. Zielińska A, Carreiró F, Oliveira AM, Neves A, Pires B, Venkatesh DN, Durazzo A, Lucarini M, Eder P, Silva AM, Santini A, Souto EB. Polymeric nanoparticles: production, characterization, toxicology and ecotoxicology. Molecules. 2020;25:3731.
14. Traini D, Young PM. Drug delivery for tuberculosis: is inhaled therapy the key to success? Ther Deliv. 2017;8:819-821.
15. Date AA, Hanes J, Ensign LM. Nanoparticles for oral delivery: design, evaluation and state-of-the-art. J Control Release. 2016;240:504-526.
16. Reinholz J, Landfester K, Mailänder V. The challenges of oral drug delivery via nanocarriers. Drug Deliv. 2018;25:1694-1705.
17. Talegaonkar S, Bhattacharyya A. Potential of lipid nanoparticles (SLNs and NLCs) in enhancing oral bioavailability of drugs with poor intestinal permeability. AAPS PharmSciTech. 2019;20:121.
18. Shete H, Patravale V. Long chain lipid-based tamoxifen NLC. Part I: preformulation studies, formulation development and physicochemical characterization. Int J Pharm. 2013;454:573-583.
19. Khatak S, Mehta M, Awasthi R, Paudel KR, Singh SK, Gulati M, Hansbro NG, Hansbro PM, Dua K, Dureja H. Solid lipid nanoparticles containing anti-tubercular drugs attenuate the *Mycobacterium marinum* infection. Tuberculosis (Edinb). 2020;125:102008.
20. Pandey R, Khuller GK. Solid lipid particle-based inhalable sustained drug delivery system against experimental tuberculosis. Tuberculosis (Edinb). 2005;85:227-234.
21. O'Neil MJ. An Encyclopedia of Chemicals, Drugs, and Biologicals. The Merck Index, 14th edition. 2006.
22. Zhang Z, Lu Y, Qi J, Wu W. An update on oral drug delivery *via* intestinal lymphatic transport. Acta Pharm Sin B. 2021;11:2449-2468.
23. Patel K, Padhye S, Nagarsenker M. Duloxetine HCl lipid nanoparticles: preparation, characterization, and dosage form design. AAPS PharmSciTech. 2012;13:125-133.
24. Rawal S, Patel B, Patel MM. Fabrication, optimisation and *in vitro* evaluation of docetaxel and curcumin co-loaded nanostructured lipid carriers for improved antitumor activity against non-small cell lung carcinoma. J Microencapsul. 2020;37:543-556.
25. Mathur P, Sharma S, Rawal S, Patel B, Patel MM. Fabrication, optimization, and *in vitro* evaluation of docetaxel-loaded nanostructured lipid carriers for improved anticancer activity. J Liposome Res. 2020;30:182-196.
26. Sinhmar GK, Shah NN, Chokshi NV, Khatri HN, Patel MM. Process, optimization, and characterization of budesonide-loaded nanostructured lipid carriers for the treatment of inflammatory bowel disease. Drug Dev Ind Pharm. 2018;44:1078-1089.
27. Kovacevic A, Savic S, Vuleta G, Müller RH, Keck CM. Polyhydroxy surfactants for the formulation of lipid nanoparticles (SLN and NLC): effects on size, physical stability and particle matrix structure. Int J Pharm. 2011;406:163-172.
28. Silva A. Segregated delivery of rifampicin and isoniazid from fixed dose combination bilayer tablets for the treatment of tuberculosis. Br J Pharm Res. 2014;4:1781-1801.
29. Vinchhi P, Patel JK, Patel MM. High-pressure homogenization techniques for nanoparticles. In: Emerging Technologies for Nanoparticle Manufacturing. Cham: Springer International Publishing; 2021. p. 263-285.
30. Gaspar DP, Faria V, Gonçalves LM, Taboada P, Remuñán-López C, Almeida AJ. Rifabutin-loaded solid lipid nanoparticles for inhaled antitubercular therapy: physicochemical and *in vitro* studies. Int J Pharm. 2016;497:199-209.
31. Singh H, Jindal S, Singh M, Sharma G, Kaur IP. Nano-formulation of rifampicin with enhanced bioavailability: development, characterization and *in-vivo* safety. Int J Pharm. 2015;485:138-151.
32. Sinhmar GK, Shah NN, Rawal SU, Chokshi NV, Khatri HN, Patel BM, Patel MM. Surface engineered lipid nanoparticle-mediated site-specific drug delivery system for the treatment of inflammatory bowel disease. Artif Cells Nanomed Biotechnol. 2018;46:565-578.
33. Khatri H, Chokshi N, Rawal S, Patel MM. Fabrication, characterization and optimization of artemether loaded PEGylated solid lipid nanoparticles for the treatment of lung cancer. Mater Res Express. 2019;6:045014.
34. Chokshi NV, Khatri HN, Patel MM. Formulation, optimization, and characterization of rifampicin-loaded solid lipid nanoparticles for the treatment of tuberculosis. Drug Dev Ind Pharm. 2018;44:1975-1989.

35. Pinheiro M, Ribeiro R, Vieira A, Andrade F, Reis S. Design of a nanostructured lipid carrier intended to improve the treatment of tuberculosis. Drug Des Devel Ther. 2016;10:2467-2475.

36. Prabhakar K, Afzal SM, Kumar PU, Rajanna A, Kishan V. Brain delivery of transferrin coupled indinavir submicron lipid emulsions-pharmacokinetics and tissue distribution. Colloids Surf B Biointerfaces. 2011;86:305-313.

37. Subedi RK, Kang KW, Choi HK. Preparation and characterization of solid lipid nanoparticles loaded with doxorubicin. Eur J Pharm Sci. 2009;37:508-513.

38. Ravi PR, Aditya N, Kathuria H, Malekar S, Vats R. Lipid nanoparticles for oral delivery of raloxifene: optimization, stability, *in vivo* evaluation and uptake mechanism. Eur J Pharm Biopharm. 2014;87:114-124.

39. Luo Y, Chen D, Ren L, Zhao X, Qin J. Solid lipid nanoparticles for enhancing vinpocetine's oral bioavailability. J Control Release. 2006;114:53-59.

40. Garanti T, Stasik A, Burrow AJ, Alhnan MA, Wan KW. Anti-glioma activity and the mechanism of cellular uptake of asiatic acid-loaded solid lipid nanoparticles. Int J Pharm. 2016;500:305-315.

41. Gao Y, Sarfraz MK, Clas SD, Roa W, Löbenberg R. Hyaluronic acid-tocopherol succinate-based self-assembling micelles for targeted delivery of rifampicin to alveolar macrophages. J Biomed Nanotechnol. 2015;11:1312-1329.

42. Jain A, Agarwal A, Majumder S, Lariya N, Khaya A, Agrawal H, Majumdar S, Agrawal GP. Mannosylated solid lipid nanoparticles as vectors for site-specific delivery of an anti-cancer drug. J Control Release. 2010;148:359-367.

43. Kumar PV, Asthana A, Dutta T, Jain NK. Intracellular macrophage uptake of rifampicin loaded mannosylated dendrimers. J Drug Target. 2006;14:546-556.

44. Vandal OH, Nathan CF, Ehrt S. Acid resistance in *Mycobacterium tuberculosis*. J Bacteriol. 2009;191:4714-4721.

45. Zhang Y, Huo M, Zhou J, Zou A, Li W, Yao C, Xie S. DDSolver: an add-in program for modeling and comparison of drug dissolution profiles. AAPS J. 2010;12:263-271.

46. Zhang X, Chen G, Zhang T, Ma Z, Wu B. Effects of PEGylated lipid nanoparticles on the oral absorption of one BCS II drug: a mechanistic investigation. Int J Nanomedicine. 2014;9:5503-5514.

47. Benito-Gallo P, Franceschetto A, Wong JC, Marlow M, Zann V, Scholes P, Gershkovich P. Chain length affects pancreatic lipase activity and the extent and pH-time profile of triglyceride lipolysis. Eur J Pharm Biopharm. 2015;93:353-362.

48. Kalaria DR, Sharma G, Beniwal V, Ravi Kumar MN. Design of biodegradable nanoparticles for oral delivery of doxorubicin: *in vivo* pharmacokinetics and toxicity studies in rats. Pharm Res. 2009;26:492-501.

49. Abdelwahed W, Degobert G, Fessi H. Investigation of nanocapsules stabilization by amorphous excipients during freeze-drying and storage. Eur J Pharm Biopharm. 2006;63:87-94.

50. Müller RH, Maassen S, Weyhers H, Mehnert W. Phagocytic uptake and cytotoxicity of solid lipid nanoparticles (SLN) sterically stabilized with poloxamine 908 and poloxamer 407. J Drug Target. 1996;4:161-170.

51. Torcello-Gómez A, Maldonado-Valderrama J, Jódar-Reyes AB, Foster TJ. Interactions between Pluronics (F127 and F68) and bile salts (NaTDC) in the aqueous phase and the interface of oil-in-water emulsions. Langmuir. 2013;29:2520-2529.

52. Wu B, Liu H, Chen G, Zhang Y, Ma Z. Effects of PEGylated lipid nanoparticles on the oral absorption of one BCS II drug: a mechanistic investigation. Int J Nanomedicine. 2014;5503.

53. Chavan SS, Ingle SG, Vavia PR. Preparation and characterization of solid lipid nanoparticle-based nasal spray of budesonide. Drug Deliv Transl Res. 2013;3:402-408.

54. Vivek K, Reddy H, Murthy RS. Investigations of the effect of the lipid matrix on drug entrapment, *in vitro* release, and physical stability of olanzapine-loaded solid lipid nanoparticles. AAPS PharmSciTech. 2007;8:E83.

55. Rowe RC, Sheskey PJ, Quinn ME. Handbook of pharmaceutical excipients. The Pharmaceutical Press and the American Pharmaceutical Association. 2009;6th ed.

56. Barzegar-Jalali M, Adibkia K, Valizadeh H, Shadbad MR, Nokhodchi A, Omidi Y, Mohammadi G, Nezhadi SH, Hasan M. Kinetic analysis of drug release from nanoparticles. J Pharm Pharm Sci. 2008;11:167-177.

57. Ferreira M, Chaves LL, Lima SA, Reis S. Optimization of nanostructured lipid carriers loaded with methotrexate: A tool for inflammatory and cancer therapy. Int J Pharm. 2015;492:65-72.

58. Jose S, Prema MT, Chacko AJ, Thomas AC, Souto EB. Colon specific chitosan microspheres for chronotherapy of chronic stable angina. Colloids Surf B Biointerfaces. 2011;83:277-283.

59. Patel MM. Formulation and development of di-dependent microparticulate system for colon-specific drug delivery. Drug Deliv Transl Res. 2017;7:312-324.

60. Xu J, Bovet LL, Zhao K. Taste masking microspheres for orally disintegrating tablets. Int J Pharm. 2008;359:63-69.

61. Alves R, Reis TV da S, Silva LCC da, Storpírtis S, Mercuri LP, Matos J do R. Thermal behavior and decomposition kinetics of rifampicin polymorphs under isothermal and non-isothermal conditions. Braz J Pharm Sci. 2010;46:343-351.

62. Silva AM, Vieira B, Carmo FA, Amaral L, Silva LCRP, Escudini CS, Lopes M, Rodrigues CR, Ribeiro AJ, Cabral L. Segregated delivery of rifampicin and isoniazid from fixed dose combination bilayer tablets for the treatment of tuberculosis. Br J Pharm Res. 2014;4:1781-1801.

Turk J Pharm Sci 2025;22(2):104-118
DOI: 10.4274/tjps.galenos.2025.12247

ORIGINAL ARTICLE

Comprehensive Investigation of Phytochemical Constituents and Biological Activities of *Scabiosa pseudograminifolia* Hub.-Mor.

Kübra ÖĞÜT[1]*, Gülmira ÖZEK[1], Nilgün ÖZTÜRK[1], Mehmet TEKİN[2], Temel ÖZEK[1],

[1]Anadolu University Faculty of Pharmacy, Department of Pharmacognosy, Eskişehir, Türkiye
[2]Trakya University Faculty of Pharmacy, Department of Pharmaceutical Botany, Edirne, Türkiye

ABSTRACT

Objectives: The aim of this study was to comprehensively investigate the phytochemical composition, including essential oils, fatty acids, and phenolic constituents, and to evaluate the antioxidant and α-amylase inhibitory activities of *Scabiosa pseudograminifolia* Hub.-Mor. (Caprifoliaceae), an endemic species growing in Sivas province of Türkiye. The plant materials were processed to obtain essential oils, and *n*-hexane, methanol, and aqueous extracts for chemical and biological evaluations.

Materials and Methods: Essential oils were obtained by hydrodistillation. Extracts were prepared using *n*-hexane, methanol, and water through maceration. The chemical compositions of the essential oil and fatty acids were analyzed using gas chromatography (GC)-mass spectrometry and GC-flame ionization detector (FID). Phenolic compounds were identified by reverse phase high performance liquid chromatography. Total phenolic and flavonoid contents, antioxidant activity [DPPH, Trolox Equivalent Antioxidant Capacity (TEAC), β-carotene bleaching, and Oxygen Radical Absorbance Capacity assays], and α-amylase inhibitory activity were all evaluated using spectrophotometric methods.

Results: Hexadecanoic acid (30.2%) and linalool (15.6%) were the main volatile compounds in the essential oil of *S. pseudograminifolia. (Z)*-3-Hexenal was the dominant leaf and flower volatile. The primary fatty acids were nonadecanoic and hexadecanoic acids. The aqueous extract exhibited the highest total phenolic (0.52±0.01 mg gallic acid equivalent/$g_{extract}$) and flavonoid (0.081±0.002 mg quercetin equivalent/$g_{extract}$) contents. Among the tested samples, the essential oil showed the strongest TEAC value (2.39±0.15 mM), while the aqueous extract demonstrated potent antioxidant activity in DPPH (IC_{55}: 0.16±0.04 mg/mL) and β-carotene bleaching assays (inhibitory $concentration_{55}$: 0.730±0.001 mg/mL). The α-amylase inhibition levels of the extracts were found to be relatively low. Chlorogenic acid was the predominant phenolic compound.

Conclusion: This study presents the first phytochemical and biological investigation of *S. pseudograminifolia* Hub.-Mor., an endemic species from Türkiye. Essential oil analysis revealed hexadecanoic acid and linalool as major constituents, while nonadecanoic and hexadecanoic acids were predominant among the fatty acids. The methanol extract showed strong antioxidant activity, and chlorogenic acid was identified as a key phenolic compound. These findings support the potential of this species as a valuable source of natural antioxidants.

Keywords: *Scabiosa pseudograminifolia*, essential oil, fatty acids, phenolics, biological activity

INTRODUCTION

The genus *Scabiosa* L. is a member of the Dipsacaceae subfamily, which is a part of the *Caprifoliaceae* family.[1,2] Although it originated in the Mediterranean region and the Near East, it is a family that has spread to different regions, from Northern Europe to East Asia, from Central Africa to South Africa.[3] The genus *Scabiosa* encompasses a total of 80 species worldwide, including 43 found in Europe, while the remaining species are distributed across Africa and Asia.[4] About 34 *Scabiosa* species were recorded in the flora of Türkiye.[5] The nomenclature of the genus is derived from the Latin term "scabiosus or scabies," *Sarcoptes scabiei* L., known as the itching mite or scab beetle,

***Correspondence:** kubraogut@anadolu.edu.tr, **ORCID-ID:** orcid.org/0000-0002-9921-5866
Received: 25.09.2024 , **Accepted:** 16.02.2025 **Publication Date:** 14.05.2025

Cite this article as: ÖĞÜT K, ÖZEK G, ÖZTÜRK N, TEKİN M, ÖZEK T. Comprehensive investigation of phytochemical constituents and biological activities of *Scabiosa pseudograminifolia* Hub.-Mor. Turk J Pharm Sci. 2025;22(2):104-118

which causes highly contagious parasitic skin infections. It is thought to be given the name *Scabiosa* due to the use of multiple species for its treatment.[6] Although the members of the genus *Scabiosa* are generally known as "Uyuz Otu" in Türkiye, they have recently been called "Yazı Süpürgesi, Gicikotu, Kavurotu, Puk, Zivan".[7]

The literature review revealed that different species of the genus *Scabiosa* are commonly employed in traditional medicine to treat specific health issues. Specific species of *Scabiosa* are extensively utilized across various industries, including food, medicinal products, and skincare;[8] *S. columbaria* L. is traditionally employed for treating diphtheria, and *S. comosa* Fisch. Ex Roem. and Schult. is utilized in Mongolian and Tibetan traditional medicine for the treatment of liver ailments.[9] Also, qingganjiuwei powder, consisting of nine herbal components including *S. comosa*, is frequently used as an anti-fibrosis agent for patients with chronic liver disease in Inner Mongolia. This medication is approved by the Inner Mongolia Region Drug Administration for the treatment of liver disorders.[10] *S. atropurpurea* L. has been employed as a diuretic agent for acne, while S. succisa L. has been utilized in the treatment of asthma, bronchial pneumonia, and influenza. Furthermore, the external application of herbs from this particular species has been suggested for the treatment of respiratory, urogenital, and some skin conditions, such as herpes, ringworm, and scabies, as well as ulcers.[11] *S. stellata* L. is utilized for the treatment of heel fissures.[12] *S. tschilliensis* Grüning is utilized for hepatic disorders.[13]

With the phytochemical studies of a few *Scabiosa* species, the presence of coumarins, flavonoids, iridoids, pentacyclic triterpenoids, iridoid glucosides, and monoterpenoid glucoindole alkaloids has been reported.[9,14-19] Depending on this phytochemical content, the *Scabiosa* genus has demonstrated antidiabetic, hepatoprotective, analgesic, anti-inflammatory, antioxidant, antibacterial, anti-melanogenesis, anti-tyrosinase and anti-parasitic properties.[10]

To the best of our knowledge, no previous study has investigated the phytochemical composition or biological activities of *S. pseudograminifolia* Hub.-Mor., an endemic species growing in Türkiye. The aim of the study was to comprehensively evaluate the chemical composition, including essential oils, fatty acids, and phenolic constituents, and to assess the antioxidant and α-amylase inhibitory activities of different extracts of this species.

MATERIALS AND METHODS

Chemicals

The chemicals utilized in this study: *n*-hexane, dimethyl sulfoxide (DMSO), methanol, ethanol, formic acid, hydrochloric acid, glacial acetic acid, Folin-Ciocalteu (FC) reagent, boron trifluoride (BF_3) reagent, and butylated hydroxyanisole (BHA), were purchased from Sigma-Aldrich (USA). The lipid extraction kit, α-amylase produced from porcine pancreas (Type VI-B, ≥10 units/mg solid), and acarbose were purchased from Sigma (USA). The standard *n*-alkanes C_8-C_{40} were purchased from Fluka in Buchs. The phenolic acids utilized in this investigation, namely caffeic acid, chlorogenic acid, ferulic acid, gallic acid (GA), protocatechuic acid, p-hydroxybenzoic acid, syringic acid, and vanillic acid, along with propylparaben as an internal standard, were acquired from Sigma-Aldrich (St. Louis, MO, USA) or Merck (GmbH, Darmstadt, Germany). The rest of the chemicals utilized in this study were obtained from Merck (Germany).

Instruments

An Agilent 5975 gas chromatography-mass spectrometry (GC-MS) system manufactured by Agilent Technologies (Santa Clara, CA, USA) was used to conduct GC-MS analyses. The SPME technique for volatiles was performed using a manual SPME holder (57330-U, SUPELCO, Bellefonte, PA) and the polydimethylsiloxanedivinylbenzene 65 µm fiber (blue type). In the microtiter assays, the sample solutions were pipetted into microplate wells using an Eppendorf® Xplorer® 12-channel pipettor with a volume range of 10-300 µL. Two types of microplates were acquired from Sigma-Aldrich: a 96-well flat-bottom white polystyrene microplate, which was non-sterile (Greiner), and a 96-deep-well round-bottom polypropylene plate with a volume of 2.2 mL. The absorbance readings were recorded using a BioTek Powerwave XS microplate reader. Agilent 1100 series autosampler system from Agilent, GL Sciences Inc. (Waldbronn, Germany). The equipment was outfitted with a system controller, a DAD detector (G 1315B, 280 nm), and a quaternary LC pump (G1311A). The separation method was conducted using a Zorbax Eclipse XDB-C18 column (150 mm, 4.6 mm, 5 µm particle size), manufactured by Agilent in Waldbronn, Germany. The Human UP 9000 System (18 mW)'s water purification system provided ultrapure water. The liquid chromatographic system (Shimadzu LC 10Avp, Kyoto, Japan) had an in-line degasser, pump, and controller connected to an SPD-M10Avp photodiode array detector with an automatic injector and Class VP chromatography manager software. A reverse-phase C18 Ultrasphere column (INERTSIL, Waldbronn, Germany), (100x4.6 mm i.d. 3 microns) was used to analyze phenolic acids.

Plant material

The plant material *S. pseudograminifolia* Hub.-Mor. was collected at Sivas, Kangal-Gürün junction. The identification of the plant was conducted by Prof. Dr. Mehmet Tekin (Trakya University Faculty of Pharmacy, Department of Pharmaceutical Botany) and it was registered in Trakya University Faculty of Pharmacy Herbarium (code: 1621).

Hydrodistillation of essential oil

The essential oil was obtained from air-dried plant parts by hydrodistillation for 3 hours using clevenger-type equipment, following the techniques outlined in the European Pharmacopoeia.[20] The essential oil yield was calculated on a moisture-free basis. The oil underwent dehydration using anhydrous sodium sulfate and was thereafter preserved in amber glass vials at 4 ˚C until the gas chromatographic and biological activity analyses.

Microsteam distillation-solid phase microextraction (MSD-SPME)

In the experiment, 1.0 g of the leaf and flower parts were separately added to a 25 mL flask containing 3.0 mL of water.[21] A distillation head with a septum for SPME holder needle entrance and a condenser was attached to a flask that was designed explicitly for refluxing rather than distillation. In the pre-experiment, the fibre underwent conditioning at a temperature of 250 ˚C for 15 minutes. The electric heater was used gradually for the evaporation of volatiles from the sample. Once the evaporation started, the fibre was removed through the needle and placed in the headspace above the samples. The MSD-SPME process was conducted at the boiling point of water. The equilibrium time refers to the interval between the introduction of SPME fibre into the flask and the commencement of the extraction process. A sufficient extraction time of 3.0 minutes was employed following the establishment of equilibrium. Following the extraction time, the carefully loaded SPME fibre was withdrawn into the needle. Later, the needle was meticulously separated from the plug and employed for thermal desorption at the inlet port of gas chromatography-mass spectrometry (GC/MS) equipment.

Lipid extraction and fatty acid derivatization

Fatty acid research involved a series of consecutive steps, which included preparing the sample, extracting total lipids, methylating fatty acids, and then analyzing the fatty acid methyl esters using GC-MS/flame ionization detector (FID).[22] The lipid extraction kit was employed to extract the total lipids from the aerial parts of the plant material. The extraction of lipids requires a dual solvent partition mechanism, which comprises an aqueous and a lipophilic solvent (for example, chloroform). The lipids were retained in the lower layer of chloroform, whereas the water-soluble chemicals were retained in the upper layer of methanol-water. In the experiment, the mill-ground plant material (0.15 g) was homogenized in extraction solvent (3.0 mL) of the kit. Following the homogenization and vortexing, 0.5 mL of the buffer solution supplied in the kit was added to the mixture and vortexed. Following that, the organic solvent phase was filtered through a special filter of the kit. 200 µL of the extract was dried under nitrogen gas and then subjected to transesterification with BF_3-methanol reagent. The mixture was subjected to reflux for 1 h at 95 ˚C. After that, *n*-hexane (1.0 mL) and distilled water (1.0 mL) were added to the reaction vessel. The mixture was vortexed and centrifuged at 500 rpm for 5 minutes. The uppermost layer, hexane, was transported in a vial, concentrated under nitrogen gas, and thereafter injected into the GC-MS/FID system.

Preparation of extracts

The extracts of *S. pseudograminifolia* were prepared by fractionating the same powdered plant material with n-hexane, methanol, and water (plant material/solvent ratio 1:10). For each extract, the maceration process involved continuous shaking for 48x2 hours under ambient conditions. The supernatants obtained were filtered using Whatman filter paper. Subsequently, the organic solvents were removed from the filtrates using reduced pressure to obtain dry extracts. However, the aqueous extracts were dried using the lyophilization technique. The dried extracts were stored in amber glass vials at 4 ˚C until further analysis.[23,24]

The dried extracts were solved in 10% DMSO-methanol (10 mg/mL) and utilized as stock solutions before biological activity screening, total phenolic content assessment, and total flavonoid content evaluation.

GC/MS analysis

The GC-MS analysis was conducted using the previously stated settings.[25] An Agilent Innowax FSC column, 60 m x 0.25 mm, with a film thickness of 0.25 µm was used, along with a carrier flow rate of 0.8 mL/min. The GC oven was initially set at 60 ˚C for 10 minutes. It was then gradually increased to 220 ˚C at a rate of 4 ˚C per minute and held at that temperature for 10 minutes. Finally, the temperature was increased to 240 ˚C at a rate of 1 ˚C per minute. The split ratio was adjusted to 40:1, while the injector temperature was set to 250 ˚C. The MS spectra were recorded at 70 eV, covering a mass range of 35 to 450 *m/z*.

Gas chromatography analysis

The GC assay was conducted with Agilent 6890N GC equipment. To achieve an equivalent elution sequence as observed in GC-MS, the elution line was divided between MS and FID detectors, and a single injection was conducted using the same column and suitable operational parameters. The temperature of the FID was set at 300 ˚C. The contents of the essential oil and fatty acid methyl esters were determined by co-injecting them with standards procured commercially or obtained from pure organic sources whenever feasible. Furthermore, the confirmation of compound identities was achieved through the comparison of their mass spectra with records available in the Wiley-NIST GC/MS Library (Wiley, NY, USA), MassFinder software 4.0 (Dr. Hochmuth Scientific Consulting, Hamburg, Germany, and Adams Library".[26] Confirmation was accomplished by utilizing the exclusive Başer Library of Essential Oil Constituents database, which was acquired through chromatographic investigations conducted on pure compounds under identical equipment and conditions. For confirmation of identified compounds, each of the compounds' relative retention indices was calculated with a C8-C40 *n*-alkane standard mixture (Fluka, Buchs, Switzerland). The FID chromatograms were used to calculate the relative percentage of the separated individual compounds without normalization.

Reverse phase high performance liquid chromatography (RP-HPLC) analysis

The extracts of *S. pseudograminifolia were subjected to RP-HPLC analysis to get* a profile of the phenolic acids. The chromatographic separation was conducted using two solvent systems: (A) a mixture of methanol, water, and formic acid in a ratio of 10:88:2 *(v/v/v)*, (B) a mixture of methanol, water, and formic acid in a ratio of 90:8:2 *(v/v/v)*, as reported previously.[27] The study employed a gradient elution program in the following manner: from 15-20 min, to 85% A; from 20-30 min, to 50% A;

from 30-35 min, to 0% A; and from 36-42 min, back to 100% A. The flow rate was 1 mL/min, and the injection volume was 10 µL. Signals were detected at 280 nm. The relevant extracts were dissolved in a mixture of methanol and water (1:1, v/v) and injected into the HPLC.

The peaks were identified using the following method: the separate phenolic acid standards were dissolved. The rate of peak normalization (peak area/peak retention time) of the relevant phenolic acids, was determined by calculating the integrated peak areas and their corresponding retention times. The quantities of these phenolic acids were then measured in the associated extracts using their calibration curves.

Total phenol content

The extracts of *S. pseudograminifolia* were evaluated for the total phenolic content measured as gallic acid (GA) equivalent (GAE) using a Folin-Ciocalteu (FC) reagent, according to previous procedure.[28] Methanol was used to prepare the stock solutions of the extracts and GA. The experimental procedure involved the combination of 20 µL of the sample solution (extract/GA), 1560 µL of ultrapure water, and 100 µL of FC reagent into a 96 deep-well plate. Following an incubation period of 1-8 minutes, 300 µL of a sodium carbonate solution (20%) was added to the mixture. The mixture was subjected to a 2-hour incubation period (at 25 °C in the dark). Subsequently, 300 µL of the mixture was put into a 96-well microplate. The absorbance readings at a wavelength of 760 nm were subsequently compared to a GA calibration curve, which was established using a 5-point calibration range spanning from 0.01 to 1.0 mg/mL. The experiment was repeated three times. The calibration curve for GA had a regression coefficient r^2 of 0.9992, calculated as y=0.7489x+0.0551. The results were expressed as mg GAE/$g_{extract,}$ and values are presented as mean ± standard deviation (SD) from triplicate experiments.

Total flavonoid content

The extracts of *S. pseudograminifolia* were evaluated for the total flavonoid content measured as quercetin equivalent (QE) using aluminum chloride as a reagent. In the experiment, 80 µL of the sample solution (extract/quercetin), 80 µL of $AlCl_3$, and 1840 µL of absolute ethanol were added into 96-deep-well. In the blank samples, 10 µL of acetic acid (15%) was added instead of aluminum chloride. Following an incubation period of 40 minutes, 300 µL of the mixture was transferred into the 96-well microplate. The absorbance values were measured at a wavelength of 415 nm using a microplate reader. The quantification of total flavonoid content was performed using a calibration curve based on quercetin. A 5-point calibration was used to plot the calibration curve within the concentration range of 0.01-1.0 mg/mL.[29] The calibration curve for quercetin had a regression coefficient r^2 of 0.9996, calculated as y = 1.857x + 0.0088. The average content value was computed using a standard error of ±. The results were quantitatively represented as mg QE/$g_{extract}$.

Trolox Equivalent Antioxidant Activity (TEAC) Test

The antioxidant potential of the extracts and essential oils of *S. pseudograminifolia* was assessed using ABTS+•, respectively, and calculated as Trolox equivalent.[30] At first, a solution of ABTS+• (7 mM) and potassium persulfate was prepared in pure water. Following a 16-hour incubation period in the dark, the aliquot of the solution was diluted with absolute ethanol until it reached an absorbance range of 0.700-0.800 at a wavelength of 734 nm. The extracts, essential oil (2 mg/mL), and Trolox (five dilutions ranging from 3.0 to 0.125 mM) were made in methanol (with 10% DMSO) as stock solutions. The experiment involved combining 10 µL sample (essential oil, extract, Trolox) with a 990 µL ABTS solution in a 96-deep well plate. Following a 30-minute incubation in the dark, a decrease in absorbance was recorded at a wavelength of 734 nm using a microplate reader. The ABTS•+ scavenging activity of the samples was quantified as TEAC and was determined using a linear equation calculated for Trolox (y=29.997x-0.6918). The calibration curve's regression coefficient was calculated to be r^2=0.9989. The experiment was conducted three times.

Free Radical Scavenging Effect (DPPH) Test

The samples' ability to scavenge DPPH radicals was assessed using a modified version of the Brand-Williams method.[31] The extracts, essential oil (2 mg/mL), and standard inhibitor (0.1 mg/mL) were prepared in methanol with 10% DMSO as stock solutions. In the experiment, 100 µL of the sample solution was combined with 100 µL of DPPH solution (0.08 mg/mL in MeOH) in 96-well flat-bottom plate cells. The mixtures were incubated in the dark for 30 minutes. The reduction in absorbance at a wavelength of 517 nm was recorded with the microplate reader. The gallic acid solution was employed in this test as the positive control. The experiments were conducted three times. The samples' free radical scavenging activity was quantified as a percentage of inhibition, which was determined using the following equation:

$$\%\ Inh = \left(\frac{Abs_{control} - Abs_{sample}}{Abs_{control}}\right) \times 100$$

The absorbance of the control includes all reagents except the test substance, is indicated as $Abs_{control,}$ Abs_{sample} represents the absorbance of the sample after the addition of DPPH (Version 12.0).

Lipid Peroxidation Inhibition (β-Carotene Bleaching Test)

The present study aimed to assess the inhibitory impact of extracts and essential oils on lipid peroxidation using the β-carotene bleaching test with some modifications.[32] A chloroform solution containing 1 mg/mL of β-carotene was prepared and subsequently combined with 200 mg of Tween-20 and 25 µL of linoleic acid to generate an emulsion. Chloroform was completely evaporated using a vacuum (at a temperature of 40 °C) and then nitrogen gas. Following that, oxygenated ultrapure water (50 mL) was added, and the mixture was vortexed.

Before each experiment, the emulsion solution was freshly prepared and stored in the dark. The standard antioxidant employed in the study was BHA. The stock solutions of the

samples were prepared in methanol (containing 10% DMSO) at a concentration of 5 mg/mL. In the experiment, 60 µL of a sample (extract/essential oil/BHA) was combined with 250 µL of an emulsion solution within a 96-well plate. The absorbance values were measured at 50 °C every 15 minutes for a total of 105 minutes at a wavelength of 492 nm. The experiments were conducted three times. The results of the experiment were calculated using the following formula:

$$\%\,AA = \left(1 - \frac{(Abs_{0\ sample} - Abs_{120\ sample})}{(Abs_{0\ control} - Abs_{120\ control})}\right) \times 100$$

Where AA is the antioxidant activity, $Abs_{0\ sample}$ and Abs_{120} sample are the absorbance values of the sample at 0 min and 120 min, and Abs_{0} control and Abs_{120} control are the absorbance values of the control at 0 min and 120 min. In this context, AA represents the antioxidant activity, whereas $Abs_{0\ sample}$ and $Abs_{120\ sample}$ indicate the absorbance values of the sample at 0 minutes and 120 minutes, respectively. Similarly, $Abs_{0\ control}$ and $Abs_{120\ control}$ represent the absorbance values of the control at 0 minutes and 120 minutes.

Oxygen Radical Absorbance Capacity (ORAC) Test

The oxygen radical absorption capacity of the extracts and essential oil of *S. pseudograminifolia* was assessed using a microtiter assay[33] with certain modifications. A fluorescent probe was employed in the assay, while 2,2'-azobis(2-amidinopropane) dihydrochloride (AAPH) was utilised as a free radical generator. The standard antioxidant employed in the study was Trolox. The stock solution was prepared by dissolving 15 mg of fluorescein in 10 mL of phosphate buffer solution (0.075 M, pH 7.4). The resulting solution was stored in the dark at 4 °C. In a 96-well plate, 25 µL of a sample (extract/essential oil/trolox) and 150 µL of fluorescein solution were combined and incubated for 30 minutes at 37 °C in the dark. The plate was shaken for 10 seconds following the addition of 25 µL of AAPH reagent after incubation. The fluorescence values were measured at 37 °C at 60-second intervals over 180 minutes. The excitation wavelength was 485 nm, and the emission wavelength was 535 nm. The under the curve (AUC) values were determined using the *SigmaPlot* program. The net AUC values were obtained using the following formula:

NET AUC= AUC_{sample}-AUC_{blank}

The standard curve was derived by graphing the net AUC and the linear relationship between the concentration of Trolox and net AUC. The calculation of ORAC values was performed using Trolox equivalents. The experiments were conducted three times.

α-Amylase Inhibition Test

Following the previously reported assay,[34] of the extracts and essential oil were tested for their capacity to inhibit the α-amylase enzyme. The inhibitor of the α-amylase enzyme employed in this study was acarbose. The extract and essential oil solutions were prepared in methanol (containing 10% DMSO) in appropriate quantities. For the experiment, 50 µL of the sample (extract/essential oil/acarbose) and 50 µL of an enzyme solution (0.8 U/mL in 20 mM sodium phosphate buffer pH 6.9) were added to a 96-well plate. The mixture was then incubated for 10 minutes in the dark at 37 °C. Following the incubation period, 50 µL of a starch solution (0.05%) was added, and the resulting mixture was incubated for an additional 10 minutes in the dark at 37 °C. Following the incubation period, the reaction was terminated by adding 25 µL of HCl solution (1M). Finally, 100 µL of I_2/KI reagent solution was added to the wells. In the absence of an enzyme solution, a buffer solution was added to the blank samples. All the reagents were present in the control wells except for the sample. The plate reader was used to record absorbance readings at a wavelength of 630 nm. The calculation of the inhibition was done using the following formula:

$$Inh = \left(\frac{(Abs_{0\ control} - Abs_{control\ blank}) - (Abs_{sample} - Abs_{sample\ blank})}{(Abs_{0\ control} - Abs_{control\ blank})}\right) \times 100$$

Statistical analysis

Quantitative data obtained from the biological activity assays were statistically evaluated. All antioxidant and α-amylase inhibition experiments were performed in triplicate, and the results are presented as mean ± standard deviation. Statistical differences between the samples were assessed using one-way ANOVA followed by Tukey's multiple comparison test, with significance accepted at $p<0.05$. Analyses were carried out using IBM SPSS Statistics version 21, developed by IBM Corp., headquartered in New York, USA.

RESULTS

The phytochemical profile of *S. pseudograminifolia* and its *in vitro* antioxidant and anti-α-amylase effects have been determined for the first time within the scope of this investigation. All these studies have contributed to closing the knowledge gap regarding *S. pseudograminifolia*. The leaves of *S. pseudograminifolia* have undergone extraction using solvents of different polarities, namely *n*-hexane, methanol, and aqueous solution. Table 1 displays the extract yields.

Chemical composition of essential oil and volatile constituents

The constituents that make up the essential oil from *S. pseudograminifolia* aerial parts have been identified using GC-MS and GC-FID techniques, and the results are presented in Table 2 and Supplementary Figure 1. In addition to this, the

Table 1. Yields of extracts

Extract type	Extract code	Amounts of extract, g	Yield*, %
n-Hexane extract	SP_H	0.151	0.43
Methanol extract	SP_M	4.733	13.44
Aqueous extract	SP_W	3.057	8.68
Essential oil	SP_{EO}	0.008	0.02

*Yield was calculated based on air dried plant weight

Table 2. Hydrodistilled essential oil compounds and volatile constituents obtained from *S. pseudograminifolia* aerial parts, leaves, and flowers using the MSD-SPME technique

RRIexp.	RRIlit.	Compound	%			References
			Hydrodistilled aerial parts	MSD-SPME of leaves	MSD-SPME of flowers	
945	945	2-Ethyl furan	0.3			[35]
950	949	2,4-Dimethylfuran	0.7			[36]
1047	1050	(*E*)-2-Butenal		0.8	0.5	[37]
1052	-	4-Methyl 2,4-pentadienal#	0.8			
1087	1098	Hexanal		0.5	4.4	[38]
1187	1187	Heptanal			0.6	[39]
1191	1149	*(E)*-3-Hexenal	1.2			[39]
1202	1198	Limonene		0.7	1.2	[40]
1211	1215	Isoamyl alcohol			1.5	[41]
1212	1211	1,8-Cineole		0.1		[40]
1223	1244	Amyl furan		0.1		[42]
1225	1225	*(Z)*-3-Hexenal		34.0	29.1	[40]
1230	1231	*(E)*-2-Hexenal			1.5	[43]
1251	1253	γ-Terpinene			0.1	[44]
1256	1231	Isocumene	8.0			[45]
1260	1262	(E)-β-Ocimene		0.2	0.2	[44]
1263	1260	Pentanol			0.2	[46]
1285	1280	*p*-Cymene		0.2	0.3	[47]
1295	1282	Terpinolene		0.2	0.3	[40]
1306	1287	Octanal		0.2	0.3	[40]
1319	1319	4-Nonanone			0.2	[48]
1331	1332	(*E*)-2-Heptenal			0.3	[37]
1332	1356	Allyl caproate		0.6		[49]
1344	1337	6-Methyl-5-hepten-2-one		1.3	0.6	[40]
1363	1351	Hexanol		1.7	7.7	[40]
1377	1340	*(E)*-3-Hexene-1-ol			0.2	[50]
1400	1400	Tetradecane		0.4		[42]
1403	1380	*(Z)*-3-Hexene-1-ol		0.9	2.0	[40]
1407	1391	2-Nonanone			0.1	[40]
1409	1392	Nonanal		1.1	0.6	[40]
1410	1400	*(E)*-2-Hexene-1-ol			0.7	[40]
1412	-	3-Octene-2-one#			0.4	[51]
1413	1388	4,8-Dimethyl-1,3,7-nonatriene		1.3		[42]
1443	1428	*(E)*-2-Octenal		0.4	0.4	[52]

combined MSD-SPME technique was utilized to investigate the plant's volatile constituents. The plant's leaves and flowers were analyzed separately for this purpose. The hydrodistilled essential oil compounds, in the order in which they were eluted

Table 2. Continued

RRIexp.	RRIlit.	Compound	%			References
			Hydrodistilled aerial parts	MSD-SPME of leaves	MSD-SPME of flowers	
1450	1444	1-Octen-3-ol		0.1	0.4	[40]
1454	1446	*trans*-Linalool oxide		0.2	0.3	[40]
1463	1449	Heptanol			0.2	[40]
1471	1479	*(E,Z)*-2,4-Heptadienal		1.9	0.4	[42]
1476	1461	Furfural			0.3	[40]
1496	1490	2-Ethyl hexanol		3.2	4.3	[53]
1499	1496	Decanal			0.3	[40]
1502	1497	*(E,E)*-2,4-Heptadienal		1.5	0.8	[53]
1514	1535	β-Burbonene		0.4		[54]
1520	1524	*(E,Z)*-3,5-Octadiene-2-one		0.9	0.8	[55]
1528	1515	Camphor		0.3	0.2	[40]
1541	1519	Benzaldehyde		1.8	3.9	[40]
1553	1543	Linalool	15.6	3.1	5.0	[40]
1559	1552	Octanol		1.3	1.1	[40]
1568	1573	*(E,E)*-3,5-Octadiene-2-one		0.5	0.6	[56]
1586	1566	(*E,E*)-2,6-Nonadienal			0.6	[47]
1589	1583	(*E,Z*)-2,6-Nonadienal			0.3	[57]
1600	1600	Hexadecane		0.5		[58]
1612	1614	Furfuryl alcohol		1.1		[59]
1619	-	4-Methyl-(2E)-undecene#		3.6	2.5	[39]
1630	-	6-Methyl-1-octanol#		4.3	2.5	[39]
1632	1638	β-Cyclocitral		1.7		[60]
1641	1616	1-Ethyl-1H-pyrrole-2-carbaldehyde#			0.2	[61]
1660	1656	Nonanol		2.9	2.1	[40]
1662	1665	Safranal		0.8		[62]
1663	1663	Phenylacetaldehyde		0.5	2.1	[63]
1678	1648	Acetophenone			0.7	[40]
1702	1670	Methyl chavicol		0.7	0.2	[40]
1719	1706	α-Terpineol	2.5	0.7	0.9	[64]
1726	1712	Dodecanal			0.5	[40]
1743	-	2-(1-Cyclopenten-1-yl) furan#		0.7		[39]
1748	-	Methoxy phenyl oxime#		1.0	0.8	[39]
1770	1751	Carvone		0.2	0.4	[65]
1775	1753	Ethyl benzaldehyde		0.3	0.3	[66]
1790	1762	Naphthalene		0.6	0.4	[67]

Table 2. Continued

RRIexp.	RRIlit.	Compound	%			References
			Hydrodistilled aerial parts	MSD-SPME of leaves	MSD-SPME of flowers	
1796	-	Octenyl cyclopentene#		2.8		39
1797	2025	*(E)*-Cinnamaldehyde			0.2	68
1807	1797	Methyl acetophenone§		0.4	0.4	69
1815	1775	Cuminaldehyde		1.2	0.9	70
1816	1839	Geraniol	2.3			40
1824	-	2,2,4-Trimethyl-3-carboxyisopropyl-isobutyl pentanoate#	0.9			39
1842	1845	*(E)*-Anethole		2.5	2.0	60
1860	1867	*(E)*-Geranyl acetone		1.2	0.3	71
1872	-	2,2,4-Trimethyl pentane-1,3-diol diisobutyrate#			0.2	39
1876	-	2-Naphthalenol		0.3		39
1878	1880	1-Isobutyl 4-isopropyl 3-isopropyl-2,2-dimethylsuccinate		0.6		58
1886	1872	2-Methyl naphthalene		0.1		72
1894	1865	Benzyl alcohol		0.4	0.2	40
1941	1904	Phenylethyl alcohol			0.4	40
1964	1936	(E)-β-Ionone		1.6	0.2	40
1995	1996	Benzothiazole		0.3	0.2	73
2022	1992	Phenol			0.1	40
2023	1995	trans-β-Ionone-5,6-epoxide		0.5		42
2025	2028	Methyl eugenol		0.2	0.1	74
2036	2041	Isopropyl myristate		0.1		75
2037	2015	Pentyl octyl benzene		0.1		76
2041	2038	Phenyl ether		0.2		77
2065	2058	Anisaldehyde		0.2	0.2	78
2066	2072	Lilial		0.2	0.1	79
2130	2131	Hexahydro farnesyl acetone	3.0	0.4	0.4	80
2144	2120	*(Z)*-3-Hexen-1-ol benzoate		0.1		81
2182	2179	3,4-Dimethyl-5-pentylidene-2(5H)-furanone		0.6	0.2	42
2194	2192	Nonanoic acid *(=Pelargonic acid)*	1.5			82
2202	2105	Thymol		0.2	0.2	83
2243	2240	Carvacrol	1.3	3.0	1.9	83
2451	2449	Dodecanoic acid *(=Lauric acid)*	10.9			84

Table 2. Continued

RRIexp.	RRIlit.	Compound	%			References
			Hydrodistilled aerial parts	MSD-SPME of leaves	MSD-SPME of flowers	
2670	2670	Tetradecanoic acid *(=Myristic acid)*	9.1			[85]
2820	2822	Pentadecanoic acid *(=Pentadecylic acid)*	1.6			[86]
2877	2890	Hexadecanoic acid (*=Palmitic acid)*	30.2			[87]
		Total	89.9	96.7	94.7	

#: Tentative identification from Wiley-NIST digital library, MSD-SPME: Microsteam distillation-solid phase microextraction, RRI_{exp}: Experimentally calculated retention index, RRI_{lit}: Retention index from literature

on the HP-Innowax FSC column, along with their relative percentages, retention indices, and method of identification, are presented in Supplementary Figures 2 and 3, and in Table 2, as well as volatile constituents extracted with the MSD-SPME technique.

Fatty acid chemical composition

This research enabled the initial assessment of the fatty acid composition of *S. pseudograminifolia*. The lipids of *S. pseudograminifolia* were isolated from the leaves and flowers with microscale techniques and subjected to transesterification with BF_3 reagent for subsequent GS-FID/MS analysis. Results of chromatographic separation and identification of the methyl ester derivatives are presented in Supplementary Figures 4 and 5, and Table 3, respectively.

Total phenolic, flavonoid contents and biological activity results

The phenolic compounds make an important contribution to the total antioxidant potential of natural products. So, basically, their phenolic contents were specified, and the characterization of the extracts was to be determined. The total phenolic contents of *S. pseudograminifolia* extracts were assessed using a FC reagent, and the results were presented in terms of GA equivalent. The total flavonoid content of *S. pseudograminifolia* extracts was assessed as the QEs. The results of spectrophotometric assays are presented in Table 4.

HPLC analysis results

Some phenolic acids in the *S. pseudograminifolia* extracts have been determined using an RP-HPLC gradient system with a modified technique.[27] The HPLC results of *S. pseudograminifolia* aqueous and methanol extracts are shown in Table 5. The amounts are given in $\mu g/g_{extract}$.

DISCUSSION

Chemical composition of essential oil and volatile constituents

In the GC-MS study of *S. pseudograminifolia,* seventeen compounds accounted for 89.9% of the total identified components. Hexadecanoic acid (30.2%), linalool (15.6%), and dodecanoic acid (10.9%) are the main components of the essential oil from the of *S. pseudograminifolia* aerial parts derived through the hydrodistillation.

We also used the MSD-SPME technique to examine volatile components of leaves and flowers. From the leaves of *S. pseudograminifolia*, we found 68 volatile constituents, which made up 96.7% of all the components found using the MSD-SPME. The main volatile components were *(Z)*-3-hexenal (34.0%), 6-methyl-1-octanol (4.3%), 4-methyl-(2*E*) undecene (3.6%), and linalool (3.1%). Additionally, from the flowers of *S. pseudograminifolia*, we found 72 volatile constituents, which made up 95% of all the components found using the MSD-SPME. The main volatile components were *(Z)*-3-hexenal (29.1%), hexanol (7.7%), linalool (5%), and hexanal (4.4%). Table 2 presents these findings.

In the published literature, there are few gas chromatographic investigations of essential oils from aerial parts *Scabiosa* species. In *S. columbaria* subsp. *columbaria* var. *columbaria* L. the major volatile compounds, were identified as 4-octadecenal (30.0%) in the flower and carvone (35.44%) in the leaf.[88] The main components of the essential oil were tricosane (15.5%), rosifoliol (15.3%), (*E*)-caryophyllene (10.7%), and α-humulene (7.9%) in the aerial parts of *S. flavida* Boiss. & Hausskn.[89] In the leaf essential oil of *S. maritima* L., the main components were hexahydrofarnesyl acetone (42.0%) and dodecanoic acid (17.2%). In the inflorescence of *S. maritima,* the main components of essential oil were 3-vinyl pyridine (23.5%) and hexahydrofarnesyl acetone (19.4%).[90] α-Thujone (34.4%), camphor (17.5%), and β-thujone (15.29%) constituted the major compounds of the fruit oil of *S. arenaria* Forssk from Tunisia, while chrysanthenone (23.4%), together with camphor (12.9%) and α-thujone (10.7%), were the main constituents essential oil of the leaf and stem. In the case of the flower oil, also chrysanthenone (38.5%), camphor (11.7%), and α-thujone (9.5%) were reported as the major compounds.[4]

The volatile components of the aerial parts was compared to that of leaves and flowers, revealing that they did not have the same major compounds. In addition, it has been observed that the chemical composition of *S. pseudoraminifolia* differs from that of other *Scabiosa* species.

Fatty acid chemical composition

A total of 20 fatty acids, accounting for 99.8% of the total oil content, were identified in the leaves of *S. pseudograminifolia*, while 23 fatty acids were detected in the flower samples, representing 78.3% of the total oil. The predominant components in the leaves were methyl nonadecanoate (21.9%), methyl hexadecanoate (20.8%), and *(Z,Z,Z)*-9,12,15-methyl octadecatrienoate. In the flowers, methyl hexadecanoate

(18.3%), *(Z,Z)*-9,12-methyl octadecadienoate (12.4%), and *(Z,Z,Z)*-9,12,15-methyl octadecatrienoate (12.2%) were the major constituents.

According to the literature, the leaves of *Scabiosa* species typically contain up to 19 fatty acids, ranging from lauric acid (C12:0) to nervonic acid (C24:1n9). Palmitic acid (C16:0), behenic acid (C22:0), lignoceric acid (C24:0), and linoleic acid (C18:3n6) are commonly reported as the dominant fatty acids. The reported proportion of saturated fatty acids ranges from 48.97% to 80.11%, while unsaturated fatty acids range from 13.62% to 25.39% (Table 3).

The detection of 20 and 23 fatty acids in the leaves and flowers of *S. pseudograminifolia*, respectively, indicates a slightly broader fatty acid diversity compared to other species in the genus. Notably, the high proportion of methyl nonadecanoate (C19:0) observed in the leaf extract-a component rarely emphasized in previous *Scabiosa* studies-may serve as a chemotaxonomic marker specific to this species. Additionally, the predominance of saturated fatty acids in both organs aligns with the characteristic lipid composition previously documented for the genus.

Total phenolic, flavonoid contents and biological activity results

An assessment was conducted to determine the antioxidant activity of the essential oil of *S. pseudograminifolia* and its *n*-hexane, methanolic, and aqueous extracts. The test results included the DPPH free radical scavenging effect, TEAC, ORAC, and β-carotene peroxidation inhibition assay (Table 4).

There is a scarcity of reports regarding phenolic and flavonoid contents of *Scabiosa* species. The overall phenolic content of *S. arenaria* varied from 34.77 to 269.09 mg GAE/$g_{extract}$, while

Table 3. Chemical composition of the fatty acids obtained from the leaves and flowers of the *S. pseudograminifolia*

RRI#	Compound	Leaves	Flowers
1402	Methyl octanoate (=*Caprylic acid methyl ester);* (8:0)		0.3
1505	Methyl nonanoate (=*Pelargonic acid methyl ester);* (9:0)		0.3
1815	Methyl dodecanoate (=*Lauric acid methyl ester*); (12:0)	0.9	0.5
1980	*Unidentified* (MA:278)	0.4	0.2
2012	*Unidentified* (MA:278)	1.0	0.5
2016	Methyl tetradecanoate (=*Myristic acid methyl ester*); (14:0)	1.9	1.0
2051	Octanedioic acid (=*Suberic acid);* (8:0)		0.4
2125	Methyl pentadecanoate (=*Pentadecylic acid methyl ester*); (15:0)	0.5	0.5
2158	Nonanedioic acid (=*Azelaic acid*); (9:0)	1.0	1.0
2223	Methyl hexadecanoate (=*Palmitic acid methyl ester*); (16:0)	20.8	18.3
2251	*(Z)*-9-Methyl hexadecenoate (=*Palmitoleic acid methyl ester*); (16:1); ω-7		0.4
2330	Methyl heptadecanoate (=*Margaric acid methyl ester*); (17:0)	0.6	0.4
2436	Methyl octadecanoate *(=Stearic acid methyl ester)*; (18:0)	7.1	5.6
2455	*(Z)*-9-Methyl octadecenoate *(=Oleic acid methyl ester)*; (18:1); ω-9	7.8	4.0
2468	*(E)*-9-Methyl octadecenoate (=*Elaidic acid methyl ester*); (18:1); ω-9	0.6	0.9
2509	*(Z,Z)*-9,12-Methyl octadecadienoate (=*Linoleic acid methyl ester);* (18:2); ω-6	5.8	12.4
2542	Methyl nonadecanoate (=*Nonadecylic acid methyl ester*); (19:0)	21.9	
2572	*(Z,Z,Z)*-9,12,15-Methyl octadecatrienoate *(=α-Linolenic acid methyl ester); (18:3)*; ω-3	10.3	12.2
2642	Methyl eicosanoate *(=Arachidic acid methyl ester)*; (20:0)	4.4	3.1
2740	Methyl heneicosanoate *(=Heneicosilicic acid methyl ester)*; (21:0)	0.6	0.6
2843	Methyl docosanoate *(=Behanic acid methyl ester)*; (22:0)	8.3	6.5
2868	*(Z)*-13-Methyl dococenoate *(=Erucic acid methyl ester)*; (22:1); ω-9	1.2	5.0
2945	Methyl trichosanoate *(=Trichosilic acid methyl ester)*; (23:0)	0.8	0.5
3050	Methyl tetracosanoate *(=Lignoceric acid methyl ester);* (24:0)	3.9	3.7
	Total	99.8	78.3

RRI# : Relative retention index of the methyl/ethyl derivative of the compound

Table 4. TPC, TFC and biological activity results of *S. pseudograminifolia* extracts

Codes	TPC (mgGAE/$g_{extract}$)	TFC (mgQE/$g_{extract}$)	DPPH (IC_{50}, mg/mL)	TEAC (mM)	ORAC[a] (TEμmol)	β-Carotene peroxidation inhibition (IC_{50}, mg/mL)	α-Amylase inhibition (%)
SP_{EO}	-	-	NE	2.39±0.15	32.6±6.8	NE	33.6
SP_{H}	0.11±0.06	NE	28.80±1.90[b]	0.26±0.14	NE	NE	NE
SP_{M}	0.50±0.01	0.067±0.008	0.19±0.03	2.21±0.20	134.0±11.0	0.730±0.001	NE
SP_{W}	0.52±0.01	0.081±0.002	0.16±0.04	2.33±0.13	248.4±15.4	1.4±0.2	NE
BHA	-	-	-	-	-	0.01±0.0005	-
GA	-	-	0.002±0.00	-	-	-	-
ACR	-	-	-	-	-	-	85.0

[a]: ORAC values are determined for essential oil and extracts at 0.1 mg/mL, [b]: IC_{50} was not calculated; the value was for 10 mg/mL, ORAC: Oxygen Radical Absorbance Capacity, TPC: Total phenol content, TFC: Total flavonoid content, SP_{EO}: The plant's essential oil, SP_{H}: The plant's *n*-hexane extract, SP_{M}: The plant's methanol extract, SP_{W}: The plant's aqueous extract code, BHA: Butylated hydroxyanisole, GA: Gallic acid, ACR: Acarbose, NE: Non-effective, TEAC: Trolox equivalent antioxidant activity.

Table 5. RP-HPLC quantitative determination of phenolic acids in *S. pseudograminifolia* extracts

	Phenolic acid amounts (μg/$g_{extract}$)							
Extracts	PA	*p*-HBA	CA	ClA	SA	*p*-CA	FA	*o*-CA
SP_{M}	0.11	0.12	0.05	4.06	0.07	0.44	0.30	0.53
SP_{W}	0.22	0.79	0.25	5.26	0.21	0.89	0.48	0.65

RP-HPLC: Reverse phase high performance liquid chromatography, SP_{M}: The plant's methanol extract, SP_{W}: The plant's aqueous extract code, PA: Protocatechic acid, *p*-HBA: *p*-Hydroxybenzoic acid, CA: Caffeic acid, ClA: Chlorogenic acid, SA: Syringic acid, *p*-CA: *p*-Coumaric acid, FA: Ferulic acid, *o*-CA: *o*-Coumaric acid

the quantities of flavonoid compounds ranged from 0.81 to 10.9 mg QE/$g_{extract}$. Previously, it has been reported that the aqueous methanol extract and fractions from *S. atropurpurea* subsp. *maritima* contained the total phenolic content ranged from 17.7 to 186.75 mg GAE/$g_{extract}$, and the total flavonoid content varied from 4.38 to 208.69 mg catechin equivalent/g. The methanolic extract of *S. sicula* was found to have a total phenolic content of 2.67 mg GAE/$g_{extract}$. In the methanolic extracts of *S. columbaria* subsp. *columbaria* var. *columbaria* from Türkiye, the phenolic content ranged from 269.833 to 640.111 μg GAE/mL, while the flavonoid content ranged from 6.060 to 13.527 μg QAE/mL.[14] In our study, we detected that the aqueous extract of *S. pseudograminifolia* exhibited the highest concentrations of phenols and flavonoids: 0.52±0.01 mg GAE/$g_{extract}$ and 0.081±0.002 mg QE/$g_{extract}$, respectively.

The literature demonstrated a strong suppression of DPPH free radicals in the aqueous extract of *S. arenaria*, with an inhibitory concentration $(IC)_{50}$ value of 0.18 mg/mL.[92] The crude extracts of *S. tschiliensis* exhibited DPPH-scavenging action, with an IC_{50} value of 25.68±1.21 μg/mL. They had much more DPPH-scavenging power than other plants from the *Scabiosa* genus that were studied, like *S. comosa* and *S. arenaria*.[93] According to the literature, the IC_{50} values for the crude extract of *S. atropurpurea* ranged from 22.42 to 415.23 mg/mL. The crude extract obtained from the leaves exhibited the most significant DPPH-scavenging activity compared to other plant parts.[94] In this study, we found that the extract's IC_{50} values ranged from 0.16 to 0.19 mg/mL, indicating no activity of the essential oil towards DPPH free radicals. The TEAC value of the methanol extract from *S. sicula* was found to be 0.34±0.01 μg/mL. This is the concentration of Trolox solution that has the same antioxidant activity as a 1 mg/mL solution of the extract.[95] The TEAC value of *S. arenaria* was 0.56 mM Trolox/$g_{extract}$,[92] leaf parts of *S. columbaria,* it was 267.381±0.012 and 242.857±0.003, respectively.[88] The essential oil (2.39±0.15) and, aqueous extract (2.33±0.13) had the highest TEAC values, respectively, in contrast to DPPH activity. ORAC tests in *Scabiosa* species are rare and are the first in the literature to be performed in hexane, methanol, and water extracts, with the highest activity observed in water extract. In terms of β-carotene bleaching kinetics, it was observed that the methanolic fraction of *S. atropurpurea* and ascorbic acid (the reference compound) exhibited the highest level of efficacy in inhibiting β-carotene oxidation. These curves were nearly identical and showed their respective inhibition percentages were strikingly similar, with values of 97.19% and 100%. The findings indicate that the *n*-hexane and chloroform extracts exhibit a moderate level of antioxidant activity, with individual levels of 64.17% and 42.91%, respectively.[96] The inhibition values for the methanol extract were 0.730±0.001 mg/mL, and those for the water extract were 1.4±0.2 mg/mL. The study revealed a significant positive connection between the antioxidant activity and the total phenolic content of each extract. The α-amylase enzyme-inhibiting effect of *S. pseudograminifolia* was found to be insufficient

HPLC analysis results

The analysis revealed that *S. pseudograminifolia* has significant amounts of chlorogenic acid, caffeic acid, protocatechic acid, *p*-coumaric acid, syringic acid, and ferulic acid (Table 5). Regarding the biological activity of extracts, the study revealed a significant positive connection between the activity and the total phenolic content of each extract. Therefore, in this investigation, we have looked at the phenolic compounds in *S. pseudograminifolia*'s methanolic and aqueous extracts as a whole.

There are quite enough studies on the phenolic composition of *Scabiosa* species in the literature. These investigations have revealed that isoorientin and 4-O-caffeoylquinic acid are the primary compounds found in *S. stellata* extract.[97] Additionally, caffeoylquinic acid, rutin, ursolic acid, cyanuric acid, sinapic acid, luteolin, apigenin, quercetin, kaempherol, and tamarixetin have also been identified. Gallic, chlorogenic, caffeic, syringic, *p*-coumaric, sinapic, ferulic, catechin hydrate, epicatechin-3-*O*-gallate, luteolin-7-*O*-glucoside, isorhamnetin 3-*O*-glucoside, rutin, isoquercetin, myricetin, kaempferol-3-*O*-rutinoside, isorhamnetin-3-*O*-rutinoside, quercetin, naringenin, luteolin, isorhamnetin, and apigenin were detected in *S. atropurpurea* subsp. *maritima* hydromethanol extract.[94]

The methanol extracts from *S. columbaria* subsp. *columbaria* var. *columbaria* contained six phenolic compounds that were identified as the main ingredients. These were GA, catechin, 4-OH-benzoic acid, 4-OH-benzaldehyde, caffeic acid, and chlorogenic acid. The methanolic extract derived from *S. columbaria* subsp. *columbaria* contains GA and caffeic acid.[88]

CONCLUSION

This research includes the first biological activity and phytochemical studies on *S. pseudograminifolia* Hub.-Mor. growing in Sivas province of Türkiye. The main constituents of the essential oil derived from *S. pseudograminifolia* were hexadecanoic acid (30.2%), linalool (15.6%), and dodecanoic acid (10.9%). The MSD-SPME method revealed that *(Z)*-3-hexenal (34.0%), 2-ethyl hexanol (3.2%), 6-methyl-1-octanol (4.3%), 4-methyl-(2*E*) undecene (3.6%), and linalool (3.1%) were were the major volatile components in the leaves of *S. pseudograminifolia*. Similarly, *(Z)*-3-hexenal (29.1%), hexanol (7.7%), linalool (5%), and hexanal (4.4%) were identified as the main volatile components in the flowers. Non-adecanoic (21.9%) and hexadecanoic (20.8%) acids were found as fatty acids in *S. pseudograminifolia*. The aqueous and methanol extracts exhibited a significant concentration of chlorogenic acid. The highest TEAC values were determined for essential oil and aqueous extract. The methanol extract of *S. pseudograminifolia* exhibited the highest levels of β-carotene peroxidation inhibition, and the aqueous extract exhibited the highest levels free radical scavenging potential. The plant's ability to inhibit α-amylase enzyme is insufficient. The elucidation of the phytochemical content and bioactivity potential of *S. pseudograminifolia* extracts supports their potential use in further pharmacological studies and contributes to the growing knowledge on underexplored endemic flora.

Ethics

Ethics Committee Approval: Not required.

Informed Consent: Not required.

Footnotes

Authorship Contributions

Concept: K.Ö., T.Ö., Design: K.Ö., T.Ö. Data Collection or Processing: K.Ö., G.Ö., N.Ö., T.Ö., M.T., Analysis or Interpretation: K.Ö., G.Ö., N.Ö., T.Ö., Literature Search: K.Ö., Writing: K.Ö., G.Ö., N.Ö., T.Ö.

Conflict of Interest: The authors declare no conflicts of interest.

Financial Disclosure: The research was financially supported by the Scientific Research Projects Department of Anadolu University (BAP No: 2103S009).

REFERENCES

1. Akimaliev A. β-sitosterol and oleanolic acid from Scabiosa soongorica. Chem Nat Compd. 1977;13:596.
2. Akyol Y, Kocabaş O, Kayacan E, Minareci E, Özdemir C. Scabiosa hispidula Boiss. (Caprifoliaceae) türüne ait anatomik bir çalışma. Nevşehir Bilim Teknol Derg. 2016;5:10-15.
3. Heywood VH. Flowering plants of the world. Oxford; Oxford University Press; 1978:239-240.
4. Besbes M, Omri A, Cheraif I, Daami M, Ben Jannet H, Mastouri M, Aouni M, Selmi B. Chemical composition and antimicrobial activity of essential oils from Scabiosa arenaria Forssk. growing wild in Tunisia. Chem Biodivers. 2012;9:829-839.
5. TÜBİVES. [cited 2021 Dec 21]. Available from: http://194.27.225.161/yasin/tubives/index.php?sayfa=hizli_ara
6. Aksoy A, Çelik J, Bozkurt M, Uysal T. Türkiye florası için yeni bir tür kaydı: Scabiosa lucida Vill. (Caprifoliaceae). Bağbahçe Bilim Derg. 2020;7:49-57.
7. Menemen Y. Türkçe Bilimsel Bitki Adları Yönergesi'nde değişiklik ve ilave öneriler. Bağbahçe Bilim Derg. 2019;6:1-3.
8. Besbes Hlila M, Omri A, Ben Jannet H, Lamari A, Aouni M, Selmi B. Phenolic composition, antioxidant and anti-acetylcholinesterase activities of the Tunisian Scabiosa arenaria. Pharm Biol. 2013;51:525-532.
9. Pinto DCGA, Rahmouni N, Beghidja N, Silva AMS. Scabiosa genus: a rich source of bioactive metabolites. Medicines (Basel). 2018;5:110.
10. Skała E, Szopa A. Dipsacus and Scabiosa species-the source of specialized metabolites with high biological relevance: A review. Molecules. 2023;28:3754.
11. Besbes Hlila M, Mosbah H, Majouli K, Ben Nejma A, Ben Jannet H, Mastouri M, Mahjoub Aouni, Boulbaba Selmi. Antimicrobial activity of Scabiosa arenaria Forssk. extracts and pure compounds using bioguided fractionation. Chem Biodivers. 2016;13:1262-1272.
12. Bammi J, Douira A. Les plantes médicinales dans la forêt de l'achach (plateau central, Maroc). 2002.
13. Chen Q, Wang Y, Ma F, Han M, Wang Z, Xue P, Lu J. Systematic profiling of the effective ingredients and mechanism of Scabiosa comosa and S. tschilliensis against hepatic fibrosis combined with network pharmacology. Sci Rep. 2021;11:2600.
14. Albayrak S, Aksoy A, Yilmaz MA, Beyzi E. Investigation of phytochemical, antioxidant and antidiabetic potentials of Scabiosa L.

(Caprifoliaceae) species with chemometric methods. Chem Biodivers. 2024;21:202301652.

15. Perdetzoglou D, Skaltsa H, Tzakou O, Harvala C. Comparative phytochemical and morphological study of two species of the Scabiosa L. genus. Feddes Repert. 1994;105:157-165.
16. Tundis R, Loizzo MR, Menichini F, Statti GA, Menichini F. Biological and pharmacological activities of iridoids: recent developments. Mini Rev Med Chem. 2008;8:399-420.
17. Ghisalberti EL. Biological and pharmacological activity of naturally occurring iridoids and secoiridoids. Phytomedicine. 1998;5:147-163.
18. Kılınc H, Masullo M, Lauro G, D'Urso G, Alankus O, Bifulco G, Piacente S. Scabiosa atropurpurea: A rich source of iridoids with α-glucosidase inhibitory activity evaluated by in vitro and in silico studies. Phytochemistry. 2023;205:113471.
19. Otang-Mbeng W, Sagbo IJ. Anti-melanogenesis, antioxidant and anti-tyrosinase activities of Scabiosa columbaria L. Processes. 2020;8:236.
20. European Pharmacopoeia. Essential Oils in Herbal Drugs, in: European Pharmacopoeia, 11th edition, p. 323-324, European Directorate for the Quality of Medicines & HealthCare (EDQM), Council of Europe, Strasbourg, France, 2023. 2023:323-324.
21. Göger G, Türkyolu Ü, Gürşen EN, Yur S, Karaduman AB, Göger F, Özek G. Phytochemical characterisation of Phlomis linearis Boiss. & Bal and screening foranticholinesterase, antiamylase, antimicrobial, and cytotoxic properties. Turk J Chem. 2021;45:387-399.
22. Möller R, Nürnberg G, Albrecht E, Ruth W, Brockmann GA, Dannenberger D. A method for analyzing fatty acids in cattle hair, with special emphasis on lauric acid and myristic acid. Eur J Lipid Sci Technol. 2019;121:1900143.
23. Göğer F, Özek G, Tekin M, Yur S, Özek T. phytochemical profiling and evaluation of Marrubium sivasense Aytaç, Akgül & Ekici for antioxidant activity and ınhibition effects on α-amylase, lipoxygenase, xanthine oxidase and tyrosinase enzymes. JOTCSA. 2019;6:281-292.
24. Özek G, Özbek M, Yur S, Göger F, Arslan M, Özek T. Assessment of endemic Cota fulvida (Asteraceae) for phytochemical composition and ınhibitory activities against oxidation, α-amylase, lipoxygenase, xanthine oxidase and tyrosinase enzymes. Records of Nat Prod. 2019;13:333-345.
25. Özek G, Özek T, Başer KHC, Duran A, Sagiroglu M, Duman H. Comparison of the essential oils of Prangos turcica A. Duran, M. Sagiroglu et H. Duman fruits obtained by different isolation techniques. J Essent Oil Res. 2006;18:511-514.
26. Adams RP. Identification of essential oil components by gas chromatography/mass spectrometry. Carol Stream 2007;456:544-545.
27. Öztürk N, Tuncel M, Tuncel NB. Determination of phenolic acids by a modified HPLC: Its application to various plant materials. J Liq Chromatogr Relat Technol. 2007;30:587-596.
28. Vl S. Analysis of total phenols and other oxidation substrates and antioxidants by means of Folin-Ciocalteu reagent. Methods Enzymol. 1999;299:152-178.
29. Yur S, Tekin M, Göger F, Başer KHC, Özek T, Özek G. Composition and potential of Tanacetum haussknechtii Bornm. Grierson as antioxidant and inhibitor of acetylcholinesterase, tyrosinase, and α-amylase enzymes. Int J Food Prop. 2017;20:2359-2378.
30. Re R, Pellegrini N, Proteggente A, Pannala A, Yang M, Rice-Evans C. Antioxidant activity applying an improved ABTS radical cation decolorization assay. Free Radic Biol Med. 1999;26:1231-1237.
31. Brand-Williams W, Cuvelier ME, Berset C. Use of a free radical method to evaluate antioxidant activity. Food Sci Technol. 1999;28:1231-1237.
32. Baderschneider B, Luthria D, Waterhouse AL, Winterhalter P. Antioxidants in white wine (cv. Riesling): I. Comparison of different testing methods for antioxidant activity. Vitis. 1999;38:127-131.
33. Gillespie KM, Chae JM, Ainsworth EA. Rapid measurement of total antioxidant capacity in plants. Nat Protoc. 2007;2:867-870.
34. Zengin G, Sarikurkcu C, Aktumsek A, Ceylan R. Sideritis galatica Bornm.: a source of multifunctional agents for the management of oxidative damage, Alzheimer's and diabetes mellitus. J Funct Foods. 2014;11:538-547.
35. Brunton NP, Cronin DA, Monahan FJ. Volatile components associated with freshly cooked and oxidized off-flavours in turkey breast meat. Flavour Fragr J. 2002;17:327-334.
36. Narain N, de Sousa Galvao M, Madruga MS. Volatile compounds captured through purge and trap technique in caja-umbu (Spondias sp.) fruits during maturation. Food Chem. 2007;102:726-731.
37. Hashizume M, Gordon MH, Mottram DS. Light-induced off-flavor development in cloudy apple juice. J Agric Food Chem. 2007;55:9177-9182.
38. Héberger K, Görgényi M. Principal component analysis of Kováts indices for carbonyl compounds in capillary gas chromatography. J Chromatogr A. 1999;845:21-31.
39. NIST Mass Spectrometry Data Center. NIST Mass Spectrometry Data Center, William E. Wallace, director, "Retention Indices" in NIST Chemistry WebBook, NIST Standard Reference Database Number 69, Eds. P.J. Linstrom and W.G. Mallard, National Institute of Standards and Technology, Gaithersburg MD, 20899, https://doi.org/10.18434/T4D303, (retrieved August 26, 2024). 2024.
40. Babushok VI, Linstrom PJ, Zenkevich IG. Retention indices for frequently reported compounds of plant essential oils. J Phys Chem Ref Data. 2011;40.
41. Kang HR, Hwang HJ, Lee JE, Kim HR. Quantitative analysis of volatile flavor components in Korean alcoholic beverage and Japanese sake using SPME-GC/MS. Food Sci Biotechnol. 2016;25:979-985.
42. Shukurlu EN, Özek G, Özek T, Vitalini S. Chemical composition of different plant parts from Lactuca serriola L.-focus on volatile compounds and fatty acid profile. Z Naturforsch C J Biosci. 2023;78:285-291.
43. Koprivnjak O, Conte L, Totis N. Influence of olive fruit storage in bags on oil quality and composition of volatile compounds. Food Technol Biotechnol. 2002;40:129-134.
44. Frizzo CD, Serafini LA, Dellacassa E, Lorenzo D, Moyna P. Essential oil of Baccharis uncinella DC. from Southern Brazil. Flavour Fragr J. 2001;16:286-268.
45. Censullo AC, Jones DR, Wills MT. Speciation of the volatile organic compounds (VOCs) in solventborne aerosol coatings by solid phase microextraction-gas chromatography. J Coat Technol. 2003;75:47-53.
46. Feng Z, Wu X, Chen V, Velie E, Zhang Z. Incidence and survival of desmoplastic melanoma in the United States, 1992-2007. J Cutan Pathol. 2011;38:616-624.
47. Menichini F, Tundis R, Bonesi M, De Cindio B, Loizzo MR, Conforti F, GA Statti., Menabeni R, Bettini R, and Menichini F. Chemical composition and bioactivity of Citrus medica L. cv. Diamante essential oil obtained by hydrodistillation, cold-pressing and supercritical carbon dioxide extraction. Nat Prod Res. 2011;25:789-799.
48. Saini R, Jaitak V, Guleria S, Kaul VK, Kiran Babu GD, Singh B, Lal B, Singh RD. Comparison of headspace analysis of volatile constituents

with GCMS analysis of hydrodistilled and supercritical fluid extracted oil of Capillipedium parviflorum. J Essent Oil Res. 2012;24:315-320.

49. Vinogradov BA. Production, composition, properties and application of essential oils, 2004, retrieved from http://viness.narod.ru. 2004.
50. Huang J, Yang M, Zong Y, Liu C, Yu H, Chen C, Tian H. Characterization of the aroma in barley leaves from different cultivars and tillering stages by HS-SPME/GC-MS, GC-O and E-nose. Food Biosci. 2024;60:104117.
51. Hu S, Ren H, Song Y, Liu F, Meng L. Analysis of volatile compounds by GCMS reveals the geographical origin of cultivated rice. 2022.
52. Thakeow P, Angeli S, Weißbecker B, Schütz S. Antennal and behavioral responses of Cis boleti to fungal odor of Trametes gibbosa. Chem Senses. 2008;33:379-387.
53. Feng T, Zhuang H, Ye R, Jin Z, Xu X, Xie Z. Analysis of volatile compounds of Mesona blumes gum/rice extrudates via GC-MS and electronic nose. Sens Actuators B Chem. 2011;160:964-973.
54. Rochat S, Egger J, Chaintreau A. Strategy for the identification of key odorants: application to shrimp aroma. J Chromatogr A. 2009;1216:6424-6432.
55. Yamaguchi K, Shibamoto T. Volatile constituents of green tea, Gyokuro (Camellia sinensis L. var Yabukita). J Agric Food Chem. 1981;29:366-370.
56. Altintas A, Kose YB, Yucel E, Demirci B, Baser KHC. Composition of the essential oil of Centaurea dichroa. Chem Nat Compd. 2004;40:604-605.
57. Senger-Emonnot P, Rochard S, Pellegrin F, George G, Fernandez X, Lizzani-Cuvelier L. Odour active aroma compounds of sea fig (Microcosmus sulcatus). Food Chem. 2006;97:465-471.
58. Tekin M, Özek G, Martin E, Özek T, Yılmaz G, Başer KHC. Essential oil characterization of Cousinia sivasica Hub.-Mor. Asteraceae Biol Divers Conserv. 2018;11:16-21.
59. Shibamoto T, Kamiya Y, Mihara S. Isolation and identification of volatile compounds in cooked meat: sukiyaki. J Agric Food Chem. 1981;29:57-63.
60. Kaya A, Başer KHC, Koca F. Essential oils of Acinos troodi (Post) Leblebici subsp. vardaranus Leblebici and subsp. grandiflorus Hartvig & Strid. Flavour Fragr J. 1999;14:50-54.
61. Welke JE, Manfroi V, Zanus M, Lazarotto M, Zini CA. Characterization of the volatile profile of Brazilian Merlot wines through comprehensive two-dimensional gas chromatography time-of-flight mass spectrometric detection. J Chromatogr A. 2012;1226:124-139.
62. Liao X, Yan J, Wang B, Meng Q, Zhang L, Tong H. Identification of key odorants responsible for cooked corn-like aroma of green teas made by tea cultivar "Zhonghuang 1". Food Res Int. 2020;136:109355.
63. Özek G, Chidibayeva A, Ametov A, Nurmahanova A, Özek T. Chemical composition of flower volatiles and seeds fatty acids of Rosa iliensis Chrshan, an endemic species from Kazakhstan. Records of Natural Products. 2022;16:225-235.
64. Schepetkin IA, Özek G, Özek T, Kirpotina LN, Kokorina PI, Khlebnikov AI, Quinn MT. Neutrophil immunomodulatory activity of nerolidol, a major component of essential oils from Populus balsamifera buds and propolis. Plants. 2022;11:3399.
65. Nyiligira E, Viljoen AM, Başer KHC, Özek T, Van Vuuren SF, Houghton PJ. Essential oil composition and in vitro antimicrobial and anti-inflammatory activity of South African Vitex species. South African Journal of Botany. 2004;70:611-617.
66. Le Guen S, Prost C, Demaimay M. Characterization of odorant compounds of mussels (Mytilus edulis) according to their origin using gas chromatography–olfactometry and gas chromatography–mass spectrometry. J Chromatogr A. 2000;896:361-371.
67. Wong KC, Tie DY. The essential oil of the leaves of Murraya koenigii Spreng. Journal of Essential Oil Research. 1993;5:371-374.
68. Sandner D, Krings U, Berger RG. Volatiles from Cinnamomum cassia buds. Z Naturforsch C J Biosci. 2018;73:67-75.
69. Schepetkin IA, Özek G, Özek T, Kirpotina LN, Khlebnikov AI, Quinn MT. Neutrophil immunomodulatory activity of (–)-borneol, a major component of essential oils extracted from Grindelia squarrosa. Molecules. 2022;27:4897.
70. Hachicha SF, Skanji T, Barrek S, Ghrabi ZG, Zarrouk H. Composition of the essential oil of Teucrium ramosissimum Desf. (Lamiaceae) from Tunisia. Flavour Fragr J. 2007;22:101-104.
71. Kundakovic T, Fokialakis N, Kovacevic N, Chinou I. Essential oil composition of Achillea lingulata and A. umbellata. Flavour Fragr J. 2007;22:184-187.
72. Soria AC, Sanz J, Martínez-Castro I. SPME followed by GC-MS: a powerful technique for qualitative analysis of honey volatiles. European Food Research and Technology. 2009;228:579-590.
73. Başer KHC, Özek G, Özek T, Duran A. Composition of the essential oil of Centaurea huber-morathii Wagenitz isolated from seeds by microdistillation. Flavour Fragr J. 2006;21:568-570.
74. Christensen LP, Jakobsen HB, Paulsen E, Hodal L, Andersen KE. Airborne Compositae dermatitis: monoterpenes and no parthenolide are released from flowering Tanacetum parthenium (feverfew) plants. Arch Dermatol Res. 1999;291:425-431.
75. Pozo-Bayón MA, Ruíz-Rodríguez A, Pernin K, Cayot N. Influence of eggs on the aroma composition of a sponge cake and on the aroma release in model studies on flavored sponge cakes. J Agric Food Chem. 2007;55:1418-1426.
76. Peng CT, Hua RL, Maltby D. Prediction of retention indexes: IV. Chain branching in alkylbenzene isomers with C10-13 alkyl chains identified in a scintillator solvent. J Chromatogr. 1992;589:231-239.
77. Johanningsmeier SD, McFeeters RF. Detection of volatile spoilage metabolites in fermented cucumbers using nontargeted, comprehensive 2-dimensional gas chromatography-time-of-flight mass spectrometry (GC×GC-TOFMS). J Food Sci. 2011;76:168-177.
78. Xiao Z, Dai S, Niu Y, Yu H, Zhu J, Tian H, Gu Y. Discrimination of Chinese vinegars based on headspace solid-phase microextraction-gas chromatography mass spectrometry of volatile compounds and multivariate analysis. J Food Sci. 2011;76:1125-1135.
79. Polatoğlu K, Arsal S, Demirci B, Başer KHC. Unexpected Irregular Monoterpene "Yomogi Alcohol" in the Volatiles of the Lathyrus L. species (Leguminosae) of Cyprus. J Oleo Sci. 2016;65:241-249.
80. Formisano C, Rigano D, Napolitano F, Senatore F, Arnold NA, Piozzi F, Rosselli S. Volatile constituents of Calamintha origanifolia Boiss. growing wild in Lebanon. Nat Prod Commun. 2007;2:1253-1256.
81. Bisio A, Ciarallo G, Romussi G, Fontana N, Mascolo N, Capasso R, Biscardi D. Chemical composition of essential oils from some Salvia species. Phytotherapy Research. An International Journal Devoted to Pharmacological and Toxicological Evaluation of Natural Product Derivatives. 1998;12:117-120.

82. Suleimenov YM, Atazhanova GA, Ozek T, Demirci B, Kulyjasov AT, Adekenov SM, Baser KHC. Essential oil composition of three species of Achillea from Kazakhstan. Chem Nat Compd. 2001;37:447-450.

83. Başer KHC, Özek T, Demirci B, Kürkçüoğlu M, Aytaç Z, Duman H. Composition of the essential oils of Zosima absinthifolia (Vent.) Link and Ferula elaeochytris Korovin from Turkey. Flavour Fragr J. 2000;15:371-372.

84. Selli S, Cabaroglu T, Canbas A, Erten H, Nurgel C, Lepoutre JP, Gunata Z. Volatile composition of red wine from cv. Kalecik Karası grown in central Anatolia. Food Chem. 2004;85:207-213.

85. Başer KHC, Özek G, Özek T, Duran A, Duman H. Composition of the essential oils of Rhabdosciadium oligocarpum (Post ex Boiss.) Hedge et Lamond and Rhabdosciadium microcalycinum Hand-Mazz. Flavour Fragr J. 2006;21:650-655.

86. Kaya A, Başer KHC, Tümen G, Koca F. The essential oil of Acinos suaveolens (Sm.) G. Don fil. Acinos arvensis (Lam.) Dandy and Acinos rotundifolius Pers. growing wild in Turkey. Flavour Fragr J. 1999;14:60-64.

87. Quijano CE, Linares D, Pino JA. Changes in volatile compounds of fermented cereza agria [Phyllanthus acidus (L.) Skeels] fruit. Flavour Fragr J. 2007;22:392-394.

88. Akar Z. Chemical compositions by using LC-MS/MS and GC-MS and antioxidant activities of methanolic extracts from leaf and flower parts of Scabiosa columbaria subsp. columbaria var. Columbaria L. Saudi J Biol Sci. 2021;28:6639-6644.

89. Javidnia K, Miri R, Javidnia A. Constituents of the essential oil of Scabiosa flavida from Iran. Chem Nat Compd. 2006;42:529-530.

90. Jalloul A Ben, Garzoli S, Chaar H, el Jribi C, Abderrabba M. Seasonal effect on bioactive compounds recovery using aqueous extraction, antioxidant activities, and volatile profiles of different parts of Scabiosa maritima L.(=Scabiosa atropurpurea subsp. maritima (L.) Arcang.). South African Journal of Botany. 2023;152:63-79.

91. Ebadi-Nahari M, Farnia P, Nikzat S, Mollaei S. A chemotaxonomic evaluation of some Scabiosa L. species in Iran. Biochem Syst Ecol. 2018;81:33-36.

92. Hafsa M Ben, Besbes M, Mahjoub MA, Mighri Z. Antimicrobial, antioxidant activities and total phenolic content of the acetonic, ethanolic and aqueous extracts of Scabiosa arenaria (Forsk). J Med Plants Nat Prod. 2009;1:59-68.

93. Wang J, Liu K, Li X, Bi K, Zhang Y, Huang J, Zhang R. Variation of active constituents and antioxidant activity in Scabiosa tschiliensis Grunning from different stages. J Food Sci Technol. 2017;54:2288-2295.

94. Ben Jalloul A, Chaar H, Tounsi MS, Abderrabba M. Variations in phenolic composition and antioxidant activities of Scabiosa maritima (Scabiosa atropurpurea sub. maritima L.) crude extracts and fractions according to growth stage and plant part. South African Journal of Botany. 2022;146:703-714.

95. Kılınç H, Masullo M, D'Urso G, Karayildirim T, Alankus O, Piacente S. Phytochemical investigation of Scabiosa sicula guided by a preliminary HPLC-ESI-MSn profiling. Phytochemistry. 2020;174:112350.

96. Ali-Rachedi F, Laoud A, Meraghni M. Antioxidant activity and acetylcholinesterase inhibitory of Scabiosa atraupurpuria sub maritima L. Extract. Research Journal of Biotechnology. 2024;19:57-63.

97. Rahmouni N, Pinto DCGA, Beghidja N, Benayache S, Silva AMS. Scabiosa stellata L. phenolic content clarifies its antioxidant activity. Molecules. 2018;23:1285.

Click the link to access Supplementary Figure 1-5: https://d2v96fxpocvxx.cloudfront.net/68f48462-babf-415b-b878-1e392d1c83af/content-images/f74cb961-a41f-4861-97c7-10bdf2156076.pdf

Turk J Pharm Sci 2025;22(2):119-130
DOI: 10.4274/tjps.galenos.2025.02772

ORIGINAL ARTICLE

Effect of *Aegle marmelos* Extract-Phospholipid Complexes in Dextran Sulfate Sodium-Induced Ulcerative Colitis in Rats

Pooja Ganpat SWAMI, Dilesh Jagdish SINGHAVI*, Rajendra Onkarappa GANJIWALE

Institute of Pharmaceutical Education and Research, Wardha, India

ABSTRACT

Objectives: Ayurvedic texts mention the use of *Aegle marmelos* fruit in colitis and other gastrointestinal ailments. The polyphenolic contents of the fruit, however, have poor bioavailability, limiting their therapeutic use. The study aimed to develop and optimise the *A. marmelos* fruit extract-phospholipid (AMEP) complex to improve the oral bioavailability of the *A. marmelos* extract (AME), and compare the *in vivo* effect of AME and AMEP in dextran sulfate sodium (DSS)-induced ulcerative colitis in rats.

Materials and Methods: The research work is the first of its kind to use a hydroalcoholic extract of A. marmelos fruit in the preparation of phospholipid complexes for ameliorating UC. The complexes were prepared using the solvent evaporation method and optimised by Box-Behnken design. The work compares the *in vivo* activity of plain AME, its phospholipid complexes, and the standard drug (mesalamine) in the alleviation of chemical-induced colitis in rats. AMEP was optimised using response surface methodology by Box-Behnken design. AMEP was characterised using scanning electron microscopy, Fourier transform infrared spectroscopy, differential scanning calorimetry, zeta analysis, and particle size analysis. A DSS-induced rat model was used *in vivo* studies to mimic ulcerative colitis. The pathogenesis of the disease was assessed by evaluating the levels of oxidative stress markers [nitric oxide (NO), malondialdehyde (MDA), and superoxide dismutase (SOD) activity], cytokines [tumor necrosis factor-alpha (TNF-α) and interleukin-6 (IL-6)], disease activity index, colon length, and histopathology.

Results: The characterization confirmed the formation of AMEP, having a particle size of 673.6±4.30 nm, polydispersity index of 0.224±0.010, and zeta potential of -42.6 mV±0.51. The NO, MDA, TNF-α, and IL-6 levels were significantly reduced ($p<0.0001$, $p<0.005$, $p<0.0001$, $p<0.01$), and the SOD level was significantly increased ($p<0.05$) in AMEP-treated groups compared to the AME-treated groups.

Conclusion: These findings suggessts that AMEP has a powerful potential to reduce the levels of oxidative markers and inflammatory cytokines, making it a promising treatment for ulcerative colitis.

Keywords: *Aegle marmelos* extract, phospholipid-complex, ulcerative colitis, Box-Behnken design

INTRODUCTION

Ulcerative colitis (UC) is a chronic idiopathic inflammatory disease of the colon. It is marked by relapses and remissions of mucosal inflammation, commencing in the rectum and extending to the proximal sections of the colon.[1] UC causes long-lasting inflammation and ulcers in the large intestine and rectum. It affects the colon's innermost lining, and the symptoms develop over time. It commonly affects adults in the age group between 30 and 40 and can be debilitating, potentially leading to serious, life-threatening complications.[2]

The current treatment regimen for UC focuses entirely on inducing remission and preventing relapses.[3] The pathogenic

***Correspondence:** dileshsinghavi@rediffmail.com, **ORCID-ID:** orcid.org/0000-0002-2544-7226
Received: 29.11.2023, **Accepted:** 23.03.2025 **Publication Date:** 14.05.2025

Cite this article as: SWAMI PG, SINGHAVI DJ, GANJIWALE RO. Effect of Aegle marmelos extract-phospholipid complexes in dextran sulfate sodium-induced ulcerative colitis in rats. Turk J Pharm Sci. 2025;22(2):119-130

heterogeneity of UC makes single-target therapy a challenge, as evidenced by the recent failures of pharmacological therapies, including tumor necrosis factor-alpha (TNF-α), anti-integrin, and Janus kinase inhibitors.[4,5] Thus, it is necessary to find alternative treatment solutions with multiple therapeutic targets.[6] The ineffectiveness of treatments, especially in chronic cases, has led to increased use of complementary and alternative medicine, in which herbal products are commonly used, in UC.[7,8]

Few plant actives and extracts have shown activity against UC, but often their usage is limited due to a lack of supporting studies.[9] *Aegle marmelos* (L.) Correa (Rutaceae) is one such plant used in the treatment of colitis and other gastroenterological disorders.[10] *A. marmelos* fruit has medicinal importance as an astringent, digestive, and stomachic agent.[11] Qualitative analysis of *A. marmelos* fruit extract (AME) confirms the presence of phenols, tannins, coumarin glycosides, flavonoids, and alkaloids. Gallic acid, quercetin, chlorogenic acid, ellagic acid, ferulic acid, kaempferol, and protocatechuic acid are some of the phenols and flavonoids reported to have been found in *A. marmelos* fruit. These compounds are profoundly important due to their antioxidant properties. However, the bioavailability of most of these compounds is poor, which limits their activity.[12,13]

A. marmelos fruit also shows the presence of marmelosin, which is a furanocoumarin (also a marker compound) with immunomodulatory potential that has antioxidant, antiproliferative, and anti-inflammatory activity.[14] It has been demonstrated that marmelosin alleviates inflammation by inhibiting the phosphorylated phosphoinositide 3-kinases/protein kinase B/nuclear factor-kappa B (PI3K/Akt/NF-κB) pathway.[15,16] It has been shown to alleviate UC symptoms by regulating the nuclear factor erythroid-2-related factor 2/antioxidant response elements/heme oxygenase-1 (Nrf-2/ARE/HO-1) pathway.[17] However, the bioavailability of marmelosin is poor, and it belongs to the Biopharmaceutics Classification System Class II category.[18]

The problem of poor bioavailability and solubility can be overcome using a method of lipid-based formulation developed recently, in which plant extracts or actives are complexed with dietary phospholipids.[19,20] The lipid-based formulations improve the solubility, oral absorption, and permeation of the actives without compromising their safety.[21,22] In the current study, we focused on preparing a cost-effective product for alleviating UC. The AME was prepared using aqueous ethanol. Since the extract contains various polyphenols, antioxidant and anti-inflammatory activity *via* multiple pathways can be achieved against colitis. The aim of the study was to formulate AMEP to enhance the solubility and absorption of the phytoactives of AME and to compare the effects of AME and AMEP (at the same dose) on rats with UC.

MATERIALS AND METHODS

Materials and reagents

Fresh fruits of *A. marmelos* were collected in January from Borgaon village in the Wardha district of Maharashtra, which had well-drained black soil. The specimens were authenticated [herb. Sheet no. Bot. Sp. 04/2020-21]. The specimen was authenticated by Dr. L.P Dalal, Head of the Department of Botany in Bajaj College of Science, Wardha, and deposited in Bajaj College of Science, Wardha. The fruits were cleaned, chopped, dried, and ground using a grinder. The resulting powder was sifted through a size #22 mesh and stored under cool and dry conditions.

A reference standard of marmelosin was obtained from Natural Remedies (Bangalore, India). Mesalamine tablets were obtained from Sun Pharmaceutical Industries Ltd. (India). 2,2-diphenyl-1-picrylhydrazyl and quercetin were bought from Research-Lab (Mumbai) and Chemika-Biochemika Reagents, respectively. Dextran sulfate sodium (DSS) was procured from Sisco Research Laboratories. Lipoid H90 was obtained as a sample from Lipoid GmbH, Ludwigshafen. Loba Chemie Pvt. Ltd. supplied the remaining chemicals.

Preparation of AME

AME was extracted using the maceration method from the powdered *A. marmelos* fruits. It was obtained using aqueous ethanol (50% *v/v*) with a 1:10 ratio of solute to solvent. It was filtered, dried, and stored in a desiccator.

Determination of marmelosin content in AME

The marmelosin content of the AME was determined through high-performance thin-layer chromatography (HPTLC) analysis. The samples were applied to pre-coated silica plates (F254, Merck) using Linomat5 (software WINCATS); a scanner (CAMAG-3) was utilised for scanning. *n*-Hexane and ethyl acetate 12:4 were used to make the mobile phase. A standard calibration curve was plotted using marmelosin solutions of concentrations 100, 200, 300, 400, and 500 µg/mL.

AME sample solutions with a concentration of 100 mg/mL were prepared. Each sample of 10 µL was applied on the silica plate, which was run in a twin-trough chamber. The plate was developed using 10% *w/v* methanolic potassium hydroxide (KOH). Peaks were recorded at 366 nm using a TLC scanner. Quantification was done using the calibration curve of marmelosin ($y=11.63x+431.5$; $R^2=0.999$), which was expressed as mg/g of extract.

Preparation and optimization of AMEP

AMEP was prepared using the solvent evaporation method and a rotary evaporator.[23] In brief, AME and PC were dispersed in absolute ethanol in a round-bottom flask in different ratios and stirred for 1-3 hours at a temperature between 35 °C and 45 °C. The solvent was then evaporated using an evaporator. The complexes were then removed and allowed to dry. The samples were then stored in desiccators.

A QbD-based approach using a Box-Behnken formulation design was used to obtain a response surface for optimization of phospholipid complexes. The influences of three independent variables, namely, (1) AME-to-phospholipid ratio *(w/w)*, (2) reaction temperature (°C), and (3) reaction time (hours), on the dependent variable of the complex, *i.e.*, the entrapment efficiency (%), were studied. The experiments were designed

using the Design Expert software package (Version 13.0.5.0, StatEase Inc.). Fifteen formulations were designed, with one centre point.

Entrapment efficiency (EE) of AMEP

The EE of the marker compound, marmelosin, was determined in the AMEP using the HPTLC method. AME and AMEP samples were prepared at a concentration of 10 mg/mL. The samples (10 µL) were applied on pre-coated silica plates (F254, Merck), using Linomat5, and a CAMAG TLC scanner3 was used for scanning. The mobile phase consisted of a 1:1 mixture of n-hexane and ethyl acetate. The plate was run in a twin-trough glass chamber. Methanolic KOH (10% *w/v*) was used for sample derivatization, and peaks were recorded at 366 nm.

$$EE\ (\%) = \frac{Marmelosin\ content\ in\ AMEP}{Marmelosin\ content\ in\ AME} \times 100 \quad (1)$$

Characterization of optimised AMEP formulation

Solubility of AMEP

The solubility of the AMEP was checked in ethanol (50% *v/v*), absolute ethanol, ethyl acetate, chloroform, dimethyl sulfoxide, methanol, and water.

Particle size, polydispersity index (PI), and zeta potential

The particle size, PI, and zeta potential of the AMEP were determined by dynamic light scattering (DLS; Horiba-DLS-7100E, Japan). The AMEP was dispersed in water prior to analysis.

Fourier transform infrared spectroscopy (FTIR)

FTIR analysis was carried out using an infrared spectrophotometer (IR affinity, model 206-73500-38, Shimadzu). The potential interactions were investigated by comparing the IR spectra of PC, AME, physical mixture of PC and AME, and AMEP in the 4000-400 cm-1 wavenumber region.

Scanning electron microscopy (SEM)

The morphology of the AMEP was studied using a Hitachi High-Tech S3700N scanning electron microscope.

Differential scanning calorimetry (DSC)

Thermograms of PC, AME, PM, and AMEP were recorded using a differential scanning calorimeter (DSC-60, Shimadzu). A heating rate of 10 °C/minute was used for the thermal analysis. The percentage weight loss of the samples was monitored from 25 °C to 400 °C.

Experimental animals

In vivo investigations utilized male Wistar rats weighing 200-280 g. The animals were kept at standard temperature (25 °C) and light (12:12 hours of light-dark cycles) conditions. They were given access to water and food *ad libitum*. Practical procedures were performed in compliance with the CPCSEA, Government of India, and, as approved by the Institutional Animal Ethic Committee study protocol (approval number: 535/PO/RERCBT/S/02/CPCSEA/IPER/IAEC/2020-2021/17, date: 19.12.2020).

Disease induction

A chemically induced colitis model was used. The animals were put into six groups at random, with six animals in each group: (1) the normal group (G-I), (2) the DSS group, or positive-control group (G-II), (3) the standard-treated group (mesalamine) [100 mg/kg body-weight (bw)] (G-III), (4) the AME-treated group (400 mg/kg bw) (G-IV), (5) the AMEP-treated group (800 mg/kg bw) (G-V), and (6) the excipient (PC) group (400 mg/kg bw) (G-VI).

Acute colitis was induced by the oral administration of 6% DSS (MW 50 kDa) in drinking water.[24] The animals of all groups except G-I were given 6% DSS in water *ad libitum* for 7 days. The animals developed severe diarrhoea and had significant weight loss. The animals of all groups (except G-I and G-II), were treated for the next 7 days with their respective treatments. Their weights were monitored, and their faeces were observed throughout the experiment.

The animals of each group were then sacrificed using the cervical dislocation method after being fasted overnight.[24] The colon was excised and cleaned with an ice-cold saline solution of 0.9% *w/v*. The colon tissues were stored in chilled phosphate-buffered saline (pH 7.4) for biochemical analysis.

Colon length and Disease Activity Index (DAI)

The length of the colon between the ileocecal junction and the proximal rectum was measured. Body weight, stool consistency, and gross rectal bleeding were noted. The DAI was used to evaluate the severity of the colitis.[25]

Biochemical evaluation

The rat colons were homogenized in ice-cold 0.01 M phosphate buffer (pH 7.4) at 4000 rpm for 15 minutes to obtain a 10% *w/v* homogenate. This was used to evaluate the antioxidant and anti-inflammatory activities in the colonic tissues. The colorimetric method was used for the analysis of nitric oxide (NO) content by the Montgomery method.[26] The superoxide dismutase (SOD) activity was determined using the Marklund and Marklund method,[27] and the malondialdehyde (MDA) activity was determined using the method of Okhawa et al.[28] inflammatory cytokines (TNF-α and IL-6) were quantified by the enzyme-linked immunosorbent assay method using commercial kits (Krishgen Biosystems).

Histological analysis

The colon tissue at the distal end was fixed for 24 hours in a 10% *v/v* formaldehyde solution and later embedded in paraffin. The sections were cut, and hematoxylin and eosin were used to stain them. The slides were examined under a light microscope.

Statistical analysis

All the data were expressed as the mean ± standard deviation. Data analysis was carried out using the GraphPad Prism 9.0 software package (GraphPad, San Diego, CA). The parametric variables were analysed using one-way ANOVA, followed by Dunnett's post hoc analysis. Student's t-test was used to compare two groups. A value of $p<0.05$ was considered to be statistically significant.

RESULTS

Marmelosin content in AME

HPTLC analysis was conducted to quantify AME by determining the marker compound, marmelosin (Figure 1). The marmelosin content in AME was determined using the standard calibration graph (Figure 2). It was found to be 0.349±0.03% *w/w*.

Phytosome formulation

Fifteen formulations were prepared using a second-order Box-Behnken design at three levels, and their entrapment efficiencies were determined. The independent variables and their levels in the formulation are provided in Table 1. The layout of the experiment design is shown in Table 2. The entrapment efficiencies of 15 formulations varied between 23.02% *w/w* and 82.77% *w/w*.

A linear model was chosen for analyzing the variable response as it had a comparatively higher R^2 value (0.9523) and a lower predicted residual sum of squares (PRESS) value.[29] The mathematical relationship as given by Design-Expert 13.0.5.0 for the measured responses is: Entrapment efficiency = +57.82-1.43*A+15.87*B+12.05*C (2).

Where A is the AME:PC ratio, B is the temperature, and C is the stirring time. The sign and value of the coefficients in equation (2) represent the tendency and magnitude of the factors' influence on the response. If the value is positive, there is a direct correlation between the factor and the response; if it is negative, there is an inverse correlation. The contour plots showing the relationship between entrapment efficiency and the independent variables can be observed in Figure 3.

The model's *f* value of 73.27 and *p* value of less than 0.0001 imply that the model is significant (Table 3). The lack-of-fit *f* value of 8.30 indicates that it is not significant in comparison to the pure error. For a good model, a non-significant lack of fit is generally considered desirable. The predicted R^2 value of 0.9125 is in reasonable agreement with the adjusted R^2 value of 0.9393, *i.e.*, the difference is less than 0.2. Adeq Precision measures the signal-to-noise ratio, which should preferably be above 4.[30] The ratio of 28.7318 indicates an adequate signal, and the model can be used to navigate the design space. The optimised formulation of AMEP was developed by

Design Expert software based on desirability criteria. The predicted value of the optimised formulation as generated by the software was 82.77% *w/w*, which similar to the actual value of formulation F6. Hence, formulation F6 was selected as the optimized batch. The optimal values of the independent variables, *i.e.*, AME-to-phospholipid ratio *(w/w)*, reaction temperature (°C), and reaction time (hours), were found to be 1:1, 55 °C, and 3 h, respectively.

Validation of the optimised model

An additional batch of AMEP was prepared using optimised independent variables to validate the model. Its entrapment efficiency was determined. The predicted entrapment efficiency obtained from the developed model and the actual values of entrapment efficiency achieved from the prepared formulation were compared. The model-predicted value of EE (%) of marmelosin in the optimized formulation of AMEP was found to be 85.16%, while the actual EE (%) from the prepared formulation of AMEP was found to be 83.15±1.04%. Thus, the

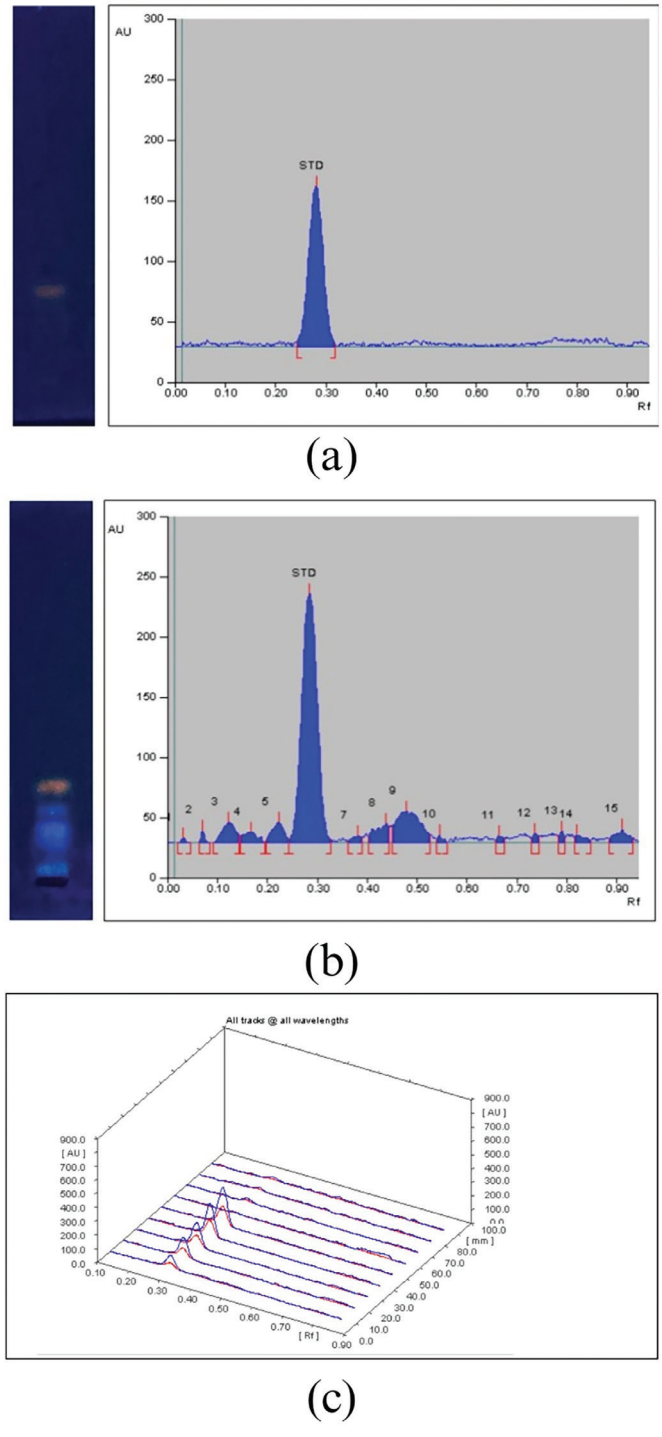

Figure 1. HPTLC chromatograms for marmelosin determination of determination of marmelosin in extract (AME). HPTLC chromatograms of (a) standard marker (marmelosin) at 366 nm; (b) AME at 366 nm; (c) 3D overlay of HPTLC chromatogram of all tracks at 254 nm (red graphs) and 366 nm (blue graphs)

HPTLC: High-performance thin layer chromatography, AME: *Aegle marmelos* fruit extract

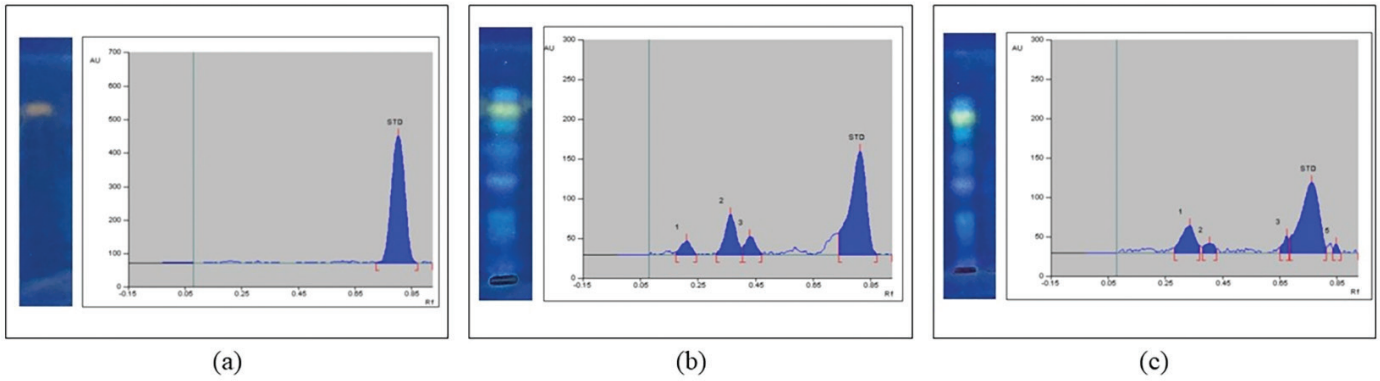

Figure 2. HPTLC chromatogram for entrapment efficiency of marmelosin formulation at 366 nm of determination of entrapment efficiency of marmelosin in formulations at 366 nm. HPTLC chromatographs of (a) standard marker (marmelosin); (b) AME; (c) AMEP

HPTLC: High-performance thin layer chromatography, AMEP: *Aegle marmelos* fruit extract-phospholipid

Table 1. Coded levels and real values for each factor

Independent variable	Actual levels at coded factor levels		
	-1	0	+1
Extract: Phospholipid ratio	1:1	2:1	3:1
Temperature (°C)	35	45	55
Stirring time (h)	1	2	3

applicability of the developed model was validated. The bias (%) was calculated using equation 3 and was found to be less than 3%,[31] suggesting the relative robustness of the model.

$$\text{Bias (\%)} = \frac{\text{predicted value} - \text{observed value}}{\text{predicted value}} \times 100 \quad (3)$$

The predicted and observed entrapment efficiency of AMEP prepared using optimised parameters is given in Table 4. The result confirms the precision and validity of the response surface methodology for the AMEP formulation method.

Solubility profile

The solubility profiles of PC, AME, and AMEP show that PC is soluble in organic solvents, while AME is soluble in polar solvents. Details regarding AMEP's solubility are not provided. AMEP forms micelles in aqueous solutions and is soluble in chloroform.

SEM, particle size, FTIR, and DSC analysis

SEM analysis was performed to observe the surface morphology. The AMEP was dispersed in water before observation under SEM. The electron micrographs showed spherical, uniform vesicles of AMEP (Figure 4a). These spherical vesicles were observed as discrete structures without aggregation.

The particle size of the dispersed AMEP was found to be 673.6±4.30 nm, and its PI was 0.224±0.010 (Figure 4b). The zeta potential was found to be -42.6 mV±0.51 (Figure 4c).

The FTIR and DSC graphs of AME, PC, PM, and AMEP are shown in Figure 5a, b.

In vivo study

DAI, weight loss and colon length

The DAI scores of all groups except the normal group increased in the first 7 days (Figure 6a). The DAI score of the positive-control or DSS group increased consistently and remained higher even on Day 14. The DAI scores of the standard-treated and AMEP-treated groups decreased more, compared with the AME-treated and excipient-treated groups, indicating better amelioration of symptoms of colitis. The animals showed progressive weight loss in the first 7 days as they consumed DSS. Weight loss in colitis is due to the loss of body fluids (diarrhea and colorectal bleeding), malabsorption, and decreased appetite, which leads to nutrient deficiencies.

The DSS group had the maximum weight loss (about 15.0%), while the standard group had the minimum weight loss (5.12%) (Figure 6b). When compared with the standard group, the weight loss was significantly lower in the AMEP-treated group (p=0.0026) compared to the AME-treated group (p<0.0001) and the excipient-treated group (p<0.0001).

The length of the colon in all the DSS-consuming groups was shorter than in the normal group. The colon length of the DSS group was found to be significantly shorter relative to the normal group (p<0.0001). The colon lengths of the standard-treated group (G-III) and the AMEP-treated group (G-V) were not significantly different (p=0.3107), however, the colon lengths of the standard group and the AME group are significantly different (p<0.05) (Figure 6c).

Biochemical evaluation

Animals consuming DSS showed increased levels of NO in colon tissues. The NO level of the DSS group was significantly higher. The NO level in all the treated groups decreased significantly compared to the DSS group. The NO level was lowest in the standard-treated group. No significant difference was observed between the decreased NO level of the standard group and the AMEP-treated group (p=0.1161). However, the difference between the NO level of the standard group and the AME-treated group was significant (p<0.0001) (Figure 7a). The SOD level of the colonic tissues decreased significantly in the DSS group (p<0.001, compared with the normal group). These changes

Table 2. Composition of experimental formulations obtained using Box-Behnken design for AMEP and their respective entrapment efficiency

Formulation	Extract: Phospholipid ratio	Temperature (°C)	Stirring time (h)	Observed entrapment efficiency* (*w/w* %)	Predicted entrapment efficiency (*w/w* %)
F1	-1	0	-1	49.75±0.95	47.20
F2	0	0	0	62.75±0.32	57.82
F3	-1	1	0	71.68±0.44	75.12
F4	1	-1	0	42.31±0.83	40.52
F5	1	0	1	67.62±0.87	68.44
F6	-1	1	1	82.77±1.05	87.16
F7	1	1	0	71.57±0.43	72.27
F8	0	-1	1	51.44±0.65	53.99
F9	0	0	0	60.17±0.41	57.82
F10	0	1	-1	63.15±0.98	61.65
F11	-1	-1	0	43.98±0.67	43.37
F12	1	0	-1	41.99±0.62	44.35
F13	0	-1	-1	23.02±0.89	29.90
F14	0	0	0	62.65±0.30	57.82
F15	-1	0	1	73.87±0.94	71.29

*Each value represents the mean ± standard deviation (n=3), AMEP: *Aegle marmelos* fruit extract-phospholipid

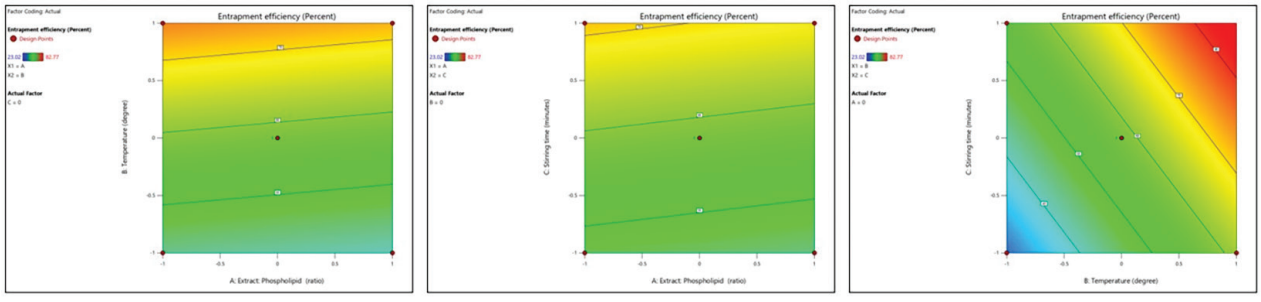

Figure 3. Contour plots showing effect of independent variables on entrapment efficiency (a) temperature and extract to phospholipid ratio; (b) stirring time and extract to phospholipid ratio; (c) stirring time and temperature

were significantly mitigated by the AME-treated, AMEP-treated, and standard groups (with $p<0.05$, 0.01, and 0.01, respectively), as compared with the normal control group (Figure 7b). DSS consumption significantly increased the colonic MDA level in all the groups ($p<0.0001$, compared with the normal group). This change was reversed in all the treated groups and was most decreased by the standard-treated group. The decreased MDA level in the standard group was not significant ($p=0.4396$), compared with the decreased MDA level in the AMEP group, but it was significant ($p<0.05$) compared with that of the AME group. Thus, AMEP decreased the MDA level more efficiently than AME. This could be because of the better bioavailability of the extract complex compared with the plain extract (Figure 7c).

The levels of the pro-inflammatory cytokines TNF-α and IL-6 increased with DSS intake. These levels increased significantly in the DSS group compared with the normal group ($p<0.001$). These increases were reduced by standard, AME, and AMEP treatments. The TNF-α reduction compared with the DSS group was highly significant in the AMEP-treated and standard-treated groups ($p<0.0001$ in both), significant in the AME-treated group ($p<0.01$), and not significant in the excipient-treated group ($p=0.2238$) (Figure 7d). The IL-6 reduction was highly significant in the standard-treated group and the AMEP-treated group ($p<0.0001$, both) compared with the DSS-treated group, but it was not significantly reduced in the AME-treated group or the excipient-treated group ($p=0.2886$, 0.6306, respectively) (Figure 7e).

Table 3. ANOVA and fit statistics results

Source	Sum of squares	Mean square	*f* value	*p* value
Model	3274.44	1091.48	73.27	<0.0001*
A. Extract: Phospholipid ratio	17.62	17.62	1.18	0.3000
B. Temperature	1987.37	1987.37	133.41	<0.0001
C. Stirring time	1144.32	1144.32	76.82	<0.0001
Residual	163.86	14.90		
Lack of fit	159.59	17.73	8.30	0.1121#
Fit statistics				
SD	3.86			
R^2	0.9523			
Adjusted R^2	0.9393			
Predicted R^2	0.9125			
Adeq precision	28.7318			

*: Significant, #: Not significant, ANOVA: Analysis of variance, SD: Standard deviation

Table 4. Predicted and observed entrapment efficiency of AMEP prepared using optimised parameters

Response variable	Predicted values (*w/w* %)	Observed values* (*w/w* %)	
Entrapment efficiency	85.16	83.15 ± 1.04	2.36

*: Mean ± standard deviation (n=3), AMEP: *Aegle marmelos* fruit extract-phospholipid

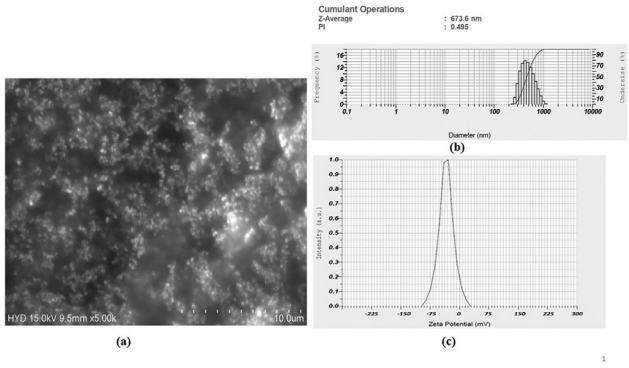

Figure 4. Characterization of optimised AMEP: (a) SEM; (b) particle size and particle index; and (c) zeta potential

AMEP: *Aegle marmelos* fruit extract-phospholipid, SEM: Scanning electron microscopy

Histopathology

The colon architecture was disrupted noticeably in the DSS-treated group (Figure 8). This disruption could be characterized as edema, crypt damage, cell infiltration, ulceration, and sub-mucosal erosion. The standard and AMEP-treated groups had fewer infiltrating cells and suffered less mucosal damage compared with the DSS-treated group. Thus, animals that were treated with the standard treatment and AMEP experienced considerable protection of colon tissue compared with the other groups.

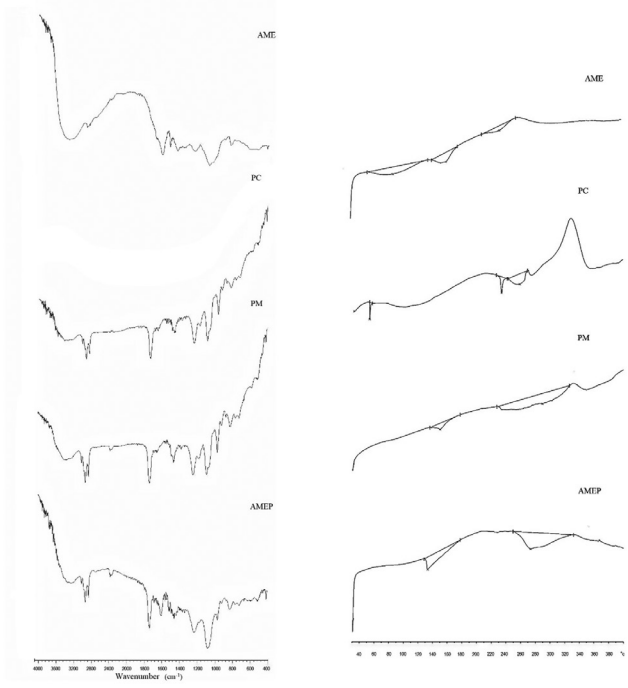

Figure 5. (a) FTIR graphs and (b) thermograms of AME, PC, a PM, and the optimised AMEP formulation

FTIR: Fourier transform infrared spectroscopy, PM: Physical mixture, AMEP: *Aegle marmelos* fruit extract-phospholipid, PC: Phosphatidylcholine

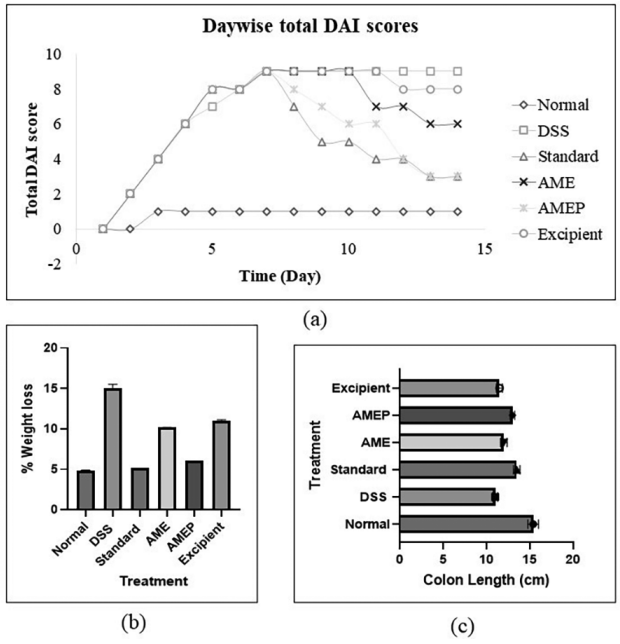

Figure 6. (a) Total DAI scores; (b) weight loss; and (c) colon length in colitis-induced rats
DAI: Disease Activity Index

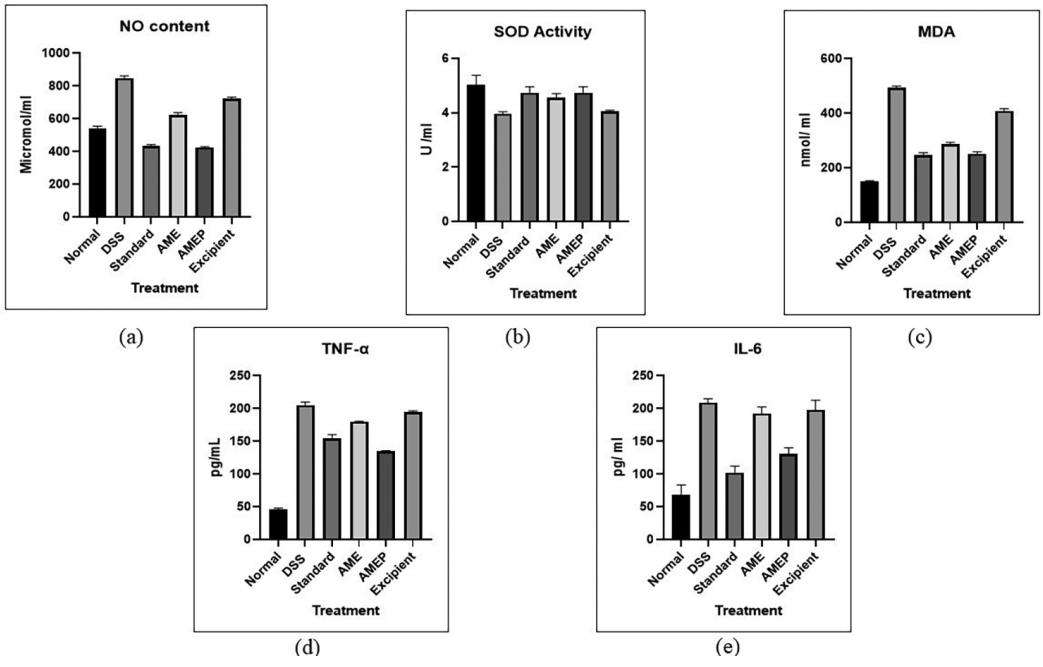

Figure 7. Concentrations of (a) NO; (b) SOD; (c) MDA; (d) TNF-α; and (e) IL-6 levels in rat colon tissues
NO: Nitric oxide, MDA: Malondialdehyde, SOD: Superoxide dismutase, TNF-α: Tumor necrosis factor-alpha, IL-6: Interleukin

DISCUSSION

The parameters that played a significant role in AMEP formulation were the AME to phospholipid ratio *(w/w)*, reaction temperature (°C), and reaction time (hours). The molar ratio of AME-to-phospholipid was not used in the study because of the diverse phytoactives present in AME. The scatterplots of these parameters revealed that there was no correlation between them.

Observing equation (2), it is clear that variables B (temperature) and C (reaction time) have a positive effect, while variables A (AME:PC ratio) have a negative effect on the entrapment efficiency of AMEP. A higher AME:PC ratio decreases entrapment efficiency. An increase in PC increased the complexation. However, higher PC concentrations made the product viscous, so ratios of AME:PC less than 1:1 were not studied. As the concentration of AME increased, the entrapment efficiency did not increase. The AME powder precipitated on the surface of

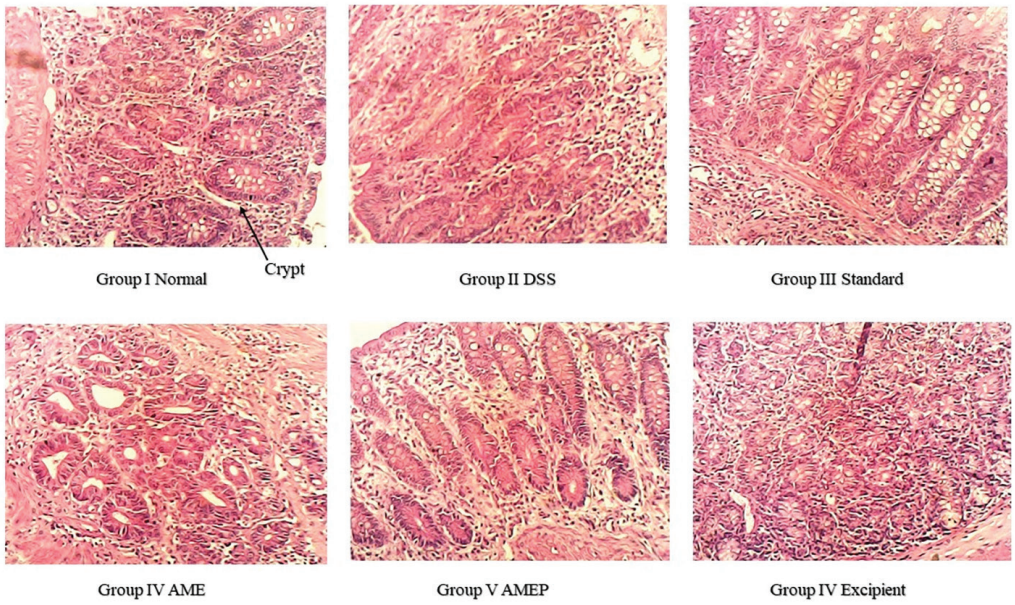

Figure 8. Histopathology of colitis-induced rats
DSS Dextran sulfate sodium, AMEP: A. marmelos fruit extract-phospholipid

the RBF as the ratio of AME to PC increased. This may be due to incomplete entrapment of AME and an insufficient amount of PC to associate with AME. Thus, the weight-by-weight ratio of 1:1 between AME and PC gave maximum entrapment efficiency. The entrapment efficiency of AMEP increased with an increase in temperature. This may be due to the increased melting of lipid at higher temperatures, which led to a decrease in its viscosity. The movement of lipid increased due to its reduced viscosity, leading to interaction with AME, forming an association. Increased stirring time improved the entrapment efficiency, which may be because of increased reaction time and enhanced movement of molecules, leading to augmented complex formation of AME and PC molecules.

The zeta potential is the surface charge of the particles. It helps assess the stability of a formulation. Values greater than -30 mV indicate good physical stability and are considered acceptable.[32] The stability of the dispersed AMEP was found to be acceptable.

In Figure 5a, the region of the FTIR spectra between 3400 and 3200 cm^{-1} shows characteristic peaks of polyphenolic compounds that are due to the polymeric hydroxyl group and hydrogen bond stretching.[33] This can be observed in the AME spectrum as intense peaks in the 3384-3203 cm^{-1} range. The -CH, -CH2, and -CH3 stretching can be observed in the 2950–2850 cm^{-1} range. The FTIR peaks at 1604 and 1560 cm^{-1} are due to aromatic bond stretching, whereas the peaks near 1200 cm^{-1} are due to phenolic C-O stretching. The FTIR spectrum of PC exhibits characteristic peaks of alkanes in the 2931-2854 cm^{-1} region, C=O stretching at 1734 cm^{-1}, P=O stretching at 1244 cm^{-1}, P-O-C stretching at 1089 cm^{-1}; and -N+(CH3)3 stretching at 968 cm^{-1}. The AME and PC peaks in the PM show additive effects, in which almost all the peaks of AME and PC have combined without shifting any peak. However, the FTIR graph of AMEP shows a shift of the P=O peak from 1244 to 1232 cm^{-1} and a shift of the P-O-C peak from 1089 to 1081 cm^{-1}. This may be due to hydrogen bond formation between hydrophilic polyphenols, present in AME, and the polar phosphate head of PC. Also, in the FTIR spectrum of AMEP, the intensity of the peak at 1604 cm^{-1} has changed, and the peak at 1560 cm^{-1} has disappeared, which indicates aromatic ring stretching. This may be influenced by polar covalency, leading to the weakening, withdrawing, or shielding of electrons in bonds. This behaviour may be caused by the packing of AME molecules in the hydrophobic cavity of PC. The AME molecules may be held by Van der Waals forces and hydrophobic interactions. Thus, the FTIR spectrum of AMEP suggests two possible interactions between AME molecules and PC. The first hydrophilic interaction is between the polar head of PC and polyphenols in AME; the second hydrophobic interaction is between the non-polar tail of PC and aromatic molecules in AME.[34]

DSC was used to examine interactions among the components used in the formulation (Figure 5b). The endothermic peaks of AME, PC, PM, and AMEP were observed. The disappearance of existing peak(s), the appearance of new peak(s), altered peak shape, altered onset of a peak, altered peak temperature, and relative peak area or enthalpy signifies an interaction in a DSC.[35] The thermogram of PC shows two sharp endothermic peaks at 55.28 °C and 234.94 °C. The first peak is mostly the melting point of PC, and the second peak is due to phase transitions, *i.e.*, isomeric or crystalline changes in the PC molecule. The AME thermogram shows broad endothermic peaks at 89.12 °C, 161.46 °C, and 234.01 °C. However, the AMEP thermogram shows two peaks at 133 °C and 273.46 °C, which are different from those observed in PC and AME. The interaction of AME with PC may have led to the disappearance of the second endothermic peak

of PC. The DSC of AMEP shows significant reductions in the enthalpy and the melting points of AME and PC. It has been reported that hydrogen bonds can be established between the hydroxyl groups of polyphenols and the polar head of PC.[36] Thus, hydroxyl groups of phenolic moieties in AME could be involved in hydrogen bonding, while aromatic rings could be involved in hydrophobic bonding. The interaction of polyphenol hydroxyl groups of AME with the polar head of PC may allow the hydrocarbon tail of PC to wrap around the polar head of PC, which contains polyphenol molecules. This may lead to the disappearance of the individual peaks of PC and AME, as well as the appearance of two distinct sharp peaks, which may be due to AMEP formation.

The DSS rat model was used to induce colitis. DSS is a sulfated polysaccharide with colitogenic activity. Intestinal inflammation results from damage to the colonic epithelial layer, allowing intestinal contents to infiltrate the underlying tissue and trigger inflammation.

The animals were observed for symptoms of colitis. The animals in the different groups consuming DSS developed symptoms of colitis to various degrees. The symptoms of colitis that were induced included increased DAI, reduced body weight, and reduced colon length. Administration of DSS also caused histological damage through surface epithelial damage, loss of goblet cells, and infiltration of inflammatory cells. The antioxidant activities of the colon tissues were decreased. This could be observed as elevated levels of MDA and NO, a decreased SOD level, and increased levels of proinflammatory cytokines (TNF-α, IL-6).[37] SOD has an antioxidant function, and a decrease in the SOD level corresponds to oxidative damage. MDA is an indicator of oxidative damage, and the MDA level is proportional to the damage.[38] The levels of oxidative stress markers (NO, SOD, and MDA) in the AMEP-treated groups were comparable to those of the standard-treated group. These levels were better controlled by AMEP than by AME. AMEP managed the anti-inflammatory cytokines more efficiently than AME.

The phytoactives exhibit poor oral bioavailability due to their poor solubility. PC being amphiphilic increases the drug solubility by its wetting function and decreases the interfacial tension between the phytoactives and the aqueous environment. The phospholipid complex formation also reduces the crystallinity of the phytoactives, and the increased amorphous nature of the complex may lead to improved solubility of the phytoactives. The phospholipid complexes have high dispersibility, which could be another reason for the improved hydrophilicity of phytoactives. Thus, improved oral bioavailability of the phytoactives may have been attributed to;

• The potential of PC to act as a chaperone molecule to cross the biological membranes and hence improve the absorption and bioavailability of phytoactives.

• The dissolution rate of poorly soluble phytoactives was improved. For poorly soluble drugs, solubility is the rate-limiting step in drug absorption.

• The increased lipophilicity and hydrophilicity of phytoactives which may have enhanced the penetration of phytoactives into intestinal mucosa and/or increased the rate and amount of phytoactives in gastrointestinal fluids, respectively.

The *in vivo* investigations have demonstrated that the anti-colitis activity of AMEP is superior to that of AME. The greater potency can be attributed to the enhanced lipophilic nature of phospholipid complexes, leading to improved bioavailability of the phytoactives.

CONCLUSION

The fruit of *A. marmelos* is underutilised with potential medicinal use. Although it is used in ethnomedicine to alleviate gastrointestinal disorders, its commercial utility for treating colitis has never been explored.

In the current study, *A. marmelos* fruit extract was prepared using a simple maceration technique, and its activity was enhanced by complexing it with phospholipid, using an easy, reproducible, and economical method.

Potential antioxidants and anti-inflammatory phytoconstituents were found in the extract. The extract was quantified, and phospholipid complexes of the extract were formulated and optimized. The *in vivo* activities of the phospholipid complexes of the extract were found to be significantly higher than the plain extract. These findings were supported by the histopathological examination of the colon. Thus, the formulation significantly improves the antioxidant and anti-inflammatory activities of AME. The activity was comparable with that of conventional mesalamine.

It can be concluded that the phospholipid complexes, of *A. marmelos* fruit extract, may provide convenient and safer alternatives to the conventional drugs used in the treatment of UC. The research may stimulate the development of commercial formulations containing phospholipid complexes of phytoactives for the treatment of UC.

Ethics

Ethics Committee Approval: Practical procedures were performed in compliance with the CPCSEA, Government of India, and, as approved by the Institutional Animal Ethic Commitee study protocol (approval number: 535/PO/RERCBT/S/02/CPCSEA/IPER/IAEC/2020-2021/17, date: 19.12.2020).

Informed Consent: Not required.

Acknowledgment

For supporting the project under the Women Scientist Scheme A (WOS-A) programme (DST/WOS-A/LS-73/2020), the authors are grateful to the Department of Science and Technology (DST), Government of India. The authors are thankful to Lipoid GmbH, Ludwigshafen, for providing gift samples of phosphatidylcholine (Lipoid H90).

Footnotes

Authorship Contributions

Concept: P.G.S., Design: P.G.S., D.J.S., Data Collection or Processing: P.G.S., Analysis or Interpretation: P.G.S., D.J.S., R.O.G., Literature Search: P.G.S., Writing: P.G.S., D.J.S, R.O.G.

Conflict of Interest: The authors declare no conflicts of interest.

Financial Disclosure: The authors declared that this study received no financial support.

REFERENCES

1. Ungaro R, Mehandru S, Allen PB, Peyrin-Biroulet L, Colombel JF. Ulcerative colitis. Lancet. 2017;389:1756-1770.
2. Langan RC, Gotsch PB, Krafczyk MA, Skillinge DD. Ulcerative colitis: diagnosis and treatment. Am Fam Physician. 2007;76:1323-1330.
3. Torres J, Billioud V, Sachar DB, Peyrin-Biroulet L, Colombel JF. Ulcerative colitis as a progressive disease: the forgotten evidence. Inflamm Bowel Dis. 2012;18:1356-1363.
4. Bilsborough J, Targan SR, Snapper SB. Therapeutic targets in inflammatory bowel disease: current and future. Am J Gastroenterol Suppl. 2016;3:27-37.
5. Ferretti F, Cannatelli R, Monico MC, Maconi G, Ardizzone S. An update on current pharmacotherapeutic options for the treatment of ulcerative colitis. J Clin Med. 2022;11:2302.
6. Al-Bawardy B, Shivashankar R, Proctor DD. Novel and emerging therapies for inflammatory bowel disease. Front Pharmacol. 2021;12:651415.
7. Lin SC, Cheifetz AS. The use of complementary and alternative medicine in patients with inflammatory bowel disease. Gastroenterol Hepatol. 2018;14:415-425.
8. Navaneethan U, Shen B. Pros and cons of medical management of ulcerative colitis. Clin Colon Rectal Surg. 2010;23:227-238.
9. Atanasov AG, Waltenberger B, Pferschy-Wenzig EM, Linder T, Wawrosch C, Uhrin P, Temml V, Wang L, Schwaiger S, Heiss EH, Rollinger JM, Schuster D, Breuss JM, Bochkov V, Mihovilovic MD, Kopp B, Bauer R, Dirsch VM, Stuppner H. Discovery and resupply of pharmacologically active plant-derived natural products: a review. Biotechnol Adv. 2015;33:1582-1614.
10. Murthy HN, Bhat MA, Dalawai D. Bioactive compounds of bael [*Aegle marmelos* (L.) Correa]. In: Murthy HN, Bapat V, eds. Bioactive compounds in underutilized fruits and nuts. Springer, Cham. Reference Series in Phytochemistry. 2019:1-28.
11. Baliga MS, Thilakchand KR, Rai MP, Rao S, Venkatesh P. *Aegle marmelos* (L.) Correa (Bael) and its phytochemicals in the treatment and prevention of cancer. Integr Cancer Ther. 2013;12:187-196.
12. Bulani VD, Kothavade PS, Kundaikar HS, Gawali NB, Chowdhury AA, Degani MS, Juvekar AR. Inclusion complex of ellagic acid with β-cyclodextrin: characterization and *in vitro* anti-inflammatory evaluation. J Mol Struct. 2016;1105:308-315.
13. Bruni R, Barreca D, Protti M, Brighenti V, Righetti L, Anceschi L, Mercolini L, Benvenuti S, Gattuso G, Pellati F. Botanical sources, chemistry, analysis, and biological activity of furanocoumarins of pharmaceutical interest. Molecules. 2019;24:2163.
14. Pynam H, Dharmesh SM. Antioxidant and anti-inflammatory properties of marmelosin from bael (*Aegle marmelos* L.): inhibition of TNF-α mediated inflammatory/tumor markers. Biomed Pharmacother. 2018;106:98-108.
15. Jiang Y, Fang H, Lin S, Chen Y, Fu Y, Tu Y, Li Q, Hui Z. Imperatorin inhibits LPS-induced bone marrow-derived macrophages activation by decreased NF-κB p65 phosphorylation. Immunopharmacol Immunotoxicol. 2023;45:581-588.
16. Ma T, Liu P, Wei J, Wei J, Zhao M, Yao X, Luo X, Xu S. Imperatorin alleviated endometriosis by inhibiting the activation of PI3K/Akt/NF-κB pathway in rats. Life Sci. 2021;274:119291.
17. Luo M, Luo Y. Imperatorin relieved ulcerative colitis by regulating the Nrf-2/ARE/HO-1 pathway in rats. Inflammation. 2021;44:558-569.
18. Liang X, Chen X, Zhao G, Tang T, Dong W, Wang C, Zhang J, Liao Z. Preparation, characterization, and pharmacokinetic evaluation of imperatorin lipid microspheres and their effect on the proliferation of MDA-MB-231 cells. Pharmaceutics. 2018;10:236.
19. Byeon JC, Ahn JB, Jang WS, Lee SE, Choi JS, Park JS. Recent formulation approaches to oral delivery of herbal medicines. J Pharm Investig. 2019;49:17-26.
20. Kuche K, Bhargavi N, Dora CP, Jain S. Drug-phospholipid complex: a go-through strategy for enhanced oral bioavailability. AAPS PharmSciTech. 2019;20:1-13.
21. Song JG, Noh HM, Lee SH, Han HK. Lipid/clay-based solid dispersion formulation for improving the oral bioavailability of curcumin. Pharmaceutics. 2022;14:2269.
22. Tan Q, Liu S, Chen X, Wu M, Wang H, Yin H, He D, Xiong H, Zhang J. Design and evaluation of a novel evodiamine-phospholipid complex for improved oral bioavailability. AAPS PharmSciTech. 2012;13:534-547.
23. Gnananath K, Nataraj KS, Rao GB. Phospholipid complex technique for superior bioavailability of phytoconstituents. Adv Pharm Bull. 2017;7:35-42.
24. Jia X, Gao Y, Liu L, Guo Y, Wang J, Ma H, Zhao R, Li B, Du Y, Yang Q. Artemisinin alleviates intestinal inflammation and metabolic disturbance in ulcerative colitis rats induced by DSS. Evid Based Complement Alternat Med. 2022;2022(1):6211215.
25. Nishiyama Y, Kataoka T, Yamato K, Taguchi T, Yamaoka K. Suppression of dextran sulfate sodium-induced colitis in mice by radon inhalation. Mediators Inflamm. 2012;2012:239617.
26. Montgomery HAC, Dymock JF. The rapid determination of nitrate in fresh and saline waters. Analyst. 1962;87:374-378.
27. Mesa-Herrera F, Quinto-Alemany D, Díaz M. A sensitive, accurate, and versatile method for the quantification of superoxide dismutase activities in biological preparations. React Oxyg Species. 2019;7:10-20.
28. Kowalczuk K, Stryjecka-Zimmer M. The influence of oxidative stress on the level of malondialdehyde (MDA) in different areas of the rabbit brain. Ann Univ Mariae Curie-Sklodowska Med. 2002;57:160-164.
29. Swamy GJ, Sangamithra A, Chandrasekar V. Response surface modeling and process optimization of aqueous extraction of natural pigments from *Beta vulgaris* using Box-Behnken design of experiments. Dyes Pigm. 2014;111:64-74.
30. Miranda G, Faria S, Bartolomeu F, Pinto E, Madeira S, Mateus A, Carreira P, Alves N, Silva FS, Carvalho O. Predictive models for physical and mechanical properties of 316L stainless steel produced by selective laser melting. Mater Sci Eng A. 2016;657:43-56.
31. Qin X, Yang Y, Fan TT, Gong T, Zhang XN, Huang Y. Preparation, characterization and *in vivo* evaluation of bergenin-phospholipid complex. Acta Pharmacol Sin. 2010;31:127-136.
32. Shah R, Eldridge D, Palombo E, Harding I. Optimisation and stability assessment of solid lipid nanoparticles using particle size and zeta potential. J Phys Sci. 2014;25:59-75.
33. Wongsa P, Phatikulrungsun P, Prathumthong S. FT-IR characteristics, phenolic profiles and inhibitory potential against digestive enzymes of 25 herbal infusions. Sci Rep. 2022;12:6631.
34. Mignet N, Seguin J, Chabot GG. Bioavailability of polyphenol liposomes: a challenge ahead. Pharmaceutics. 2013;5:457-471.

35. Maiti K, Mukherjee K, Gantait A, Saha BP, Mukherjee PK. Curcumin-phospholipid complex: preparation, therapeutic evaluation and pharmacokinetic study in rats. Int J Pharm. 2007;330:155-163.

36. Karonen M. Insights into polyphenol-lipid interactions: chemical methods, molecular aspects and their effects on membrane structures. Plants. 2002;11:1809.

37. Pavan E, Damazo AS, Arunachalam K, Almeida PO de A, Oliveira DM, Venturini CL, Figueiredo F de F, Cruz TCD da, Silva JV da, Martins DT de O. *Copaifera malmei* Harms leaves infusion attenuates TNBS-ulcerative colitis through modulation of cytokines, oxidative stress and mucus in experimental rats. J Ethnopharmacol. 2021;267:113499.

38. Tsikas D. Assessment of lipid peroxidation by measuring malondialdehyde (MDA) and relatives in biological samples: analytical and biological challenges. Anal Biochem. 2017;524:13-30.

Turk J Pharm Sci 2025;22(2):131-139
DOI: 10.4274/tjps.galenos.2025.26723

ORIGINAL ARTICLE

The Effect of Sub-Minimal Inhibitory Concentrations of Daptomycin and Linezolid on Biofilm Formation of Methicillin Resistant *Staphylococcus aureus* Isolated from Clinical Samples

Halil BAL[1]*, Nurten ALTANLAR[2], Sulhiye YILDIZ[3]

[1]Sivas Cumhuriyet University Faculty of Pharmacy, Department of Pharmaceutical Microbiology, Sivas, Türkiye
[2]Ankara University Faculty of Pharmacy, Department of Pharmaceutical Microbiology, Ankara, Türkiye
[3]Lokman Hekim University Faculty of Pharmacy, Department of Pharmaceutical Microbiology, Ankara, Türkiye

ABSTRACT

Objectives: The aim of this study was to determine the development of *in vitro* resistance and changes in biofilm forming abilities in methicillin-resistant *Staphylococcus aureus* (MRSA) isolates exposed to sub-minimal inhibitory concentrations (sub-MICs) of daptomycin and linezolid; and to investigate the presence of the methicillin resistance gene (*mecA*) and the biofilm-associated genes (*icaA*, *icaD*) by polymerase chain reaction.

Materials and Methods: This study was carried out with thirty-two MRSA isolates. The susceptibility of the isolates to daptomycin and linezolid was investigated by the broth microdilution method, and MIC values were determined (1st MIC). After serial passages, the 2nd MIC and the 3rd MIC values were similarly detected. Before and after serial passages, the biofilm-forming abilities of MRSA isolates were examined using the microtiter plate (MTP) method.

Results: When the daptomycin and linezolid 1st MIC and 3rd MIC values of the isolates were compared, there was a 2-8 fold increase in linezolid *($p<0.05$)* and a 4-32 fold increase in daptomycin *($p<0.05$).* According to the MTP method, 20 (62.5%) of the 32 isolates formed biofilm at various levels, while 12 (37.5%) did not form biofilm. After the second series of passages, biofilm formation was observed in 19 (59.4%) isolates with daptomycin ($p>0.05$) and in 16 (50%) isolates with linezolid ($p>0.05$). The *mecA* gene was found in all isolates. Also, *icaA* and *icaD* genes were detected in 31 (96.9%) of 32 MRSA isolates.

Conclusion: MRSA isolates exposed to sub-MICs of the antibiotics daptomycin and linezolid were observed to form biofilms at varying levels or to lose their ability to form biofilms. The induction, reduction or eradication of biofilm depended on the type of antibiotic and the MRSA isolate.

Keywords: Biofilm, daptomycin, linezolid, MRSA, sub-minimal inhibitory concentration

INTRODUCTION

Staphylococcus aureus is an opportunistic pathogenic bacterium. These bacteria are found in the body parts of healthy individuals, such as the nose, intestines, skin, skin glands and mucous membranes.[1] *S. aureus* is resistant to many antibiotics, including various mechanisms. In the early 1940s, shortly after the clinical use of penicillin, penicillin-resistant isolates appeared that produced beta-lactamase. In 1959, the

***Correspondence:** halilbal@cumhuriyet.edu.tr, **ORCID-ID:** orcid.org/0000-0002-0017-3425
Received: 31.10.2023 **Accepted:** 28.03.2025 **Publication Date:** 14.05.2025

Cite this article as: BAL H, ALTANLAR N, YILDIZ S. The effect of sub-minimal inhibitory concentrations of daptomycin and linezolid on biofilm formation of methicillin-resistant *Staphylococcus aureus* isolated from clinical samples. Turk J Pharm Sci. 2025;22(2):131-139

problem was solved with beta-lactamase-resistant methicillin, but in 1961, methicillin-resistant *Staphylococcus aureus* (MRSA) isolates were identified.[2]

MRSA is resistant not only to beta-lactam group antibiotics but also to several other antibiotics, including macrolides and tetracyclines. MRSA isolates have become the leading cause of nosocomial infections worldwide due to limited treatment options.[3] Vancomycin is used for serious MRSA infections. In treatment with vancomycin, the occurrence of less sensitive isolates, poor clinical results, and increased nephrotoxicity with high-dose therapy has been observed. In the early 2000s, daptomycin and linezolid began to be used in the treatment of MRSA infections. Linezolid is used orally or intravenously to treat skin and soft tissue infections and pneumonia. Daptomycin is recommended for the secondary treatment of bacteremia, the treatment of right valve endocarditis, and complicated skin infections.[4-7] Minimal inhibitory concentration (MIC) was defined through sensitivity and antibiotic dosing studies on bacteria. The MIC is the lowest concentration of antibiotic that inhibits the visible growth of bacteria under *in vitro* conditions. During treatment, the antibiotic concentration between two consecutive doses should be higher than the MIC. After a certain period, the concentration applied in the various tissues becomes lower than the MIC value. These antibiotic concentrations below MIC are defined as sub-MIC. Bacteria can be exposed to sub-MIC levels of non-lethal antibiotics in humans, animals, and the environment. Although sub-MICs do not kill bacteria, they can affect various virulence factors such as morphology, surface properties, pathogenicity, biofilm formation, and toxin production.[8] Sub-MICs can affect the emergence of resistant isolates, mutation, recombination, and horizontal gene transfer. In addition, as a signal molecule, it can affect bacterial virulence, altering biofilm formation, quorum sensing, and gene expression.[9-11] This study aimed to investigate the effects of sub-MICs of daptomycin and linezolid on biofilm formation of MRSA isolates and the presence of methicillin resistance gene (*mecA*) and biofilm-associated genes *(icaA and icaD)* of MRSA isolates by polymerase chain reaction.

MATERIALS AND METHODS

This study was conducted with 32 MRSA (abscess, bronchoalveolar lavage, catheter tip, joint fluid, prosthetic-tissue, tracheal aspirate, tissue, wound) isolates. MRSA isolates were obtained from Ankara University Faculty of Medicine Hospitals (Ankara University İbni Sina Hospital and Ankara University Cebeci Central Laboratory). Ethics Committee approval was obtained from Ankara University Faculty of Medicine Clinical Research Ethics Committee (approval number: 08-499-18, dated: 07.05.2018).

Gram staining, catalase, tube coagulase, DNase, and mannitol fermentation tests were performed on MRSA isolates. Then, following the cefoxitin disk diffusion test, the *mecA* gene was investigated by polymerase chain reaction (PCR), and all MRSA isolates were confirmed.[12-16] The susceptibilities of MRSA isolates to daptomycin (DEVA Holding, Türkiye) and linezolid (Haver Farma, Türkiye) were determined by the broth microdilution method.[16] Antibiotic susceptibility experiments were performed in 96-well U-bottom microtiter plates (Eppendorf, Germany) using cation-adjusted Mueller-Hinton broth (CAMHB) medium (Becton Dickenson BBL, Sparks, MD, USA). For the daptomycin MIC test, the calcium concentration in CAMHB medium was adjusted to 50 mg/L.

Linezolid was dissolved in 10% dimethyl sulfoxide (DMSO, Sigma-Aldrich) at a final concentration of 640 µg/mL, and daptomycin was dissolved in sterile distilled water at a final concentration of 160 µg/mL. Two-fold serial dilutions of linezolid (32-0.0625 µg/mL) and daptomycin (8-0.0156 µg/mL) were prepared in CAMHB medium. A 0.5 McFarland culture was prepared in CAMHB and added to the wells. The final bacterial concentration in each well was $5x10^5$ colony-forming units (CFU)/mL. The wells with bacterial suspension without antibiotics were used as positive controls, and the wells with only CAMHB medium were used as negative controls. Microtiter plates were incubated at 35 °C for 24 hours. After incubation, MIC values were determined considering the susceptibility breakpoints approved by the European Committee on Antimicrobial Susceptibility Testing for *S. aureus* (S≤1 µg/mL for daptomycin, S≤4 µg/mL for linezolid).[17] Each experiment was repeated three times. *S. aureus* ATCC 29213 was used as a quality control strain.

Sub-MIC exposure and serial passage

Serial passage experiments were performed for each strain with ½ MIC values (sub-MICs), which were determined against daptomycin and linezolid. Each MRSA strain was passaged through its respective sub-MICs on the first day and incubated at 35 °C for 24 hours. On the second day, each strain was transferred to CAMHB (Becton Dickenson BBL, Sparks, MD, USA) medium and incubated at 35 °C for 24 hours. After sixteen consecutive days, the first series of passages was completed. After the first series of passages, MICs and sub-MICs values were determined again. Similarly, second serial passages were performed to determine the third MIC values.[16-18] *S. aureus* ATCC 29213 used as quality control strain.

Microtiter plate biofilm assay

Biofilm-forming abilities of MRSA isolates were determined by the microtiter plate method (MTP).[19] Biofilm formation levels of all isolates before and after serial passages were examined. Bacteria suspension was prepared in 1% glucose supplemented Tryptic Soy Broth (TSB, Merck, Germany) medium and 0.5 McFarland ($1x10^8$ CFU/mL) turbidity was adjusted. The bacterial suspension was diluted to 1/20 and 20 µL was added to the wells in the flat-bottom microtiter plate with 96 wells (BD Falcon 96 Flat Bottom Transparent, Corning, USA) 180 µL of TSB (Merck, Germany) medium supplemented with 1% glucose was added to the reach a concentration of $5x10^5$ CFU/mL. Microtiter plates were incubated (35 °C, 24 hours). After incubation, it was discharged, washed three times with sterile phosphate buffer solution (Sigma-Aldrich S.R.L., Milan, Italy) using a micropipette, inverted, and left to dry. After the microtiter plates dried, 150 µL of methanol (Merck, Darmstadt,

Germany) was added for fixation, left for 20 minutes, the methanol was removed, and the microtiter plates were left to dry. After the drying process, 0.1% safranin (Sigma-Aldrich, St. Louis, MO) dye was added and left for 15 minutes; the microtiter plates were washed and turned over and left to dry. Three wells were used for each bacterium. TSB (Merck, Germany) medium supplemented with 1% glucose was used as a negative control. *S. aureus* ATCC 6538, *S. epidermidis* ATCC 35984 were used as positive controls. The optical density cut-off value was determined and the results interpreted.[19]

DNA isolation of MRSA isolates

DNA isolation from MRSA samples was performed with a DNA isolation kit (Thermo Scientific GeneJET, Van Allen Way, Carlsbad, California) according to the manufacturer's recommendations.

mecA, icaA, icaD genes amplifications

Amplifications of the methicillin resistance gene *(mecA)* and biofilm-associated genes (*icaA* and *icaD*) were determined by conventional PCR.[20,21] The PCR reaction (50 µL): 35.35 µL (ddH_2O), 2 µL (10 µM each of the primers), 0.4 µL (25 mM dNTPs, GeneDireX Inc. USA), 0.25 µL (5U/µL Taq DNA polymerase, GeneDireX Inc. USA), 5 µL (10X PCR buffer), 5 µL (template DNA). PCR amplification conditions for the *mecA* gene: initial denaturation, 94 °C/5 min; denaturation, 94 °C/30 s; annealing, 55 °C/30 s; extension, 72 °C/1 min; 40 cycles; final extension, 72 °C/5 min. PCR amplification conditions for the *icaA* and *icaD* genes: (initial denaturation: 92 °C/5 min), (denaturation: 92 °C/1 min), (annealing: 49 °C/50 s), (extension: 72 °C/1 min), (30 cycles), (final extension: 72 °C/7 min). Positive controls (*S. aureus* ATCC 6538 and *S. aureus* ATCC 43300), negative control (sterile distilled water).

Statistical analysis

The data were analyzed using SPSS version 24 software (SPSS Inc., IBM, Chicago, IL, USA). Wilcoxon Signed-rank test was used for changes in MIC values and biofilm formation of isolates; Mann-Whitney U test was used for comparison of MIC values; McNemar's test was used for comparison of biofilm formation experiments. *P* value of <0.05 was considered statistically significant.

RESULTS

The *mecA* gene was detected by conventional PCR, and a 533 bp amplicon was obtained. The *mecA* gene was detected in all 32 MRSA. This result was confirmed genotypically for methicillin resistance of all isolates (Figure 1). According to the initial MIC values, all MRSA isolates were found to be susceptible to daptomycin and linezolid. After serial passages with the antibiotics daptomycin and linezolid, there was an increase in the second and third MIC values in all MRSA strains. When we evaluated the first MIC and third MIC results of daptomycin, we observed that there was a 4-32-fold increase in MIC values. A significant difference was found between the first and third MIC values of daptomycin (z=-4.945; $p<0.05$). When linezolid's initial MIC and third MIC values were compared, there was a 2- to 8-fold increase. There was a statistically significant difference between the first MIC and third MIC values of linezolid (z=-5.018; $p<0.05$). In the third MIC value, it was observed that 10 (31.25%) of the samples (Samples IDs: 4, 17, 18, 19, 20, 22, 25, 26, 28, 32) were resistant to daptomycin, whereas all were susceptible to linezolid (Tables 1 and 2). According to the MTP method, 20 (62.5%) of 32 MRSA produced various levels of biofilm (Table 3). Twelve (37.5%) did not produce biofilm. Amplification of the *icaA* and *icaD* genes associated with biofilm formation was performed by conventional PCR.

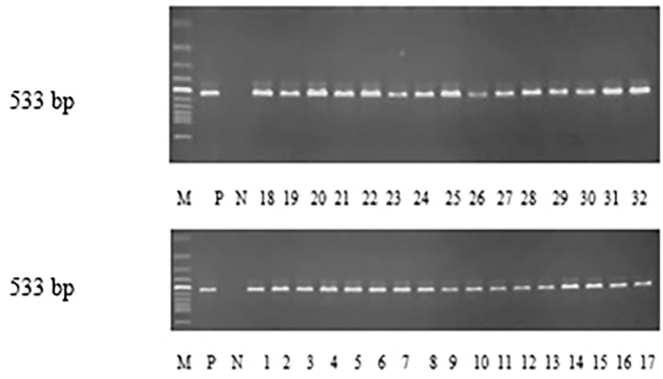

Figure 1. Agarose gel electrophoresis (*mecA* gene, 533 bp) in MRSA isolates. 1-32; [positive samples (533 bp)]. M: 100 bp DNA ladder (Thermo Fisher Scientific, St. LeonRot, Germany) P: (*Staphylococcus aureus* ATCC 43300) positive control, N: Negatif control (sterile distilled water)
MRSA: Methicillin-resistant *Staphylococcus aureus*

Amplicons of 1315 bp for the *icaA* gene and 381 bp for the *icaD* gene were obtained.[22] (96.9%) of 32 MRSA were positive for both *icaA* and *icaD* genes, and 1 (3.1%) strain was negative for both *icaA* and *icaD* genes (Figures 2 and 3). After the second series of passages performed with daptomycin, it was found that 19 (59.4%) of the 32 MRSA were biofilm producers, 13 (40.6%) were not biofilm producers (Table 3). There was no statistically significant difference between the biofilm formation levels of MRSA before serial passages and the biofilm formation levels after the second serial passages performed with daptomycin (z=-0.171; $p>0.05$).

After the second series of passages with linezolid, it was observed that 16 (50%) of 32 MRSA were biofilm producers, 16 (50%) were non-biofilm producers (Table 3). There was no statistically significant difference between the biofilm formation levels of MRSA isolates before serial passages and those levels after the second serial passages performed with linezolid (z=-0.531, $p>0.05$). When we compared the effect of linezolid and daptomycin on the biofilm formation levels of the isolates after the second series of passages, there was no statistically significant difference between the two antibiotics ($p>0.05$).

DISCUSSION

During treatment, the concentration of the antibiotic varies in different body parts. Due to contamination from human activities, sub-MICs of antibiotics are found in sewage, soil, and many aquatic environments.[23] Bacteria in these environments

may be exposed to sub-MICs of antibiotics. sub-MICs can have various effects on bacteria (selection of resistant isolates, genotypic and phenotypic variability, and bacterial signaling).[9] "By Müller et al.[24] *S. aureus* HG001, *S. aureus* SG511 strains were exposed to the sub-MICs of daptomycin by serial passage for 4 months, they found that MIC values increased 100-fold in *S. aureus* HG001 and 800-fold in *S. aureus* SG511." As a result of genetic, proteomic, and transcriptomic analyses, they determined that the cell wall structure thickens and the autolysis rate decreases in both isolates. Similarly, in another study involving daptomycin, a 16-fold increase in MIC values and a significant increase in carotenoid pigment synthesis

Table 1. Linezolid MIC values of MRSA isolates

MRSA sample no.	LNZ 1st MIC (ug/mL) Susceptible (S) Resistant (R)		LNZ 2nd MIC (ug/mL) Susceptible (S) Resistant (R)		LNZ 3rd MIC (ug/mL) Susceptible (S) Resistant (R)		Total increase in fold LNZ	*p* value
1	0.5	S	1	S	1	S	2	$p<0.05$
2	0.25	S	0.5	S	2	S	8	$p<0.05$
3	0.5	S	1	S	2	S	4	$p<0.05$
4	0.5	S	1	S	2	S	4	$p<0.05$
5	0.5	S	1	S	2	S	4	$p<0.05$
6	1	S	2	S	2	S	2	$p<0.05$
7	1	S	2	S	2	S	2	$p<0.05$
8	0.25	S	1	S	2	S	8	$p<0.05$
9	0.5	S	1	S	2	S	4	$p<0.05$
10	0.25	S	0.5	S	2	S	8	$p<0.05$
11	0.25	S	1	S	2	S	8	$p<0.05$
12	0.25	S	1	S	2	S	8	$p<0.05$
13	0.25	S	1	S	2	S	8	$p<0.05$
14	0.25	S	1	S	2	S	8	$p<0.05$
15	1	S	2	S	2	S	2	$p<0.05$
16	0.5	S	2	S	2	S	4	$p<0.05$
17	1	S	2	S	2	S	2	$p<0.05$
18	0.5	S	1	S	2	S	4	$p<0.05$
19	0,25	S	1	S	2	S	8	$p<0.05$
20	0.5	S	1	S	2	S	4	$p<0.05$
21	0.25	S	1	S	2	S	8	$p<0.05$
22	0.5	S	1	S	2	S	4	$p<0.05$
23	0.5	S	1	S	1	S	2	$p<0.05$
24	0.5	S	1	S	2	S	4	$p<0.05$
25	0.25	S	1	S	2	S	8	$p<0.05$
26	0.5	S	1	S	2	S	4	$p<0.05$
27	0.5	S	1	S	2	S	4	$p<0.05$
28	0.5	S	1	S	2	S	4	$p<0.05$
29	0.5	S	1	S	2	S	4	$p<0.05$
30	0.5	S	1	S	2	S	4	$p<0.05$
31	0.5	S	1	S	1	S	2	$p<0.05$
32	0.5	S	1	S	2	S	4	$p<0.05$
S. aureus ATCC 29213	1	S	2	S	2	S	2	$p<0.05$

LNZ: Linezolid, MRSA: Methicillin-resistant *S. aureus*, *S. aureus: Staphylococcus aureus* No.: Number, MIC: Minimal inhibitory concentration

were determined in MRSA strains.[25] "In Lahiri and Alm[26] in their experiments with *S. aureus* ATCC 29213 strain, found a 16-fold increase in the MIC value of ceftaroline, while the MIC values of non-β-lactam antibiotics (vancomycin, levofloxacin, linezolid) remained in a 2-fold dilution." They stated that this situation is not a general resistance mechanism, but may be associated with a mechanism specific to β-lactam. In our study, after serial passages with daptomycin and linezolid antibiotics, an increase in the 2nd and 3rd MIC values was observed in all MRSA isolates. Staphylococcal biofilms can appear on medical devices such as catheters, prosthetic joints, and implants.[27] Staphylococcal biofilm expression can be influenced by different physical

Table 2. Daptomycin MIC values of MRSA

MRSA sample no.	DAP 1st MIC (ug/mL) Susceptible (S) Resistant (R)		DAP 2nd MIC (ug/mL) Susceptible (S) Resistant (R)		DAP 3rd MIC (ug/mL) Susceptible (S) Resistant (R)		Total increase in fold DAP	*p* value
1	0.0625	S	0.125	S	1	S	16	$p<0.05$
2	0.0625	S	0.25	S	1	S	16	$p<0.05$
3	0.125	S	0.125	S	1	S	8	$p<0.05$
4	0.125	S	0.25	S	2	R	16	$p<0.05$
5	0.0625	S	0.125	S	0.5	S	8	$p<0.05$
6	0.125	S	0.125	S	1	S	8	$p<0.05$
7	0.125	S	0.125	S	0.5	S	4	$p<0.05$
8	0.0625	S	0.25	S	1	S	16	$p<0.05$
9	0.03125	S	0.125	S	0.25	S	8	$p<0.05$
10	0.0625	S	0.125	S	0.5	S	8	$p<0.05$
11	0.0625	S	0.125	S	0.25	S	4	$p<0.05$
12	0.0625	S	0.25	S	0.5	S	8	$p<0.05$
13	0.0625	S	0.125	S	0.25	S	4	$p<0.05$
14	0.0625	S	0.5	S	0.5	S	8	$p<0.05$
15	0.0625	S	0.125	S	0.25	S	4	$p<0.05$
16	0.0625	S	0.25	S	0.25	S	4	$p<0.05$
17	0.25	S	0.5	S	2	R	8	$p<0.05$
18	0.0625	S	0.5	S	2	R	32	$p<0.05$
19	0.0625	S	0.5	S	2	R	32	$p<0.05$
20	0.25	S	0.5	S	2	R	8	$p<0.05$
21	0.125	S	0.125	S	0.5	S	4	$p<0.05$
22	0.0625	S	0.25	S	2	R	32	$p<0.05$
23	0.125	S	0.25	S	0.5	S	4	$p<0.05$
24	0.25	S	0.5	S	1	S	4	$p<0.05$
25	0.25	S	0.5	S	2	R	8	$p<0.05$
26	0.125	S	0.5	S	2	R	16	$p<0.05$
27	0.125	S	0.5	S	1	S	8	$p<0.05$
28	0.0625	S	0.25	S	2	R	32	$p<0.05$
29	0.0625	S	0.25	S	0.5	S	8	$p<0.05$
30	0.125	S	0.25	S	1	S	8	$p<0.05$
31	0.125	S	0.5	S	1	S	8	$p<0.05$
32	0.0625	S	0.5	S	2	R	32	$p<0.05$
S. aureus ATCC 29213	0.25	S	0.5	S	0.5	S	2	$p<0.05$

DAP: Daptomycin, MRSA: Methicillin-resistant *S. aureus*, *S. aureus: Staphylococcus aureus* No.: Number, MIC: Minimal inhibitory concentration

and chemical factors and is induced in response to sub-MICs of certain antibiotics and external stress.[28-30] Numerous studies are showing that sub-MICs of some antibiotics affect bacterial biofilms *in vitro*. This is clinically important because bacteria may be exposed to sub-MICs at the beginning of the dosing regimen or between doses.[31] Adhesion factors and

Table 3. Biofilm formation levels of MRSA isolates

MRSA sample no.	Before serial passages	Daptomycin (after 2nd serial passages)	Linezolid (after 2nd serial passages)
1	I	I	I
2	III	II	0
3	I	III	II
4	II	III	II
5	0	III	0
6	III	II	III
7	III	III	0
8	I	III	I
9	0	0	0
10	I	I	III
11	0	I	II
12	0	0	0
13	0	0	0
14	I	0	0
15	I	III	I
16	I	II	III
17	II	III	II
18	0	0	0
19	0	0	0
20	III	0	0
21	0	I	0
22	0	0	0
23	I	I	II
24	III	I	III
25	0	0	0
26	II	0	0
27	II	0	II
28	0	III	III
29	I	III	II
30	III	I	0
31	III	0	III
32	0	0	0
Total biofilm*	20	19	16
S. aureus ATCC 29213	0	0	0
S. aureus ATCC 43300	III	III	III

0: No biofilm production, I: Weak biofilm production, II: Moderate biofilm production, III: Strong biofilm production, MRSA: Methicillin-resistant *Staphylococcus aureus*, *($p<0.05$)

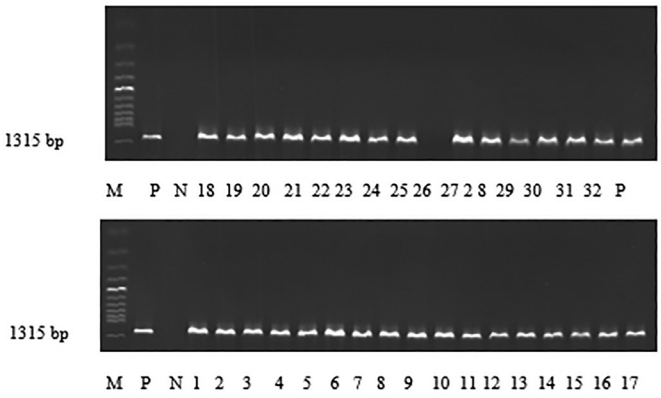

Figure 2. Agarose gel electrophoresis (*icaA* gene, 1315 bp) in MRSA isolates. M: 100 bp DNA ladder (Thermo Fisher Scientific, St. LeonRot, Germany). P: Positive control (*Staphylococcus aureus* ATCC, 43300), *icaA* positive samples (1-25, 27-32), *icaA* negative sample (26), N: Negative control (steril distilled water)

MRSA: Methicillin-resistant *Staphylococcus aureus*

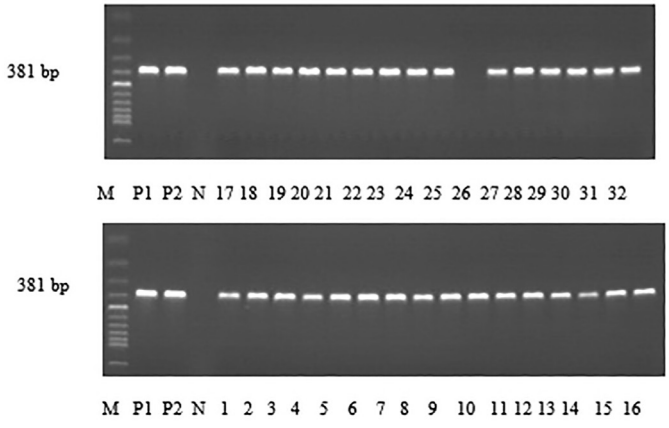

Figure 3. Agarose gel electrophoresis (*icaD* gene, 381 bp) in MRSA isolates. P1: Positive control (*Staphylococcus aureus* ATCC, 43300), P2: Positive control (*Staphylococcus aureus* ATCC 6538), *icaD* positive samples (1-25, 27-32), *icaD* negatif sample (26), N: Negative control (steril distilled water), M: 100 bp DNA ladder (Thermo Fisher Scientific, St. LeonRot, Germany), MRSA: Methicillin-resistant *Staphylococcus aureus*

polysaccharide intracellular adhesion (PIA) molecules are required for staphylococci to form biofilms. The *icaADBC* operon is located in the intercellular adhesion (ica) locus. The *icaADBC* operon contains four genes *(icaA, icaD, icaB, icaC)* encoding the proteins required for PIA production.[32,33] Cramton et al.[34] reported that *Staphylococcus* strains had *icaA* and *icaD* genes, but they could not form biofilms *in vitro*, which may be due to a point mutation in the locus. Arciola et al.[22] stated that the expression of *icaA* and *icaD* genes can be affected by various environmental factors such as medium content and anaerobic environment. Biofilm formation of *S. aureus* is explained by mechanisms independent of *ica* genes.[35] The *ArlRS* gene system in *S. aureus* is effective in autolysis, biofilm formation, capsule synthesis, and virulence.[35,36] Toledo-Arana et al.[37] reported that mutations in the ArlRS system increased biofilm formation and that the biofilm formation of the ArlRS mutant strain was not affected by the deletion of the *icaADBC* locus.34 Similarly, in our study, *icaA* and *icaD* genes were negative in 1 (3.1%) out of 32 MRSA isolates. This strain formed biofilm by the MTP. It was found to be compatible with these studies.

Some studies show that sub-MICs of antibiotics such as vancomycin, cephalexin, oxacillin, and cephalothin, which are effective on the cell wall, can induce biofilm formation of *S. aureus*.[38-40] In a similar study, Sritharadol et al.[41] observed that low mupirocin concentrations induced biofilm formation, especially in the MRSA USA 300 clone. In another study, Lázaro-Díez et al.[42] reported that sub-MICs of ceftaroline induce bacterial attachment and biofilm formation in some MRSA strains, and it is important to use effective bactericidal concentrations of ceftaroline in the treatment of biofilm MRSA-related infections. Kaplan et al.[43] stated that sub-MIC concentrations of methicillin, ampicillin, amoxicillin, and cloxacillin-induced biofilm formation were observed in.

At least one of the USA300, USA400, and USA500 MRSA strains. The induction depended on the antibiotic type and the strain, and methicillin-induced biofilm formation was observed in all three isolates. As a result of the second series of passage experiments in our study, it was determined that the induction, reduction, or destruction of biofilm formation varies according to the antibiotic and isolate, which aligns with our findings.

CONCLUSION

In this study, it was observed that the MIC values of daptomycin and linezolid in MRSA isolates increased after serial passages. After the second series of passages, it was determined that changes in the biofilm formation levels of the isolates varied by isolate and antibiotic type. Biofilm is a factor that complicates the treatment process and requires additional costs. Sub-MICs can affect biofilm formation in bacteria. In the treatment process, it is important to select the appropriate antibiotic, adjust the antibiotic dose range, and prevent random contact of antibiotics with the environment. In this way, the exposure of bacteria to sub-MICs can be reduced, preventing antibiotic resistance and biofilm formation.

Ethics

Ethics Committee Approval: Ethics Committee approval was obtained from Ankara University Faculty of Medicine Clinical Research Ethics Committee (approval number: 08-499-18, dated: 07.05.2018).

Informed Consent: Not required.

Footnotes

Authorship Contributions

Concept: H.B., N.A., S.Y., Design: H.B., N.A., S.Y., Data Collection or Processing: H.B., N.A., S.Y., Analysis or Interpretation: H.B., N.A., S.Y., Literature Search: H.B., N.A., S.Y., Writing: H.B., N.A., S.Y.

Conflict of Interest: The authors declare no conflicts of interest.

Financial Disclosure: The authors declared that this study received no financial support.

REFERENCES

1. Lakhundi S, Zhang K. Methicillin-resistant *Staphylococcus aureus*: Molecular characterization, evolution, and epidemiology. Clin Microbiol Rev. 2018;31:e00020-18.
2. Palavecino E. Community-acquired methicillin-resistant *Staphylococcus aureus* infections. Clinics in laboratory medicine. 2004;24:403-418.
3. Gonçalves E, Carvalhal R, Mesquita R, Azevedo J, Coelho MJ, Magalhães R, Ferraz MP, Manso MC, Gavinha S, Pina C, Lopes Cardoso I. Detection of *Staphylococcus aureus* (MRSA/MSSA) in surfaces of dental medicine equipment. Saudi J Biol Sci. 2020;27:1003-1008.
4. Rodvold KA, McConeghy KW. Methicillin-resistant *Staphylococcus aureus* therapy: past, present, and future. Clin Infect Dis. 2014;58 Suppl 1:S20-S27.
5. Molloy L. Methicillin-resistant *Staphylococcus aureus*: A pharmacotherapy primer. Journal of Pediatric Health Care: Official publication of National Association of Pediatric Nurse Associates & Practitioners. 2017;31:2:246-256.
6. Foster TJ. Antibiotic resistance in *Staphylococcus aureus*. Current status and prospects. FEMS Microbiol Rev. 2017;41:430-449.
7. Hashemian SMR, Farhadi T, Ganjparvar M. Linezolid: a review of its properties, function, and use in critical care. Drug Des Devel Ther. 2018;12:1759-1767.
8. Sato Y, Unno Y, Ubagai T, Ono Y. Sub-minimum inhibitory concentrations of colistin and polymyxin B promote *Acinetobacter baumannii* biofilm formation. PLoS One. 2018;13:e0194556.
9. Andersson DI, Hughes D. Microbiological effects of sublethal levels of antibiotics. Nat Rev Microbiol. 2014;12:465-478.
10. Liu B, Zhang X, Ding X, Wang Y, Zhu G. Regulatory mechanisms of sub-inhibitory levels antibiotics agent in bacterial virulence. Appl Microbiol Biotechnol. 2021;105:3495-3505.
11. Chen J, Zhou H, Huang J, Zhang R, Rao X. Virulence alterations in *Staphylococcus aureus* upon treatment with the sub-inhibitory concentrations of antibiotics. J Adv Res. 2021;31:165-175.
12. Procop GW, Church DL, Hall GS, Janda WM, Koneman EW, Schrecken-Berger PC. Woods. In: GL (ed). Koneman's color atlas and textbook of diagnostic microbiology, 7th ed. Wolters Kluwer, Philadelphia. 2017a; PA. Page: 693.
13. Procop GW, Church DL, Hall GS, Janda WM, Koneman EW, Schrecken-Berger PC, WOODS. In: GL (ed). Koneman's color atlas and textbook of diagnostic microbiology, 7th ed. Wolters Kluwer, Philadelphia. 2017b; PA. Page: 702.
14. Pumipuntu N, Kulpeanprasit S, Santajit S, Tunyong W, Kong-Ngoen T, Hinthong W, Indrawattana N. Screening method for *Staphylococcus aureus* identification in subclinical bovine mastitis from dairy farms. Vet World. 2017;10:721-726.
15. EUCAST Disk disk diffusion method for antimicrobial susceptibility testing. 2021a;Version 9.0.
16. EUCAST The European Committee on Antimicrobial Susceptibility Testing. Routine and extended internal quality control for MIC determination and disk diffusion as recommended by EUCAST. 2021b; Version 11.0.
17. EUCAST Breakpoint tables for interpretation of MICs and zone diameters. Version 2021c; 11.0.
18. Woodburn KW, Jaynes JM, Clemens LE. Evaluation of the antimicrobial peptide, RP557, for the broad-spectrum treatment of wound pathogens and biofilm. Front Microbiol. 2019;10:1688.
19. Stepanović S, Vuković D, Hola V, Di Bonaventura G, Djukić S, Cirković I, Ruzicka F. Quantification of biofilm in microtiter plates: overview of testing conditions and practical recommendations for assessment of biofilm production by *Staphylococci*. APMIS. 2007;115:891-899.
20. Radenovic M, Asanin J, Aksentijevi C K, Misic D. Investigation of presence of methicillin resistant *Staphylococci* in students of the faculty of veterinary medicine at the university of belgrade. Archives of Veterinary Medicine. 2017;9:17-28.
21. Branko S, Vlado T, Dragan V, Karabasil N, Mirjana D, Jasna D, Vera K. Detection of *icaA* and *icaD* genes of *Staphylococcus aureus* isolated in cases of bovine mastitis in the republic of serbia. Acta Veterinaria-Beograd. 2017;67:168-177.
22. Arciola CR, Campoccia D, Speziale P, Montanaro L, Costerton JW. Biofilm formation in *Staphylococcus* implant infections. A review of molecular mechanisms and implications for biofilm-resistant materials. Biomaterials. 2012;33:5967-5982.
23. Sandegren L. Selection of antibiotic resistance at very low antibiotic concentrations. Ups J Med Sci. 2014;119:103-107.
24. Müller A, Grein F, Otto A, Gries K, Orlov D, Zarubaev V, Girard M, Sher X, Shamova O, Roemer T, François P, Becher D, Schneider T, Sahl HG. Differential daptomycin resistance development in *Staphylococcus aureus* strains with active and mutated gra regulatory systems. Int J Med Microbiol. 2018;308:335-348.
25. Mishra NN, Rubio A, Nast CC, Bayer AS. Differential adaptations of methicillin-resistant *Staphylococcus aureus* to serial *in vitro* passage in daptomycin: Evolution of daptomycin resistance and role of membrane carotenoid content and fluidity. Int J Microbiol. 2012;2012:683450.
26. Lahiri SD, Alm RA. Identification of non-PBP2a resistance mechanisms in *Staphylococcus aureus* after serial passage with ceftaroline: Involvement of other PBPs. J Antimicrob Chemother. 2016;71:3050-3057.
27. Kwiecinski JM, Jacobsson G, Horswill AR, Josefsson E, Jin T. Biofilm formation by *Staphylococcus aureus* clinical isolates correlates with the infection type. Infect Dis (Lond). 2019;51:446-451.
28. Götz F. *Staphylococcus* and biofilms. Mol Microbiol. 2002;43:1367-1378.
29. Rachid S, Ohlsen K, Witte W, Hacker J, Ziebuhr W. Effect of subinhibitory antibiotic concentrations on polysaccharide intercellular adhesin expression in biofilm-forming Staphylococcus *epidermidis*. Antimicrob Agents Chemother. 2000;44:3357-3363.
30. Rossatto FC, Pinto JB, Costa GA, Frazzon AP. *In vitro* biofilm formation ability of *Staphylococci* under different growth conditions. Int J Appl Microbiol Biotechnol Res. 2017;5:2:12-19.
31. Odenholt I. Pharmacodynamic effects of subinhibitory antibiotic concentrations. Int J Antimicrob Agents. 2001;17:1-8.
32. Silva V, Almeida L, Gaio V, Cerca N, Manageiro V, Caniça M, Capelo JL, Igrejas G, Poeta P. Biofilm formation of multidrug-resistant MRSA strains isolated from different types of human infections. Pathogens. 2021;10:970.
33. Kadkhoda H, Ghalavand Z, Nikmanesh B, Kodori M, Houri H, Taghizadeh Maleki D, Karimi Bavandpour A, Eslami G. Characterization of biofilm formation and virulence factors of *Staphylococcus aureus* isolates from paediatric patients in Tehran, Iran. Iran J Basic Med Sci. 2020;23:691-698.

34. Cramton SE, Gerke C, Schnell NF, Nichols WW, Götz F. The intercellular adhesion (ica) locus is present in *Staphylococcus aureus* and is required for biofilm formation. Infect Immun. 1999;67:5427-5433.

35. Arciola CR, Campoccia D, Ravaioli S, Montanaro L. Polysaccharide intercellular adhesin in biofilm: Structural and regulatory aspects. Front Cell Infect Microbiol. 2015;5:7.

36. Crosby HA, Tiwari N, Kwiecinski JM, Xu Z, Dykstra A, Jenul C, Fuentes EJ, Horswill AR. The *Staphylococcus aureus* ArlRS two-component system regulates virulence factor expression through MgrA. Mol Microbiol. 2020;113:103-122.

37. Toledo-Arana A, Merino N, Vergara-Irigaray M, Débarbouillé M, Penadés JR, Lasa I. *Staphylococcus aureus* develops an alternative, ica-independent biofilm in the absence of the arlRS two-component system. J Bacteriol. 2005;187:5318-5329.

38. Mirani ZA, Jamil N. Effect of sub-lethal doses of vancomycin and oxacillin on biofilm formation by vancomycin intermediate resistant *Staphylococcus aureus*. J Basic Microbiol. 2011;51:191-195.

39. Haddadin RN, Saleh S, Al-Adham IS, Buultjens TE, Collier PJ. The effect of subminimal inhibitory concentrations of antibiotics on virulence factors expressed by *Staphylococcus aureus* biofilms. J Appl Microbiol. 2010;108:1281-1291.

40. Subrt N, Mesak LR, Davies J. Modulation of virulence gene expression by cell wall active antibiotics in *Staphylococcus aureus*. J Antimicrob Chemother. 2011;66:979-984.

41. Sritharadol R, Hamada M, Kimura S, Ishii Y, Srichana T, Tateda K. Mupirocin at subinhibitory concentrations induces biofilm formation in *Staphylococcus aureus*. Microb Drug Resist. 2018;24:1249-1258.

42. Lázaro-Díez M, Remuzgo-Martínez S, Rodríguez-Mirones C, Acosta F, Icardo JM, Martínez-Martínez L, Ramos-Vivas J. Effects of subinhibitory concentrations of ceftaroline on methicillin-resistant *Staphylococcus aureus* (MRSA) biofilms. PLoS One. 2016;11:e0147569.

43. Kaplan JB, Izano EA, Gopal P, Karwacki MT, Kim S, Bose JL, Bayles KW, Horswill AR. Low levels of β-lactam antibiotics induce extracellular DNA release and biofilm formation in *Staphylococcus aureus*. mBio. 2012;3:e00198-12.

Turk J Pharm Sci 2025;22(2):140-153
DOI: 10.4274/tjps.galenos.2025.48840

ORIGINAL ARTICLE

Pre-Formulation Studies of Lipid-Based Formulation Approach for a Poorly Water-Soluble Biopharmaceutics Classification System Class II Model Drug: Bosentan

Duygu YILMAZ USTA, Zeynep Şafak TEKSİN*

Gazi University Faculty of Pharmacy, Department of Pharmaceutical Technology, Ankara, Türkiye

ABSTRACT

Objectives: This study aimed to perform pre-formulation studies, formulation development, and formulation optimization for self-nanoemulsifying drug delivery systems (SNEDDS), a lipid-based formulation approach to improve the low solubility of bosentan monohydrate (BOS).

Materials and Methods: Pseudo-ternary phase diagrams were created for pre-formulation studies and formulation design for SNEDDS. The SNEDDS was optimized with BBD. The optimized BOS-loaded SNEDDS formulation was characterized by droplet size (DS), polydispersity index (PDI), dispersibility, an efficiency test of self-nanoemulsification, % transmittance, turbidity, robustness, and the effects of pH, viscosity, and thermodynamic and long-term stability studies. The *in vitro* dissolution studies were performed in distilled water containing 1% sodium lauryl sulfate, which is a Food and Drug Administration-recommended medium, and in biorelevant media. *Ex vivo* studies were conducted in biorelevant media.

Results: The optimum BOS-loaded SNEDDS had a DS of 16.76 nm and PDI of 0.200. The characterization studies satisfied SNEDDS requirements (does not deteriorate when diluted at different pHs; resistant to thermodynamic changes; self-emulsifying within 1 minute; Grade A; and transparent) for both blank and BOS-loaded SNEDDS. In long-term stability studies, it was found to be stable for six months. When *in vitro* dissolution was compared to the performance of the commercial product (Tracleer®), the BOS-loaded SNEDDS showed 2.88, 7.63, 3.83, and 4.23 increases in the percentages of cumulative dissolution in fasted state simulated intestinal fluid (FaSSIF), fed state simulated intestinal fluid (FeSSIF), FaSSIF-V2, and FeSSIF-V2, respectively. The *ex vivo* permeation study showed 12.2-, 19.1-, 20.3-, and 13.1-fold increases in drug permeation in FaSSIF, FeSSIF, FaSSIF-V2, and FeSSIF-V2 for the SNEDDS formulation, as compared to the commercial product, respectively.

Conclusion: Pre-formulation and formulation studies were carried out successfully, and lipid-based optimum BOS-loaded SNEDDS were obtained. The present study confirms the potential of optimum BOS-loaded SNEDDS, which was found to be stable over the long term, to increase the drug's solubility, *in vitro* dissolution, and *ex vivo* permeability. This formulation approach has been promising for further *in vivo* studies, to improve the oral bioavailability of BOS.

Keywords: Bosentan, experimental design, lipid-based formulation, self-nanoemulsifying drug delivery system, SNEDDS, pre-formulation studies

***Correspondence:** zsteksin@gmail.com, **ORCID-ID:** orcid.org/0000-0001-6359-5935
Received: 22.03.2024, **Accepted:** 28.03.2025 **Publication Date:** 14.05.2025

Cite this article as: YILMAZ USTA D, TEKSİN ZŞ. Pre-formulation studies of lipid-based formulation approach for a poorly water-soluble Biopharmaceutics Classification System class II model drug: Bosentan. Turk J Pharm Sci. 2025;22(2):140-153

INTRODUCTION

Many known and newly discovered drug candidates show limited solubility in water, which affects variable bioavailability and poor oral absorption. Advances in oral drug delivery systems can provide formulation options to resolve the solubility limitations of such compounds, thereby enabling the drug to be administered in a form that overcomes poor solubility problems by changing the formulation rather than the molecular structure. Different conventional techniques are used to increase solubility.[1] However, lipid formulations have emerged as a successful new approach to increasing the solubility of poorly soluble drugs belonging to the Biopharmaceutics Classification System (BCS) class II.

Self-nanoemulsifying drug delivery systems (SNEDDS) are one of the most common and commercially applicable lipid-based approaches for poorly water-soluble drugs. This system consists of oil, surfactant, cosurfactant, and active substance, and the agitation of this mixture forms *o/w* nanoemulsions in the gastrointestinal tract. As a result of the small droplet size (DS), the nanoemulsified drug can be effectively taken along the lymphatic path without undergoing hepatic first-pass effects.[2,3]

Bosentan monohydrate (BOS) is a BCS class II drug (solubility water: 1 mg/100 mL, pKa: 5.8, log P: 4.94) for the treatment of pulmonary arterial hypertension (PAH).[4-6] The bioavailability of BOS is approximately 50%. Despite the potential benefit of PAH treatment, the use of BOS is controversial due to its considerable cost.[7] Therefore, it would be crucial for both pharmacoeconomics and treatment to find a dosage form that produces the same or greater therapeutic efficacy with a lower dose.

The design of experiments has recently become common practice in both industry and academia. This systematic approach provides an understanding of the interactions among the variables.[8] Box-Behnken design (BBD) is a 3-factor, 3-level statistical approach used for this purpose. The interaction effects of the amounts of components of the optimum SNEDDS formulation, developed in our study, on the response variables were evaluated using BBD.[9]

Existing micro and nanoemulsion studies in the literature report that formulations formed of varied lipids increased the % cumulative dissolved of BOS because of the enhancement of its solubility.[10,11] This study focused on identifying, formulating, and optimizing different formulation components for oral delivery of BOS *via* SNEDDS, a lipid-based formulation approach, to increase solubility, dissolution, and permeability compared to the commercial product (Tracleer®). For this purpose, a solubility-based screening was conducted for groups of formulation components. Then, pseudo-ternary phase diagrams were created, and formulation combinations were obtained. Researchers continued the studies by selecting the most suitable formulation by analyzing their pseudo-ternary phase diagrams and fundamental formulation characteristics of SNEDDS. The selected formulation was optimized with BBD and examined in terms of physicochemical properties, as well as *in vitro* and *ex vivo* characterization, and stability. It was evaluated whether it could be a candidate for *in vivo* studies.[2,12] This study includes pre-formulation part of the previous studies. After this detailed pre-formulation study, further *in vivo* studies were conducted successfully.

MATERIALS AND METHODS

Materials

Methanol, acetonitrile, triethylamine, and sodium lauryl sulfate were purchased from Merck (Germany). Methanol and phosphoric acid were purchased from Sigma-Aldrich (France). Cremophor® RH 40 was purchased from BASF (Germany). Black seed oil, flaxseed oil, sesame oil, cotton oil, olive oil, and grape seed oil were purchased from ZadeVital® (Türkiye). Corn oil, oleic acid, and sunflower oil were purchased from the Turkish drug market. Imwitor® 988, Imwitor® 948, Miglyol® 812, Miglyol® 818, and Miglyol® 840 were provided as samples by Oleochemicals (Germany). Captex® 355 and Capmul® MCM C8 were provided as samples by Abitec (USA). Propylene glycol dicaprolate/dicaprate Labrafac®, Labrasol®, Capryol® 90, Maisine®, and Peceol® were provided as samples by Gattefossé (France). BOS was provided by Abdi İbrahim (Türkiye). Biorelevant media were purchased from biorelevant.com (UK). All chemicals and reagents were of analytical grade.

Bosentan monohdyrate quantification

BOS was quantified using a ultraviolet (UV)-spectrophotometer (Cary 60 UV-visible, Agilent, Germany) for solubility studies, and an high performance liquid chromatography (HPLC) system from Agilent (1020 Series, Germany) for *in vitro* and *ex vivo* quantification analysis.

Detailed information on UV and HPLC analysis methods has been given in the previous study.[12] The chromatographic separation was performed using the XSelect® HSS C 18, 250x4.6 mm, 5 µm (Waters, Ireland) at 220 nm. The separation was achieved using the mobile phase composed of a buffer solution, prepared by adding 1 mL of triethylamine to 1 L of distilled water and adjusting with phosphoric acid to a pH of 2.5, acetonitrile in a 45:55 *(v/v)* ratio. The flow rate was 1.5 mL/min, and the injection volume was 100 µL.

Solubility studies

Various oils, surfactants, and cosurfactants such as medium-chain triglycerides (Captex® 355, Labrafac®, Miglyol® 812, Miglyol® 818, and Miglyol® 840), medium-chain mono and diglycerides (Capmul® MCM C8, Imwitor® 988, and Imwitor® 948), edible oils (corn oil, sunflower oil, black seed oil, flaxseed oil, sesame oil, cotton oil, olive oil, oleic acid, and grape seed oil), long-chain mono and diglycerides (Maisine® and Peceol®), and propylene glycol ester (Capryol® 90) were investigated and screened for BOS solubility and lipid-based SNEDDS formulation. Solubility studies were performed as described in our previous study.[12] Components of BOS with the highest solubility were selected for pseudo-ternary phase diagram studies (Table 1).

Table 1. Evaluation of different formulation

	Self-emulsifying mixture composition (*w/w* %)				HLB	PDI*	Zeta potential*	Z-average (d.nm)*	Self-emulsification time (sec.)	Dispersibility	Self-emulsion area
	S_{mix}	Oil	Surfactant	Cosurfactant							
F1	1:4	Maisine® 39.0	Labrasol® 12.2	Tween® 20 48.8	10.3	0.628±0.144	-8.44±0.12	434±27	288	Grade D	615.3
F2	1:4	Maisine® 42.2	Labrasol® 11.6	Tween® 80 46.2	9.0	0.751±0.034	-7.16±0.26	764±52	352	Grade D	639.7
F3	1:4	Maisine® 40.1	Solutol® HS 15 12.0	Tween® 20 47.9	10.2	0.713±0.148	-5.88±0.17	468±23	136	Grade D	504.3
F4	1:4	Maisine® 42.0	Solutol® HS 15 11.6	Tween® 80 46.4	9.1	0.972±0.006	-6.56±0.80	571±3	523	Grade D	434.3
F5	4:1	Capryol® 90 33.3	Tween® 20 53.3	Transcutol® HP 13.3	11.1	0.499±0.005	-5.15±0.19	165±2	70	Grade A	684.4
F6	4:1	Capryol® 90 22.2	Labrasol® 62.2	Tween® 20 15.6	12.5	0.524±0.009	-1.53±0.24	95±4	36	Grade C	550.2
F7	4:1	Capryol® 90 22.2	Labrasol® 62.2	Tween® 80 15.6	12.2	0.624±0.207	-0.47±0.05	156±53	28	Grade C	437.7
F8	4:1	Capryol® 90 22.2	Solutol® HS 15 62.2	Tween® 20 15.6	13.1	0.134±0.004	-3.05±0.15	12±0.3	177	Grade A	473.9
F9	9:1	Peceol® 10.1	Cremophor® RH 40 80.9	Labrasol® 9.0	13.5	0.149±0.008	-6.86±	14±0.2	60	Grade A	788.5

*n=3, HLB: Hydrophilic-lipophilic balance, PDI: Polydispersity index, S_{mix}: Surfactant: cosurfactant ratio, Z-average: Droplet size diameter, sec: Second, d.nm: Diameter values in nanometers

Construction of pseudo-ternary phase diagram and selection of SNEDDS formulation

The oils (Maisine®, Peceol®, and Capryol® 90), a mixture of surfactants (Solutol® HS 15, Tween® 20, Labrasol®, and Cremophor® RH 40) with cosurfactants (Tween® 20, Tween® 80, Labrasol®, and Transcutol® HP) at different ratios, were mixed at weight ratios of 9:1-1:9, according to the solubility study results. The optimum surfactant: cosurfactant ratio (S_{mix}) was determined. The pseudo-ternary phase diagram was constructed with a homogeneous mixture of SNEDDS components and water. The endpoint of the transparency-to-turbidity transition was noted and determined by identifying the nanoemulsifying area.[13] The candidate system was examined for specific SNEDDS formulation properties such as hydrophilic-lipophilic balance (HLB), polydispersity index (PDI), zeta potential, DS, self-emulsification time, and dispersibility, based on the center of the obtained pseudo-ternary phase diagrams. According to the lipid formulation classification system (LFCS), a candidate formulation was selected by considering the properties that SNEDD system formulations should have, such as Type IIIB formulations containing that contain relatively limited amounts of glyceride lipid (<20%) and larger quantities (20-50%) of hydrophilic components (HLB>12). These formulations do not undergo significant phase changes or potential loss of solvent capacity upon aqueous dilution and have a narrow DS (50-100 nm).[1] After the candidate formulation was optimized with BBD, characterization studies were carried out for the resulting formulation.

Experimental design

Design Expert® V10 (Stat-Ease Inc., MN) was used to evaluate design parameters with a 3-factor, 3-level BBD. Formulation components, their main effects, and interaction effects were investigated. As determined by BBD, 15 experimental studies (containing three central points) were studied to define the precision of the design, assess experimental error, and optimize the performance of the SNEDDS. The program determined the low, middle, and high levels of the independent variables low, middle, and high levels. The levels (3-levels) coded as -1 (low), 0 (middle), and +1 (high) for each independent variable (3-factors) were chosen from the self-nanoemulsification area in the pseudo-ternary phase diagram. The amounts of oil (Peceol®) (X1), surfactant (Cremophor® RH 40) (X2), and cosurfactant (Labrasol®)

(X3) were chosen as independent variables, while particle size (Y1) and PDI (Y2) were the dependent variables. The response surface methodology was used to determine the ideal formulation composition. The models were validated by the multiple correlation coefficients (R^2), the lack of fit tests, and the analysis of variance (ANOVA) tests.

Preparation of lipid-based formulations

BOS was dissolved in the optimum SNEDDS formulation (Peceol®, Cremophor® RH 40, and Labrasol® were selected as oil, surfactant, and co-surfactant, respectively) obtained with BBD. The components were mixed at 37 ˚C until a homogeneous preparation was obtained.

Characterization of SNEDDS

PDI and DS

The PDI and DS were examined after diluting 1 mL formulation with 250 mL of distilled water at 25±0.5 ˚C. All the PDI and DS measurements were carried out by Malvern (Nano ZS, Malvern Instruments, UK).

Efficiency test of self-nanoemulsification

Self-emulsification time and formulation dispersibility are measured to characterize the spontaneous formation of SNEDDS.[14] For dispersibility, SNEDDS formulations were added to 500 mL of water at 37±0.5 ˚C, at 50 rpm. For self-emulsification time, SNEDDS formulations were added to 250 mL of water under the same conditions. The formulations' final appearance and time of emulsification are evaluated by a grading system.[15]

% transmittance and turbidity

The transmittance studies of the optimum SNEDDS formulations were conducted at 638 nm using a UV spectrophotometer.[16] The transparency of the formulations is verified if the % transmittance is greater than 99%.

For the optimum SNEDDS formulation and self-nanoemulsion, turbidity measurements were carried out at 25±0.5 ˚C, with readings from 0 to 200 NTU.

Viscosity

The viscosity was measured and evaluated as described in our previous study.[12] The SNEDDS formulation (0.5 mL) was placed in a Brookfield viscometer (DV III+Rheometer, USA). The viscosity studies were carried out in triplicate.

Robustness and pH effect

The effect of volume and pH change on the DS of the aqueous medium used to dilute the optimum SNEDDS was examined. The optimum SNEDDS formulation was diluted in 1:100, 1:250, and 1:500 ratios in aqueous media without enzyme at pH 1.2 and 6.8.

Morphological imaging

Transmission electron microscopy (TEM) was used to image the droplet's morphology. Distilled water was used to dilute the formulation. It was then stirred with a magnetic stirrer, and a drop of the sample was placed on a copper grid with a phosphotungstic acid solution (1% *w/v*) for 5 min at room temperature (FEI, USA).[17]

Thermodynamic and long-term stability studies

The studies were carried out for heating-cooling cycles (3 cycles, 4˚C - 45˚C), centrifugation (at 3500 rpm for 30 min), and freeze-thaw (3 cycles, -21 ˚C - 25 ˚C). Each cycle should be at least 48 hours for each of the heating-cooling and freezing-thawing cycles. After the successful thermodynamic studies, the optimum formulation was evaluated with PDI and DS.

The physical and chemical stability of the optimum formulation was evaluated under different storage conditions, namely 4˚C, 25±2˚C/60±5% relative humidity (RH), and 40±2 ˚C/75±5% RH. The optimum formulation was evaluated at 0, 1, 3, and 6 months for physical appearance, PDI, and DS.

Dissolution study

The *in vitro* dissolution study was conducted in United States Pharmacopeia apparatus II (Variant, USA) at 37±0.5 ˚C and 50 rpm in 900 mL of dissolution medium. The 1% SLS in distilled water, which is Food and Drug Administration (FDA)-recommended media (before the updated 09/15/2023 revision in the FDA dissolution database), and biorelevant media were used as media. Based on satueferation solubility, the relative sink condition was calculated for the dissolution study. This evaluation was conducted for the FDA-recommended medium only. To prepare a supersaturated solution, an excess dose of BOS and 10 mL of dissolution medium were added to vials (at 37 ˚C, n=3). Samples were taken from the vials at the end of 24 hours and analyzed with a UV spectrophotometer. The relative sink condition values of the FDA medium, 1% SLS containing distilled water, were evaluated at the 24th hour under the temperature conditions of the dissolution studies 37 ˚C. The ratio of saturation solubility to drug concentration (CS/CD) was calculated by dividing the dose by 900 mL of dissolution medium to represent the sink condition for commercial products and SNEDDS formulation. One g of SNEDDS formulation was placed in a Capsugel® capsule (00el, Belgium), which was placed in a sinker that would prevent it from floating, then left in the dissolution medium. The samples (5 mL) were withdrawn at 0.25, 0.5, 0.75, 1, and 1.5 h. They were filtered and analyzed at 220 nm by HPLC (1220 LC Agilent, Germany).[12] The dissolution profiles of commercial products (125 mg) and optimum SNEDDS formulation (28 mg) were compared and evaluated by the DDSolver® (with similarity factor) (f2).

Ex vivo permeability studies

Ex vivo permeability studies used a Franz diffusion cell (diffusional area: 1 cm^2, cell chamber capacity 2.5 mL). Biorelevant media and goat intestine membranes were used for the study. One mL of optimum SNEDDS and commercial product suspension were used, and the study was carried out at 37 ˚C for 10 h. The samples were analyzed using HPLC at 220 nm.[12] The steady-state section of the permeation profile and the ratio of concentration to flux in the donor chamber were used to calculate the permeability coefficient (*P*) and flux values, respectively.

Flux (J, µg. cm-2. h-1) is the amount of active substance penetrating a unit area per unit of time. Equation 1 was used to determine the slope of the linear portion in the graph showing the quantity of BOS that permeated the acceptor compartment vs. time.

$$J=dQ/A\,dt \qquad \text{(Equation 1)}$$

Q is the amount of penetrating drug, A is the area of the tissue/membrane, and t is time.

Statistical analysis

Student *t-tests* and one-way ANOVA were used for statistical analysis. The significance of the difference, which is at a 0.05 probability level, was assessed using IBM® SPSS® 22.

RESULTS

Solubility studies

The oil with a higher solubilization capacity of the drug has a higher drug loading potential.[18,19] In Figure 1, BOSs solubility was significantly higher in synthetic oils than in other edible oils, showing high solubility in medium-chain mono/diglyceride and long-chain mono/diglyceride groups.

Construction of pseudo-ternary phase diagram and selection of SNEDDS formulation

The red areas in the pseudo-ternary phase diagram represent the areas where a system without any active substance forms a self-nanoemulsion, as defined by water titration (Figure 2). The most suitable combinations for each SNEDD system were determined by trying ratios from 9:1 to 1:9.

The HLB values are a critical factor in the formulation of SNEDDS. Based on the HLB values, suitable components for the *o/w*, (required HLB values: 8-18) emulsion were selected, and the total HLB values for SNEDD systems were calculated (Table 1). PDI, zeta potential, DS, self-emulsification time, and dispersibility characterizations were made for nine different SNEDDS combinations based on the centers of the obtained areas (Table 1).

Experimental design

The BBD program presented 15 formulations based on the experimental design. The influence of independent variables on dependent variables was examined (Table 2). The best-fit models were found for the SNEDDS PDI and DS dependent variables. The correlation coefficients of the equations were evaluated using experimental values and were found to fit the data well, yielding the R^2 values present in Table 3. The 'Prob>*f*' values must be less than 0.05 for the model terms to be significant ($p<0.05$ in all cases) (Table 4).

Tables 3 and 4 contain the model that fitted the experimental data and the ANOVA results for DS and PDI of SNEDDS. The DS responses for SNEDDS formulation were evaluated, and the 2-factor interaction (2 FI) model was selected by Design Expert® as the appropriate model. In the model, the terms A, B, C, AB, and AC were significantly effective ($p<0.0001$). For the PDI responses in the Peceol formulation, the terms A, B, and AB were found to be significant for SNEDDS. The contour and surface graphs of the independent factors statistically impacted the DS responses (Figures 3a and 3b for A, B, and AB and Figures 3c and 3d for A, C, and AC).

For the optimum SNEDDS from the F9 SNEDDS formulation, the PDI was found to be 0.149±0.008. The DS was 14.44±0.21 nm (Figure 4). Twenty-eight milligrams of BOS could be dissolved in 1 gram of the SNEDDS formulation. Other characterization

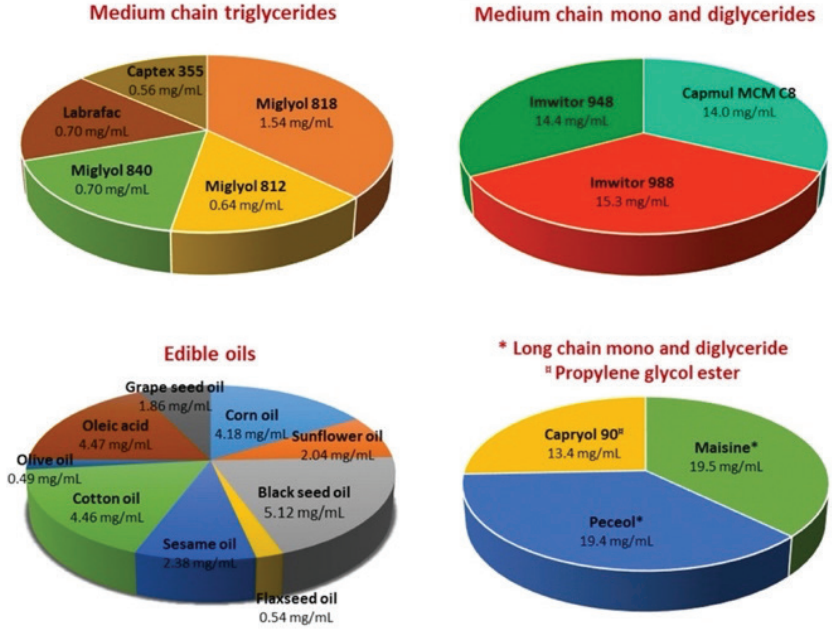

Figure 1. Solubility of BOS in different oil groups

BOS: Bosentan monohydrate

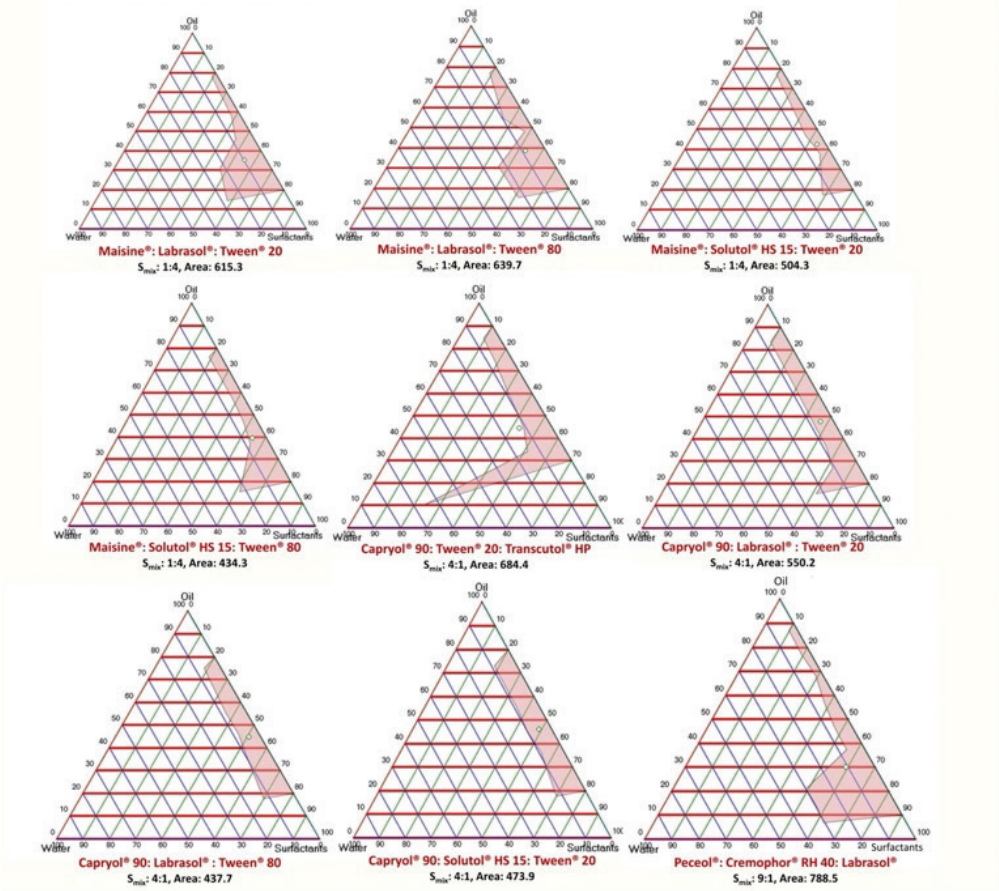

Figure 2. The pseudo-ternary phase diagrams of different oils, surfactants, and cosurfactants

Table 2. Variables used in the Box-Behnken design for optimum SNEDDS formulation

	Levels, actual (coded)		
	Low (-1)	**Medium (0)**	**High (+1)**
Independent variables			
X_1: Amount of Peceol added (g)	0.9	1.45	2
X_2: Amount of Cremophor RH 40 (g)	4.5	5.85	7.2
X_3: Amount of Labrasol (g)	0.5	0.65	0.8
Dependent variables			
Y_1: Droplet size (nm)		<100 nm	
Y_2: PDI		<0.2	

PDI: Polydispersity index, SNEDDS: Self-nanoemulsifying drug delivery systems

Table 3. Model fitting for DS and PDI of optimum SNEDDS formulation

	BFM	**Lack of fit**	**R^2**	**Adjusted R^2**	**Predicted R^2**
DS model	2FI	0.1424	0.9985	0.9973	0.9928
Equation	Y_1=87.26+62.28*A-41.04*B+9.23*C 27.46*AB+9.10*AC				
	BFM	**Lack of fit**	**R^2**	**Adjusted R^2**	**Predicted R^2**
PDI model	Quadratic	0.7479	0.9878	0.9659	0.9059
Equation	Y_2=0.95+0.28*A-0.11*B+0.17*AB				

Pred R^2: Predictive R^2, Adj R^2: Adjusted R^2, BFM: Best fitted model, DS: Droplet size, PDI: Polydispersity index

Table 4. Statistical analysis of the fitted model for DS and PDI of optimum SNEDDS formulation

Dependent variables	DS (Y_1)			PDI (Y_2)		
	Independent variables	*f* value	*p* value	Independent variables	*f* value	*p* value
	A	3312	<0.0001	A	204	<0.0001
	B	1438	<0.0001	B	29.4	0.0029
	C	72.7	<0.0001	C	2.53	0.1723
	AB	322	<0.0001	AB	39.0	0.0015
	AC	35.3	0.0003	AC	0.19	0.6798
	BC	4.99	0.0560	BC	2.73	0.1593
				A2	104	0.0002
				B2	0.85	0.3999
				C2	27.3	0.0034
Model ANOVA						
	f value:	864		*f* value:	45.1	
	R^2:	0.9985		R^2:	0.9878	
	p:	<0.0001		p:	0.0003	

DS: Droplet size, PDI: Polydispersity index, SNEDDS: Self-nanoemulsifying drug delivery systems, ANOVA: Analysis of variance

studies were carried out on the BOS-loaded optimum SNEDDS formulation.

Characterization of SNEDDS

PDI and DS

All formulations developed according to BBD were confirmed to be in the nanometer sizes, with DS ranging from 15.9 to 215 nm and PDI ranging from 0.121 to 1.000. The BOS-loaded SNEDDS formulation was diluted 250-fold with distilled water, and the PDI and mean DS were found. The PDI for the BOS-loaded SNEDDS formulation prepared with the optimum formulation was 0.200±0.025, and the DS was 16.76±1.78 nm (Figure 4).

Efficiency test of self-nanoemulsification

The formulation created a clear and fine system with an emulsification time of less than 1 minute. The results are shown in Table 5. The BOS-loaded SNEDDS formulation passed this test in Grade A, and it is hypothesized that it will form nanoemulsions when dispersed in GI fluid.

% transmittance and turbidity

Evaluated SNEDDS formulation showed a transmittance of over 99%, confirming the nanoemulsification efficiency of the SNEDDS.[20] Turbidity results are given in Table 5.

Viscosity

The SNEDDS formulation result is shown in Table 5.

Robustness and pH effect

Diluting the SNEDDS formulation 100, 250, and 500 times with distilled water and pH 1.2 and pH 6.8 phosphate buffer, which simulate the gastrointestinal system, revealed the effect of robustness and dilution media (Table 5).[21] Precipitation was not seen in either alkaline or acidic environments, indicating that the formulation is stable in dispersion.

Morphological imaging

The spherical shapes ranging from 10 to 100 nm were visualized using TEM pictures (Figure 5).

Thermodynamic and long-term stability studies

The SNEDDS formulation passed the heating-cooling cycle, centrifugation study, and freeze-thaw test. The DS and PDI results for the SNEDDS formulation are shown in Table 6. The study indicated that the SNEDDS formulation showed no precipitation or phase separation.[22]

The SNEDDS formulation was found to be physically stable for six months at 4 °C, 25±2 °C/60±5% RH, and 40±2 °C/75±5% RH (Table 6).

Dissolution studies

The dissolution profiles of SNEDDS formulation (28 mg BOS) and commercial products (Tracleer® 125 mg film tablet) were compared under conditions of 1% SLS in distilled water and biorelevant media (Figure 6).

The relative sink condition values (CS/CD) for the distilled water medium containing 1% SLS, which is the dissolution medium recommended by the FDA, were found to be greater than 3 for both the commercial product (10.3) and Peceol® SNEDDS formulation (47.6). The C_S/C_D values greater than 3 are considered to provide sink conditions.[23]

In the distilled water with 1% SLS, more than 80% of the BOS was released from the formulation and commercial product after 15 min, and 100% release was obtained from both within 30 min. In addition, for the SNEDDS formulation, more than

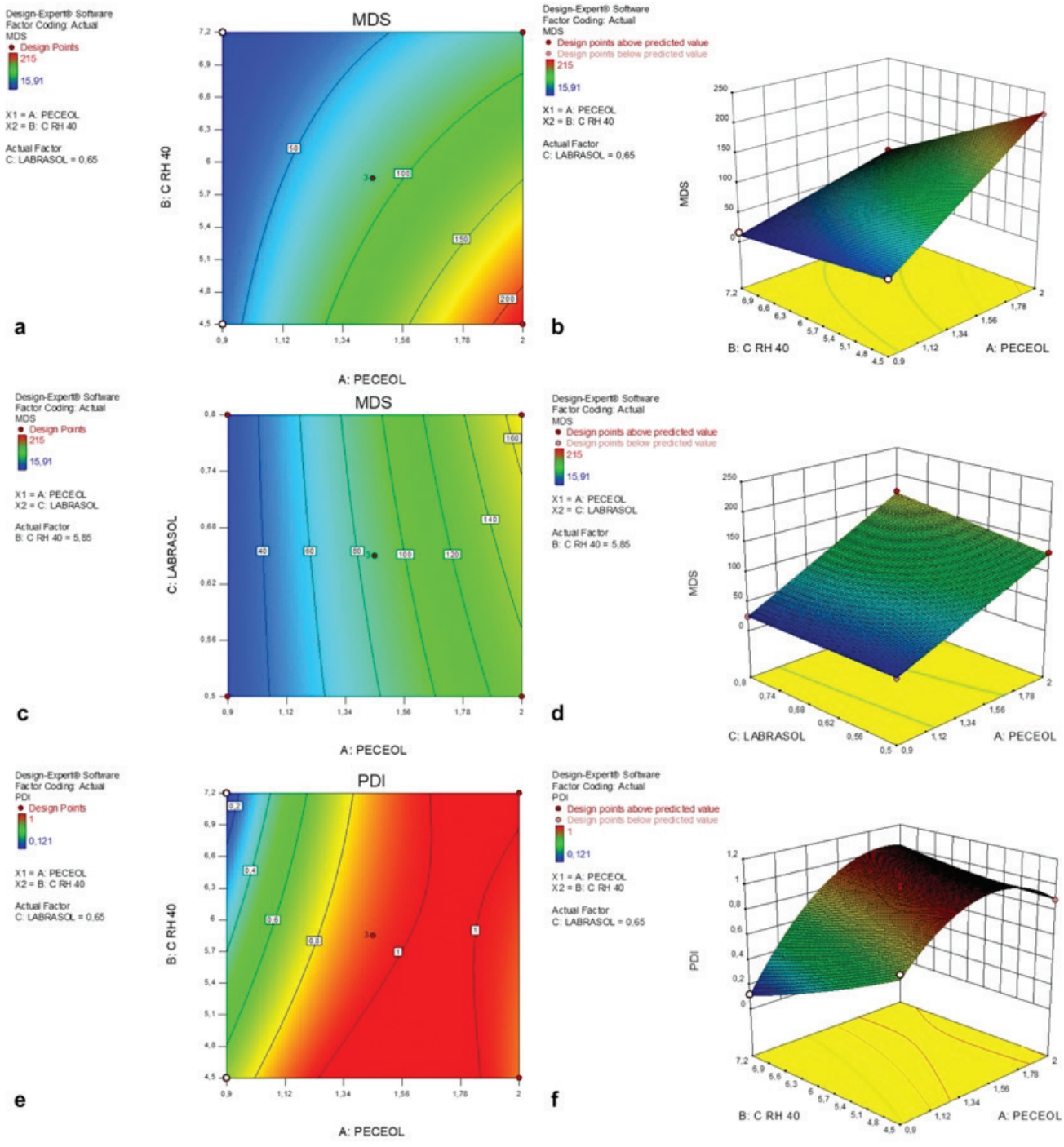

Figure 3. a) Surface and b) contour graphs of Peceol® and Cremophor® RH 40 for droplet size, c) Surface and d) contour graphs of Peceol® and Labrasol® for droplet size, e) Surface and f) contour graphs of Peceol®, Cremophor® RH 40 and Peceol®-Cremophor® RH 40 for PDI

MDS: Mean diffusional size, PDI: Polydispersity index, RH: Relative hydrophobicity

80% of the releases were obtained in 30 minutes for FaSSIF, FeSSIF, and FeSSIF-V2, while the release in FaSSIF-V2 was 77% in 30 minutes and exceeded 80% at the end of 90 minutes. However, within 90 minutes, the commercial products were able to release almost 32%, 11%, 22%, and 2% in FaSSIF, FeSSIF, FaSSIF-V2, and FeSSIF-V2, respectively.

SNEDDS formulation and commercial product dissolution profiles did not give similar dissolution curves with f_2=14 for FaSSIF, f_2=9 for FeSSIF, f_2=14 for FaSSIF-V2, and f_2=9 for FeSSIF-V2.

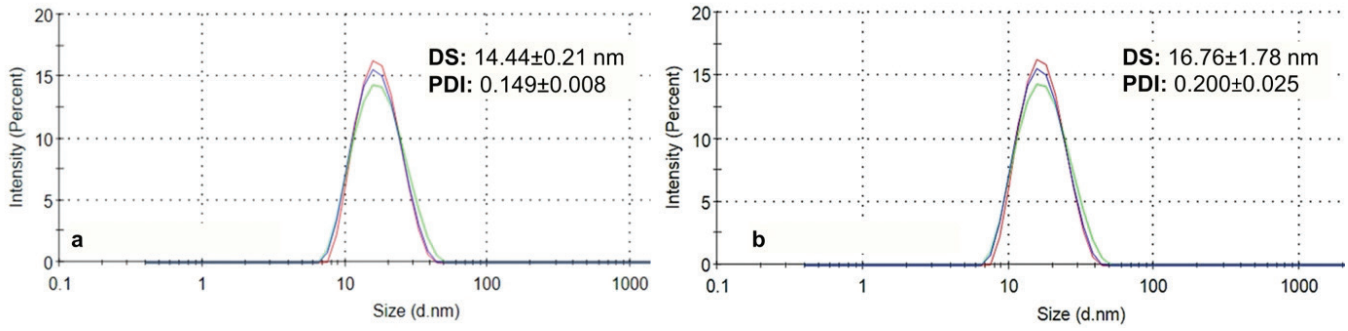

Figure 4. Droplet size and droplet size distributions (PDI) of optimum SNEDDS formulation and BOS-loaded SNEDDS formulation
BOS: Bosentan monohydrate, PDI: Polydispersity index, SNEDDS: Self-nanoemulsifying drug delivery systems

Table 5. Characterization of BOS-loaded SNEDDS formulation

Dispersibility	Self-emulsification time (sec.)	Transmittance %	Turbidity (NTU)	Viscosity (cP)
Grade A	54±6	No dilution 99.9±0.1	No dilution 12.4±0.2	474
		250-time dilution 99.6±0.0	250-time dilution 10.9±0.3	

Robustness and effect of pH		DS (nm)	PDI
Distilled water	1:100	15.4±1.2	0.173±0.030
	1:250	16.8±1.8	0.200±0.025
	1:500	25.2±10.9	0.178±0.051
pH 1.2	1:100	18.0±1.4	0.205±0.026
	1:250	27.0±15.4	0.201±0.057
	1:500	34.5±20.9	0.225±0.035
pH 6.8	1:100	16.0±0.8	0.128±0.045
	1:250	17.0±1.3	0.165±0.032
	1:500	21.0±1.2	0.230±0.017

*Mean ± standard deviation, BOS: Bosentan monohydrate, SNEDDS: Self-nanoemulsifying drug delivery systems, NTU: Nepholometric turbidity units, cP: Centipoise, DS: Droplet size, PDI: Polydispersity index

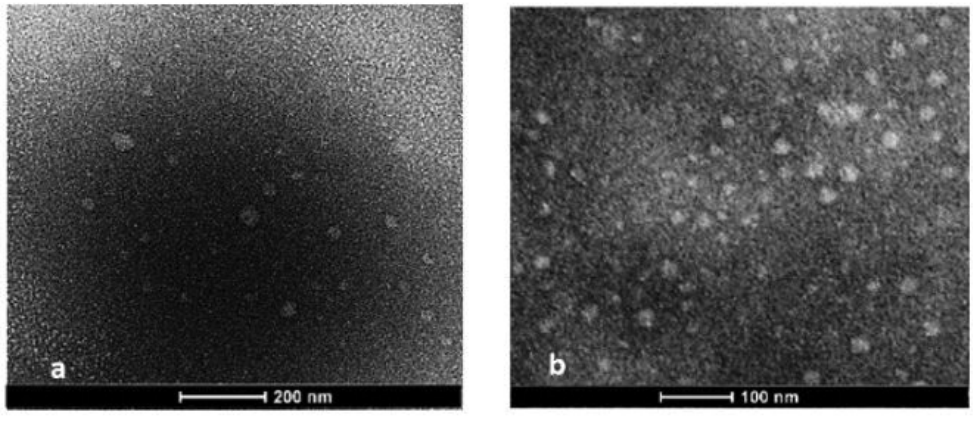

Figure 5. Morphology of a) optimum SNEDDS formulation and b) BOS-loaded SNEDDS formulation
BOS: Bosentan monohydrate, SNEDDS: Self-nanoemulsifying drug delivery systems

Table 6. Thermodynamic and long-term stability studies of BOS-loaded SNEDDS formulation

	Thermodynamic stability			Long term stability			
	DS (nm)*	PDI*		Time (month)	PA	DS (nm)*	PDI*
CS	15.4±0.7	0.136±0.027	4 °C	0	Clear	14.4±0.2	0.149±0.008
				1	Clear	23.2±6.9	0.186±0.043
				3	Clear	17.2±2.8	0.202±0.044
				6	Clear	17.0±1.2	0.176±0.063
Heating cooling	16.7±1.9	0.175±0.080	25±2 °C 60±5% RH	0	Clear	14.4±0.2	0.149±0.008
				1	Clear	24.3±2.3	0.190±0.072
				3	Clear	15.4±0.2	0.154±0.043
				6	Clear	18.3±1.9	0.208±0.058
Freeze thaw	16.6±1.8	0.229±0.038	40±2 °C 75±5% RH	0	Clear	14.4±0.2	0.149±0.008
				1	Clear	18.0±3.3	0.201±0.031
				3	Clear	15.2±0.6	0.128±0.039
				6	Clear	16.0±1.1	0.141±0.065

*Mean ± standard deviation, DS: Droplet size, PDI: Polydispersity index, CS: Centrifugation study, PA: Physical appearance, BOS: Bosentan monohydrate, SNEDDS: Self-nanoemulsifying drug delivery systems, RH: Relative hydrophobicity

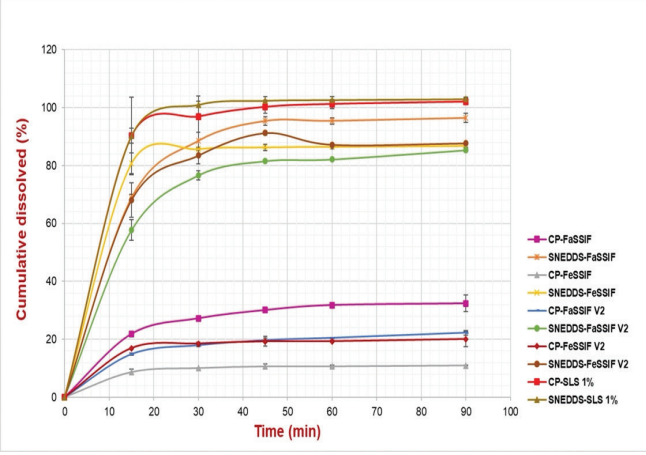

Figure 6. *In vitro* dissolution profiles of commercial product and BOS-loaded SNEDDS for 1% SLS in distilled water, FaSSIF, FeSSIF, FaSSIF-V2, and FeSSIF-V2 (n=3, mean ± SD)

CP: Commercial product, SD: Standard deviation, BOS: Bosentan monohydrate, SLS: Sodium lauryl sulfate, FaSSIF: Fasted state simulated intestinal fluid, FeSSIF: Fed state simulated intestinal fluid

Ex vivo permeability studies

The results of the SNEDDS formulation and the commercial product are shown in Figure 7. Compared to the commercial product, the SNEDDS formulation increased drug permeability by 12.2, 19.1, 20.3, and 13.1-fold in FaSSIF, FeSSIF, FaSSIF-V2, and FeSSIF-V2, respectively.

DISCUSSION

BOS is a weakly acidic drug, and pH is very important for such substances.[24] While BOS is less soluble in water: low pH aqueous solutions, its solubility increases specifically as pH increases (pH 1.1 and 4.0: 0.001 mg/mL, pH 5.0: 0.002 mg/mL, and pH 7.5: 0.43 mg/mL).[25] For solubility studies, the high solubility of the drug in the synthetic oil phase allowed less use of surfactants and cosurfactants, which are other components required for the system. The use of fewer surfactants and cosurfactants reduced the toxicity associated with these substances.

According to the solubility results, the construction of the pseudo-ternary phase diagram was carried out to identify the self-nanoemulsifying area for the SNEDDS.[26] Transparent isotropic areas are regions where nanoemulsions spontaneously form. S_{mix} ratios must be high to maintain droplet stability and to obtain smaller droplets, thus increasing the surface area.[27] The elevated S_{mix} ratios enhance water uptake capacity and maximize the nanoemulsion area for SNEDDS. Also, the choice of constituents in an SNEDDS is based on both HLB values and solubility. It is known that surfactants and cosurfactants with an HLB of 12-15 generally show better self-nanoemulsification.[28] For all these, the most suitable candidate SNEDDS formulation, which meets the requirements of being an SNEDDS according to LFCS (DS<100 nm; 0.200<PDI; dispersibility: Grade A) and also considering the size of the self-emulsification areas, was determined to be the optimum formulation,

recognized as the F9 SNEDD formulation (Table 1).[1,29,30] Optimization studies with BBD experimental design were continued with the F9 formulation. F9 formulation consists of Peceol® (HLB=1), Cremophor® RH 40 (HLB=15), and Labrasol® (HLB=14), serving as the oil, surfactant, and cosurfactant, respectively.

The experimental design study aimed to minimize DS (<100 nm) and PDI (<0.2) for F9 SNEDDS formulation, to obtain optimal SNEDDS. BBD has been proposed to study the relationship

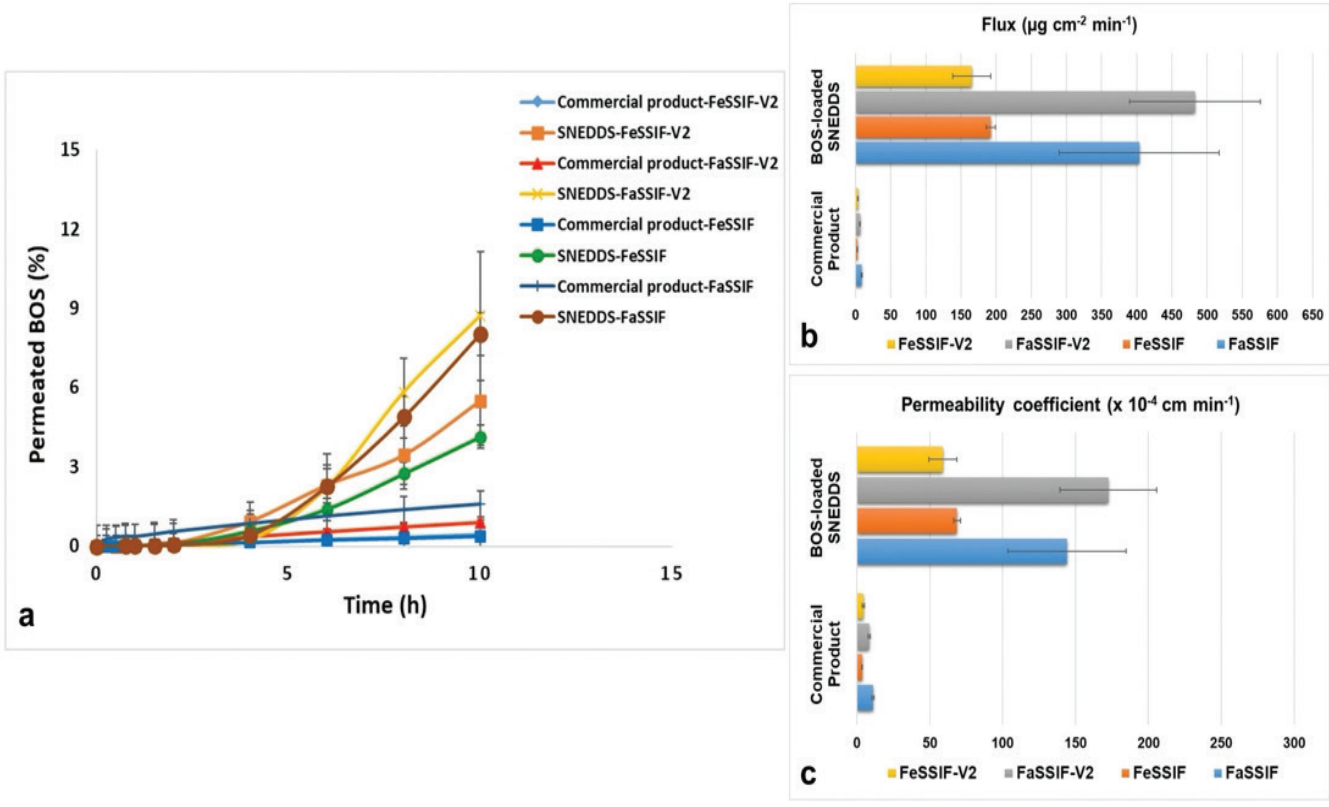

Figure 7. a) *Ex vivo* permeation profiles of commercial product and SNEDDS, b) flux values calculated from the permeation-time profiles of BOS across goat intestine membrane, c) permeability coefficients calculated from the permeation-time profiles of BOS across goat intestine membrane in FaSSIF, FeSSIF, FaSSIF-V2, and FeSSIF-V2 (n=3)

BOS: Bosentan monohydrate, FaSSIF: Fasted state simulated intestinal fluid, FeSSIF: Fed state simulated intestinal fluid, SNEDDS: Self-nanoemulsifying drug delivery systems

between dependent and independent factors, along with experimental parameters and response variables, and has been used successfully in many studies.[29] Another advantage of BBD is that it includes combinations in which all variables are simultaneously examined at their highest or lowest values.

In SNEDDS formulations, the DS should be smaller than 100 nm. In the evaluation of the graphs in Figure 3a and 3b, with the quantity of Labrasol, the cosurfactant, kept constant, the effect of Peceol®-Cremophor® RH 40 interaction on the DS was examined. It was observed that DS decreased when the amount of Peceol® selected as oil was decreased and the amount of Cremophor® RH 40 used as a surfactant was increased. The effect of the interaction of the quantity of Peceol®-Labrasol® on the DS was investigated by keeping the surfactant Cremophor® RH 40 constant (Figures 3c and 3d). It was observed that smaller DSs were obtained by decreasing the amount of Peceol® selected as oil while increasing the amount of Labrasol®, which has a relatively minor effect on the formulation, used as cosurfactant. Figures 3e and 3f, corresponding to the variables A, B, and AB, show the surface and contour graphs of the independent variables that have a statistically significant effect on the PDI responses in the model equation proposed by the software as a result of the design. When the impact of the interaction of Peceol®-Cremophor® RH 40 levels on PDI was evaluated, it was observed that as the quantity of Peceol® decreased, the DS reduced, while the quantity of Cremophor® RH 40, used as a surfactant enhancer, increased. The intended characterization features for developing the SNEDDS formulation were DS<100 nm and PDI<0.2. The test results were reported in a 95 percent confidence interval based on the best results from the formulation's characterization properties, the model results, and the experimental design.

The emulsion's PDI and DS are significant determinants in self-emulsification since they specify the rate and extent of *in vivo* drug release. As the DS of the nanoemulsion gets smaller, the surface area will increase, and the increased surface area will enhance the bioavailability of the drug, which has poor water solubility.[31] However, the volume of liquid in the stomach and its pH vary between individuals. It is essential to ensure that homogeneous nanoemulsions are formed at different dilution conditions, and the SNEDDS should disperse quickly and completely without precipitation when subjected to aqueous dilution under the agitation of GIT due to peristaltic activity.[30] Furthermore, there was a strong relationship between the SNEDDS' visual appearance and the formulation's turbidity. With smaller DSs, transparent systems exhibit a higher transmittance

percentage. Furthermore, the lower viscosity of the system indicates that SNEDDS has a propensity to create an oil-in-water *(o/w)* type nanoemulsion.The SNEDDS characterization studies have confirmed that transparent systems with suitable viscosity, small size, and homogeneous distribution, which are resistant to different dilution conditions, were obtained.

According to thermodynamic stability studies, stable emulsion formulations may withstand centrifugal stress and a wide range of temperature fluctuations without leading to drug precipitation or phase separation.[32] No change in the physical appearance of SNEDDS formulation was observed during the stability studies. The SNEDDS formulation remained transparent with no turbidity or Precipitation. The PDI and DS were similar in all the storage conditions for the SNEDDS formulation. It can be concluded that the SNEDDS formulation would stay stable at 25±2 ˚C/60±5% RH for long-term stability conditions, and at 4 ˚C and at 40±2 ˚C/75±5% RH for accelerated conditions, for six months.

In drug development, the quality of the drug product is utilized to evaluate how the formulation parameters would affect bioavailability, with *in vitro* dissolution tests being the most important measurement of performance.[33] When employed to examine solubility and dissolution, the classic dissolution media in the pharmacopeia provides useful information. However, these media are inadequate in reflecting physiological conditions, especially with BCS Class II poorly water-soluble drugs.[23]

Aqueous solutions of poorly water-soluble drugs such as BOS do not reach sufficient solubility in the physiological pH 1.2-6.8 range. BOS is a BCS Class IIa active substance with pH-dependent solubility and acidic properties.[34] A weak acid's saturation solubility, and consequently the rate and amount of dissolution, can be significantly influenced by the rate at which it ionizes. Weakly acidic drugs have low solubility in the stomach, and their solubility in the intestine increases with increasing pH. Because of their composition, biorelevant media produce more consistent results for simulating *in vivo* conditions. BCS Class II drugs have better results in *in vitro* dissolution compared to compendial media.[35]

The reason for the lower release of BOS, an active substance of BCS Class II, in the FeSSIF and FeSSIF-V2 media is that the active substance exhibits poor acidic properties. The pH values of FeSSIF (pH 5.0) and FeSSIF-V2 (pH 5.8) are less than FaSSIF (pH 6.5), and FaSSIF-V2 (pH 6.5).[36] The SNEDDS formulation, in comparison to the commercial product (Tracleer®), enhanced the percent cumulative dissolution by 2.98, 7.88, 3.84, and 4.37-fold in FaSSIF, FeSSIF, FaSSIF-V2, and FeSSIF-V2, respectively (Figure 6). The results of the commercial product and SNEDDS were analyzed, and the increases obtained with the formulation were significant ($p<0.05$). The enhanced dissolution rate of BOS from the developed SNEDDS could be because the SNEDDS formulation resulted in the spontaneous formation of a nanoemulsion with a much faster and smaller DS compared to the BOS commercial product. These results show that biorelevant media could better forecast the *in vivo* performance for BOS-loaded SNEDDS formulation. Hence, this greater availability of dissolved BOS from the formulation could enhance oral bioavailability.

In an *ex vivo* permeability studies study, biorelevant media were used as buffers to better simulate *in vivo* conditions. Furthermore, because it includes a significant level of surfactant and does not reflect *in vivo* conditions, the medium with 1% SLS was not included in the *ex vivo* studies. Although BCS Class II drugs do not inherently have a permeability problem, increased solubility may relatively enhance their permeability. BOS is a weakly acidic active compound, and its solubility is pH-dependent. The increase in the pH of the medium and the SNEDDS formulation strategy enhances the solubility and permeability of BOS. In comparison to FeSSIF (pH 5.0) and FeSSIF-V2 (pH 5.8), which are used for formulation and commercial product testing, BOS showed higher permeability in FaSSIF and FaSSIF-V2 (pH 6.5) (Figure 7). The results of the commercial product and SNEDDSs were analyzed, and the increases obtained with the formulation were significant ($p<0.05$).

The formulation was developed with the data obtained from our pre-formulation studies mentioned in this publication.[2] The main purpose of the studies was to develop the SNEDDS formulation, in which BOS is the most soluble, and then to develop the solid SNEDDS. Based on F9, Maisine®, a long-chain mono and diglyceride group oil with high BOS solubility, was preferred while the other components were kept constant. It was found that a formulation with a DS of 17 nm and a PDI of 0.180, consisting of 10.11% Maisine®, 80.90% Cremophor® RH 40, and 8.99% Labrasol®, and 30 mg BOS in 1 g SNEDDS, exhibited dispersibility of: Grade A, a self-emulsification time of 47 seconds, transmittance greater than 99%, and a viscosity of 571 cP. Similar results to those of the Maisine® SNEDDS formulation were obtained, as shown in Table 1 and Table 5. The dissolution study results did not show statistical significance ($p>0.05$). However, the dissolution of BOS per gram in Maisine® SNEDDS formulation (30 mg) was found to be relatively greater than that of the F9 (28 mg) formulation. Therefore, further studies were conducted using the Maisine® formulation.

CONCLUSION

With this study, the BOS-loaded SNEDDS formulation was effectively developed, characterized, and evaluated. The SNEDDS was optimized using the BBD. The *in vitro* evaluation of SNEDDS indicated characteristics of a self-nanoemulsifying system, including transparency, robustness to dilution, thermodynamic stability, and rapid dissolution. The formulation was found stable in long-term stability studies. An *in vitro* dissolution study was carried out to assess the biorelevant media performance of BOS. According to the findings, solubility *in vitro* was significantly improved for the formulation compared to the commercial product. Due to its increased solubility, SNEDDS improved the permeability of BOS. It can be concluded that the SNEDDS of BOS is a promising lipid-based drug delivery system to increase bioavailability. Further, *in vivo* studies are needed to test the performance of BOS-loaded SNEDDS formulation.

Ethics

Ethics Committee Approval: Not required.

Informed Consent: Not required.

Acknowledgment

The authors would like to thank Gattefossé (France) for providing Labrafac®, Labrasol®, Capryol® 90, Maisine®, and Peceol®. Oleochemicals (Germany) for Imwitor® (948-988) and Miglyol® (812-818-840); Abitec (USA) for Captex® 355 and Capmul® MCM C8, and Abdi İbrahim (Türkiye) for BOS.

Footnotes

Authorship Contributions

Concept: D.Y.U., Z.Ş.T., Design: D.Y.U., Z.Ş.T., Data Collection or Processing: D.Y.U., Z.Ş.T., Analysis or Interpretation: D.Y.U., Z.Ş.T., Literature Search: D.Y.U., Z.Ş.T., Writing: D.Y.U., Z.Ş.T.

Conflict of Interest: The authors declare no conflicts of interest.

Financial Disclosure: This study was supported by a grant from the Scientific and Technological Research Council of Türkiye (project number: 217S602, TUBITAK).

REFERENCES

1. Feeney OM, Crum MF, McEvoy CL, Trevaskis NL, Williams HD, Pouton CW, Charman WN, Bergström CAS, Porter CJH. 50 years of oral lipid-based formulations: provenance, progress and future perspectives. Adv Drug Deliv Rev. 2016;101:167-194.
2. Yilmaz Usta D, Olgac S, Timur B, Teksin ZS. Development and pharmacokinetic evaluation of Neusilin® US2-based S-SNEDDS tablets for bosentan: fasted and fed states bioavailability, IVIS® real-time biodistribution, and *ex-vivo* imaging. Int J Pharm. 2023;643:123219.
3. Timur B, Yilmaz Usta D, Teksin ZS. Investigation of the effect of colloidal structures formed during lipolysis of lipid-based formulation on exemestane permeability using the *in vitro* lipolysis-permeation model. J Drug Deliv Sci Tec. 2022;77:103797.
4. Gaine SP, Rubin LJ. Primary pulmonary hypertension. Lancet. 1998;352:719-725.
5. Sajedi-Amin S, Barzegar-Jalali M, Fathi-Azarbayjani A, Kebriaeezadeh A, Martínez F, Jouyban A. Solubilization of bosentan using ethanol as a pharmaceutical cosolvent. J Mol Liq. 2017;232:152-158.
6. Panigrahi KC, Jena J, Jena GK, Patra CN, Bhanoji Rao ME. QBD-based systematic development of bosentan SNEDDS: formulation, characterization and pharmacokinetic assessment. J Drug Deliv Sci Technol. 2018;47:31-42.
7. You R, Qian X, Tang W, Xie T, Zeng F, Chen J, Zhang Y, Liu J. Cost effectiveness of bosentan for pulmonary arterial hypertension: a systematic review. Can Respir J. 2018;8:1-12.
8. Hosny KM. Development of saquinavir mesylate nanoemulsion-loaded transdermal films: two-step optimization of permeation parameters, characterization, and *ex vivo* and *in vivo* evaluation. Int J Nanomedicine. 2019;14:8589-8601.
9. Yadav P, Rastogi V, Verma A. Application of Box-Behnken design and desirability function in the development and optimization of self-nanoemulsifying drug delivery system for enhanced dissolution of ezetimibe. Future J Pharm Sci. 2020;6:7.
10. Vadlamudi HC, Yalavarthi PR, Basaveswara Rao MV, Rasheed A, Tejeswari N. *In vitro* characterization studies of selfmicroemulsified bosentan systems. Drug Dev Ind Pharm. 2017;43:989-995.
11. Gunnam S, Kovvasu SP, Karthan J, Chakravarthy JK. Formulation and evaluation of self-emulsifying drug delivery system of bosentan. Asian J Pharm. 2018;12:S822.
12. Usta DY, Timur B, Teksin ZS. Formulation development, optimization by Box-Behnken design, characterization, *in vitro*, *ex-vivo*, and *in vivo* evaluation of bosentan-loaded self-nanoemulsifying drug delivery system: a novel alternative dosage form for pulmonary arterial hypertension treatment. Eur J Pharm Sci. 2022;174:106159.
13. Üstündağ Okur N, Çağlar EŞ, Arpa MD, Karasulu HY. Preparation and evaluation of novel microemulsion-based hydrogels for dermal delivery of benzocaine. Pharm Dev Technol. 2017;22:500-510.
14. Thakur PS, Singh N, Sangamwar AT, Bansal AK. Investigation of need for natural bioenhancer for a metabolism susceptible drug-raloxifene, in a designed self-emulsifying drug delivery system. AAPS PharmSciTech. 2017;18:2529-2540.
15. Shukla SN, Modi DC, Shah DP. A review on solid self-nanoemulsifying drug delivery system: an approach for bioavailability enhancement. World J Pharm Sci. 2016;5:302-316.
16. Patel J, Dhingani A, Garala K, Raval M, Sheth. Quality by design approach for oral bioavailability enhancement of Irbesartan by self-nanoemulsifying tablets. Drug Deliv. 2014;21:412-435.
17. Parmar K, Patel J, Sheth N. Self nano-emulsifying drug delivery system for embelin: design, characterization and *in-vitro* studies. Asian J Pharm Sci. 2015;10:396-404.
18. Pouton CW. Lipid formulations for oral administration of drugs: non-emulsifying, self-emulsifying and 'self microemulsifying' drug delivery systems. Eur J Pharm Sci. 2000;11:S93-S98.
19. Pouton CW. Formulation of poorly water-soluble drugs for oral administration: physicochemical and physiological issues and the lipid formulation classification system. Eur J Pharm Sci. 2006;29:278-287.
20. Agrawal AG, Kumar A, Gide PS. Self emulsifying drug delivery system for enhanced solubility and dissolution of glipizide. Colloids Surf B Biointerfaces. 2015;126:553-560.
21. Patel G, Shelat P, Lalwani A. Statistical modeling, optimization and characterization of solid self-nanoemulsifying drug delivery system of lopinavir using design of experiment. Drug Deliv. 2016;23:3027-3042.
22. Azeem A, Rizwan M, Ahmad FJ, Iqbal Z, Khar RK, Aqil M, Talegaonkar S. Nanoemulsion components screening and selection: a technical note. AAPS PharmSciTech. 2009;10:69-76.
23. Incecayir T, Olgac S, Usta DY, Teksin ZS. Role of surfactants on dissolution behavior of tamoxifen. Dissolution Technol. 2021;28:6-15.
24. Klumpp L, Leigh M, Dressman J. Dissolution behavior of various drugs in different FaSSIF versions. Eur J Pharm Sci. 2020;142:105138.
25. The US Food and Drug Administration. Medication Guide for Tracleer®. 2003.
26. Senapati PC, Sahoo SK, Sahu AN. Mixed surfactant based (SNEDDS) self-nanoemulsifying drug delivery system presenting efavirenz for enhancement of oral bioavailability. Biomed Pharmacother. 2016;80:42-51.
27. Sanka K, Suda D, Bakshi V. Optimization of solid-self nanoemulsifying drug delivery system for solubility and release profile of clonazepam using simplex lattice design. J Drug Del Sci Tech. 2016;33:114-124.
28. Liu CH, Chang FY, Hung DK. Terpene microemulsions for transdermal curcumin delivery: effects of terpenes and cosurfactants. Colloids Surf B Biointerfaces. 2011;82:63-70.

29. Bravo-Alfaro DA, Ochoa-Rodríguez LR, Villaseñor-Ortega F, Luna-Barcenas G, García HS. Self-nanoemulsifying drug delivery system (SNEDDS) improves the oral bioavailability of betulinic acid. J Mol Liq. 2022;364:119946.

30. Zhao Y, Wang C, Chow AH, Ren K, Gong T, Zhang Z, Zheng Y. Self-nanoemulsifying drug delivery system (SNEDDS) for oral delivery of zedoary essential oil: formulation and bioavailability studies. Int J Pharm. 2010;383:170-177.

31. Siddalingam R, Subramaniam P. Self-nanoemulsifying drug delivery systems of poorly soluble drug dutasteride: formulation and *in-vitro* characterization. J App Pharm Sci. 2017;7:011-022.

32. Kanuganti S, Jukanti R, Veerareddy PR, Bandari S. Paliperidone-loaded self-emulsifying drug delivery systems (SEDDS) for improved oral delivery. J Dispers Sci Technol. 2012;33:506-515.

33. Usta DY, Incecayir T. Modeling of *in vitro* dissolution profiles of carvedilol immediate-release tablets in different dissolution media. AAPS PharmSciTech. 2022;23:201.

34. Tsume Y, Mudie DM, Langguth P, Amidon GE, Amidon GL. The Biopharmaceutics Classification System: subclasses for *in vivo* predictive dissolution (IPD) methodology and IVIVC. Eur J Pharm Sci. 2014;57:152-163.

35. Mudie DM, Samiei N, Marshall DJ, Amidon GE, Bergström CAS. Selection of *in vivo* predictive dissolution media using drug substance and physiological properties. AAPS J. 2020;22:34.

36. Biorelevant. What are the differences between FaSSIF and FaSSIF v2? 2018. Available at: https://biorelevant.com/blog/what-are-the-differences-between-fessif-and-fessif-v2/